June 2021

RAPID CELL PHENOTYPING USING ARRAY-BASED SENSORS: APPLICATIONS IN CANCER STEM CELL THERAPY AND HIGH-CONTENT SCREENING

Yingying Geng
University of Massachusetts Amherst

RAPID CELL PHENOTYPING USING ARRAY-BASED SENSORS: APPLICATIONS IN CANCER STEM CELL THERAPY AND HIGH-CONTENT SCREENING

A Dissertation Presented

by

Yingying Geng

Submitted to the Graduate School of the
University of Massachusetts Amherst in partial fulfillment
of the requirements for the degree of

DOCTOR OF PHILOSOPHY

May 2021

Molecular and Cellular Biology Program

RAPID CELL PHENOTYPING USING ARRAY-BASED SENSORS: APPLICATIONS IN CANCER STEM CELL THERAPY AND HIGH-CONTENT SCREENING

A Dissertation Presented

by

Yingying Geng

Approved as to style and content by:

_____
Vincent M. Rotello, Chair

_____
Arthur M. Mercurio, Member

_____
Barbara A. Osborne, Member

_____
Alexander Suvorov, Member

_____
Thomas J. Maresca, Department Head
Molecular and Cellular Biology Program

DEDICATION

To God, all of this work is to glorify you;

To my parents Zhanjun Geng and Qiaozhen Guo, my brother Yukai Geng and Yuqiang Geng, my husband SuoAn, and my daughter Joanna; this Ph.D. journey would not have been possible without your love and support.

ACKNOWLEDGMENTS

My deep gratitude goes first to my research advisor Vincent M. Rotello, who inspired me with his passion for science, led me by his example, and guided me with his expertise. I am grateful for the freedom and opportunity that he has provided me to explore the scientific areas that interest me the most. I truly enjoyed working in the collaborative and open-communicating research environment that he created in the lab.

I would like to thank the valuable suggestions and support from my committee members: Professor Arthur Mercurio, Professor Barbara Osborne, and Professor Alexander Suvorov. I would especially thank Professor Author Mercurio for his guidance and valuable collaborations on the CSC work.

My appreciation also extends to my colleagues and collaborators in the Rotello and Mercurio groups. I would like to thank Dr. Hira Goel, John Amante, and Melanie Walker for the productive collaboration on the CSC project. I would like to thank Professor Michelle Farkas, Joseph Hardie, Javier Mas-Rosario for the valuable collaboration on the macrophage project. I would especially thank Dr. Ngoc Le for being a great mentor and friend throughout my Ph.D. journey. I would also like to acknowledge the help and kindness that I received over the past few years from the past and present Rotello lab members including Professor Tatsuyuki Yoshii, Dr. Gulen Tonga, Dr. Rubul Mout, Dr. Ryan Landis, Aritra Nath Chattopadhyay, Xianzhi Zhang, Dave Luther, Sanjana Gopalakrishnan, Puspam Keshri, Jiadi Sun, Sawinee Ngernpimai, Jessa Marie Makabenta, Dr. Akash Gupta, Cheng-Hsuan Li, Dr. Will Peveler, Yuanchang Liu, and Mingdi Jiang.

Additionally, I would like to thank Carol, Carrie, and Sarah for their administrative support. I am also particularly thankful to Robert Sabola for his technical support during our relocation of the cell culture facility.

Finally, I would like to express my sincere love and appreciation to my family both at Amherst and in China. I would like to thank my parents for their unconditional love and support in my entire life; my brother, Yukai, for mentoring and guiding me in my difficult times; my little brother, Yuqiang, for bringing laughter and joy to my life. I would also like to thank my beloved husband, SuoAn, who has consistently supported and encouraged me. Without his love and companionship, this Ph.D. journey would have been extremely difficult. I would also like to thank my 3-month old daughter, Joanna, for teaching me to be a mom with joy and patience. I am grateful to have a family from Amherst Chinese Christian Church. They have shown me what Christ's love is like on earth and guided me to receive an awakening spiritual life. I would like especially thank Pastor David Wang for mentoring me through difficult times. He has taught me a new way of serving by living out Jesus' teaching.

ABSTRACT

RAPID CELL PHENOTYPING USING ARRAY-BASED SENSORS: APPLICATIONS IN CANCER STEM CELL THERAPY AND HIGH-CONTENT SCREENING

MAY 2021

YINGYING GENG

B.S., UNIVERSITY OF RICHMOND

Ph.D., UNIVERSITY OF MASSACHUSETTS AMHERST

Directed by: Professor Vincent M. Rotello

Cell surface harbors rich information regarding the status of cell health. Being able to monitor and detect its changes in response to stimuli will provide crucial information in drug discovery, disease diagnosis, and human health. Despite the efforts and breakthroughs made possible through the specific sensing approach, there are significant challenges in extracting the information on the cell surface in a quantitative and reliable way. To address this challenge, I took the approach of array-based, hypothesis-free sensing in which the engineered sensors selectively interact with target analytes, producing a distinct pattern of response that enables analyte identification. This signature-based pattern recognition is particularly powerful in identifying the subtle changes on complex analytes (e.g. cell surfaces), rather than identifying specific elements within them. In this dissertation, I have applied such sensing strategy to facilitate the drug discovery process with the goal of rapidly identifying potential therapeutic candidates. Specifically, I utilize nanomaterials and polymers to construct effective nanosensors to phenotype mammalian cells. The first part of the thesis focuses on sensing a key target in cancer: cancer stem cells (CSCs). Utilizing a supramolecular nanoparticle-fluorescent protein sensor array, we successfully

discriminated breast CSCs from non-CSCs, as well CSCs that had differentiated *in vitro*. Furthermore, we integrated array-based sensing with nanoparticle surface engineering to screen and identify a candidate nanoparticle that not only induces CSC differentiation but also renders them more susceptible to drug treatment. The second part of the thesis demonstrates the power of array-based sensing in immunotherapies with the example of profiling different macrophage polarization states. I developed a novel sensor system that employs only two sensor elements to generate a high data density of five channels. Such high-content information enabled us to quantitatively discriminate among major macrophage polarization states as well as multiple less-characterized phenotypes in a matter of minutes. Overall, array-based sensing provides a simple and robust tool for cell phenotyping and holds promises for addressing challenging questions in biomedicine.

TABLE OF CONTENTS

Page

LIST OF TABLES

Table Page

LIST OF FIGURES

Figure Page

CHAPTER 1

INTRODUCTION

1.1 Biosensing: specificity v.s. selectivity

Sensing is a crucial process in our daily lives, monitoring our health and governing our safety. Nowadays, sensors are widely used in industry, medicine, and technologies to ensure a good quality of life. In order to build an efficient biosensor, two essential processes must occur: analyte recognition and signal transduction. Initially, the recognition element in the sensor needs to bind or interact with the target analyte. This could occur either through specific or selective interactions. Second, the recognition event between analyte and each receptor in the array needs to be transduced to a measurable outcome such as a colorimetric, fluorogenic, and electrochemical signal. Lastly, appropriate statistical methods need to be implemented to the collected data for analyte classification or identification.

Depending on the type of interactions that the sensor elements have with target analytes, two major types of sensing exist: specific and selective sensing. In the biological world, most sensing happens through specific interactions *via* a lock-and-key format. Specific sensors, as the name suggests, bind only to a single analyte regardless the presence of other components. The key criteria of an efficient specific sensor is the use of high affinity recognition element including antibodies,[1] lectins,[2] aptamers[3], and enzymes.[4] This approach has been successfully developed into many commercially available products such as pregnancy tests,[5] diabetic monitoring device[6] and so on. Perhaps, the most profound application of specific sensing is in the example of using biomarkers for disease diagnosis and treatment. Over the past few decades, a list of cell surface receptors with different

expression levels in cancer cells have been identified.[7,8,9] As a result, a range of cancer detection methods (e.g. electromagnetic imaging, [10] immunostaining, [11] and flow cytometry [12]) have been developed to sense the up- or down- regulation of these biomarkers. Furthermore, better understanding of how to design molecules that specifically bind to these biomarkers is crucial in developing efficient anticancer therapies. For instance, targeting ligands that have low binding affinity towards normal cells have been engineered and attached to drug delivery vehicles to guide the systems to site-specific cancer cells, while avoiding off-target toxicity.[13,14]

Specific sensing works the best the sensing environment is relatively simple with a minimum amount of cross-reactivity. However, most biological and physiological relevant samples are very complex, and the target analyte often co-exists with other molecules, making cross-reactivity in specific sensing unavoidable. Interestingly, the challenge of cross-reactivity in specific sensing presents the opportunity for selective sensing.

Selective sensing or array-based sensing works through an entirely different principle than specific sensing, where cross-reactivity is the key feature. Array-based sensors have a set of receptors that are engineered to be semi-specific/selective to target analytes so that they are flexible to interact with different analytes or different components of the analyte. Such interactions then generate a unique pattern containing comprehensive information for each analyte (Figure 1.1).[15] The cross-reactivity of the sensor receptors ensures that different aspects of the target analyte information can be extracted and used for classification and identification.[16] It is particularly powerful when the sensing samples are complex and dynamic such as proteins in biofluids,[17] bacteria,[18] and mammalian cells.[19] Since the responses produced from array-based sensors often have a high

dimension, an additional step of data processing through statistical methodologies is often needed.

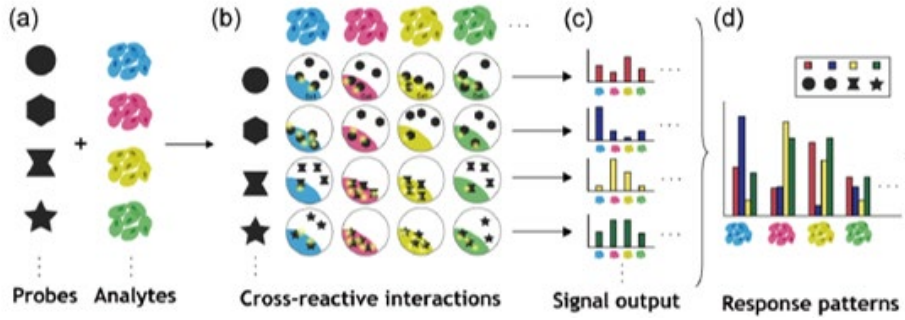

Figure 1.1. Schematic illustration of the working principle of array-based sensing. Adapted from reference 15. Copyright (2021) Japan Society for Analytical Chemistry.

1.2 Cell phenotyping using array-based sensors

1.2.1 Challenges of specific sensing in cell phenotyping

Cell phenotyping has become an important tool for understanding and treating cancers. Cell surface not only provides a physical barrier to the outside, but also reflects intracellular events. The components of the mammalian cell membrane have been found to exhibit different physicochemical properties among different cell types, as well as between healthy and disease cells.[20,21,22] Therefore, being able to monitor and detect cell surface changes in response to external stimuli will provide crucial information in disease diagnosis and drug discovery.

Commonly used methods in studying cell surfaces are mainly through biomarkers. While providing useful information, biomarker-based strategies face a set of challenges. First, this approach requires a specific hypothesis in which the analyte-target interactions are well-understood. However, such information might take years of research work. If the biomarker is not known or well-characterized, it is difficult to design sensors with targeted

specificity. Second, as cells progress from normal to disease state, changes in multiple biomarker expression levels would occur, requiring a large number of antibodies built in the specific sensing method to achieve accurate disease diagnosis.[23,24] In addition, many of the identified surface markers are shared between disease cells and normal cells at different expression levels, making off-target effect a challenging hurdle to overcome. Furthermore, cell phenotyping methods (e.g. flow cytometry, fluorescent imaging) usually involve multi-step processing of cells and specialized instrumentations, which are not only labor-intensive but also incompatible with high-throughput screening assays in drug development.

1.2.2 Opportunity of cell phenotyping using selective array-based sensors

The complex surface composition of intact living cells makes them excellent targets for array-based sensing. Array-based sensing is initially inspired by the mammalian olfactory system where a limited set of olfactory receptors can sense thousands of different odorants through cross-interactivity and pattern recognition.[25,26] Array-based sensing mimics such process by using synthetic materials including nanomaterials, polymers, and proteins. Unlike biomarker-based approach, array-based sensing utilizes a set of cross-reactive receptors to selectively interact with target analytes, producing a distinct pattern of response for each analyte (Figure 1.2). The strategy is ideal for cell phenotyping because changes in cellular responses yield variations in surface composition (e.g., protein, lipids, glycans, etc.) that result in different fingerprints. In this way, each cellular state can be rapidly assessed.[27,28,29]

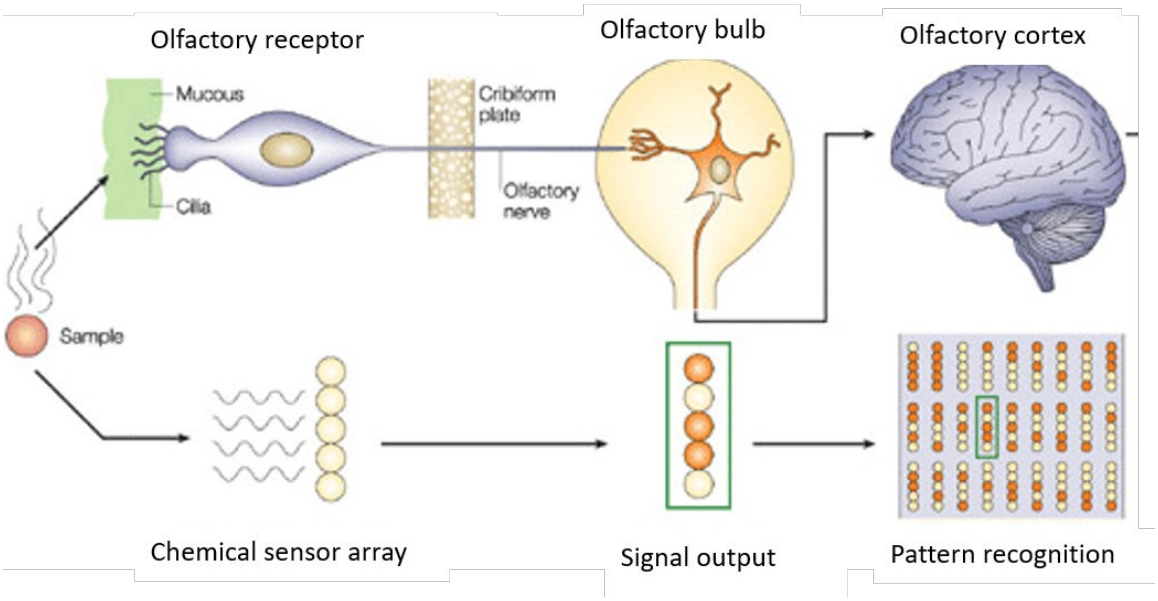

Figure 1.2. Schematic illustration of how array-based sensing mimics the human olfactory system. Adapted from reference 26.

Traditionally array-based sensing is widely used in non-biological samples such as explosives,[30] volatile-organic compounds,[31] metal ions,[32] and environmental toxins.[33] In the past few decades, however, there is an emerging trend of applying array-based sensing in complex biological analytes with the goal of advancing medicine. Much research work has looked to provide diagnostic information through cell surface profiles.[34] A wide range of sensor arrays have been reported to detect the differences between non-cancerous, cancerous, and metastatic cell lines. For instance, Tao and coworkers utilized dual-ligand functionalized gold nanoclusters to construct a sensor array and achieved separation of ten triple-negative breast cancer cell lines from multiple patients, with varying degrees of metastasis.[27] Recently, Kurita group designed a one-component sensor array using a dansyl-modified polylysine that not only differentiated eight types of human cell lines but could also differentiated the cell mixtures containing cells of different subtypes.[35]

1.3 Applying array-based sensing in phenotypically plastic cells: cancer stem cells

1.3.1 EMT and phenotypic plasticity of CSCs

Epithelial-mesenchymal transition (EMT) is a normal process that enables cells to carry out essential functions such as wound healing and embryogenesis.[36] During EMT, epithelial cells that are normally held together by tight cell-cell junctions gradually lose their assembly and become more spindle-like (Figure 1.3).[37] Such changes in morphology is orchestrated by EMT-inducing transcription factors (ZEB, SNAIL, and TWIST) which inhibit the expression of epithelial genes (e.g. E-cadherin, cytokeratin) and activate the expression of mesenchymal genes (e.g. N-cadherin, Fibronectin). The resulting mesenchymal cells can also revert to their epithelial state via mesenchymal-epithelial transition (MET).[38]

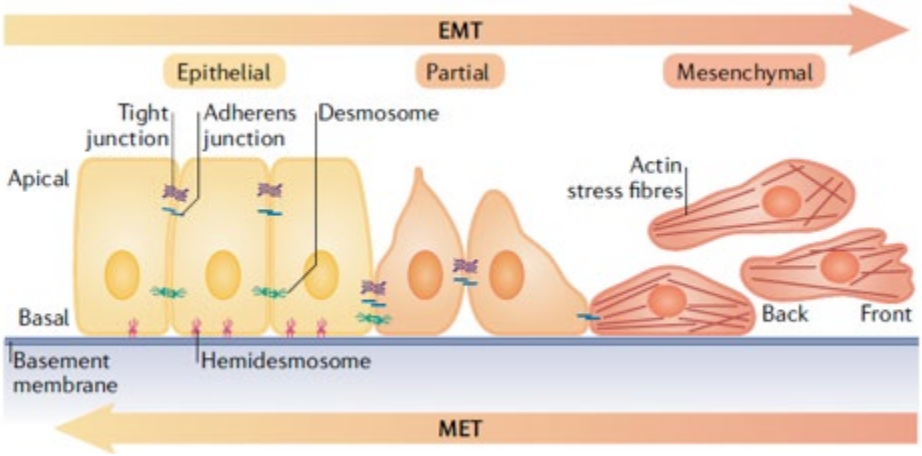

Figure 1.3. The process of epithelial-mesenchymal transition. Adapted from reference 37.

Activation of EMT in carcinoma cells can lead to a population of cells with stem cell-like properties. These cells, termed as cancer stem cells (CSCs), have the ability to self-renew and differentiate into multiple lineages of cells that comprise the tumor.[39] The plastic nature of CSCs is demonstrated in their ability to differentiate into non-CSCs and non-CSCs de-differentiate into CSCs. Interestingly, the interconversion between CSCs and

non-CSCs is not a two-state process, rather a spectrum of phenotypes can exist along the EMT spectrum. It is well documented that EMT activation can be induced by several signaling pathways including the transforming growth factor-β (TGFβ), WNT, and NOTCH pathways. Depending on the tumor type and the external stimuli received by cells, different EMT-transcription factors will be involved, resulting in multiple intermediate states.[40,41] In addition, a diverse line of research has shown that partial EMT can give rise to CSCs expressing both epithelial and mesenchymal traits.[42,43] As discussed earlier, most biomarker-based methods require a set of defined markers. The phenotypic plasticity of CSCs makes it challenging to target these intermediate states of CSCs.

1.3.2 Partial EMT and CSC heterogeneity

A consequence of EMT activation is the enrichment of mesenchymal cells with stem cell properties, termed as CSCs. Interestingly, CSCs are not homogeneous, rather subpopulations with distinct functions have been reported.[44,45] One contributor to CSC heterogeneity could be the degree of EMT activation. A common way of inducing EMT is by adding the growth factor TGF-β to cultured cells. In contrast to the shorter exposure time (a few days), which is routinely used by researchers, a recent study reveals that the prolonged exposure (weeks) to TGF-β stabilized cells in the mesenchymal state. The stabilized EMT gave rise to a larger $CD44^{+}CD24^{-}$ stem cell population than cells under a shorter-exposure since the resulting mesenchymal cells could not be reverted to the epithelial state when TGF-β was withdrawn.[46] This suggests that when CSCs were enriched using TGF-β, cells reside in a more mesenchymal state but have the ability to revert to the epithelial state. Therefore, the CSCs generated are likely a mixed mesenchymal and epithelial populations. The heterogeneity of CSC is further evident in

the findings that the enriched mesenchymal cell population can be further stratified into subtypes with distinct morphology, EMT-associated gene expression, self-renewal and tumor initiating abilities.[44,45] In addition, the reversibility of EMT program makes partial EMT a common phenomenon in both normal and carcinoma cells. Although partial EMT is important for cancer cells to gain motility during tumor invasion and dissemination,[47] it also contributes to the complex of CSC heterogeneity. Since it is rare for cells to stay in a locked end of the EMT spectrum, fully mesenchymal or fully epithelial, CSCs generated through EMT are likely to have an intermediate level of EMT activation with a mixed expression of epithelial and mesenchymal traits. [48]

1.3.3 EMT promotes stemness in CSCs.

Stemness, the ability of cells to self-renew and form mammospheres from a single cell, is a key characteristic of CSCs. Although a number of studies have shown that EMT promotes stemness in a range of different tumor types including breast, colon, lung, pancreatic, and ovary carcinomas[37], the detailed mechanisms remain unclear. Understanding the mechanism of how CSCs acquire stemness will offer insights on developing therapies targeting such property. Recent studies on several signaling pathways have revealed specific mechanisms of how EMT induces stemness. Specifically, Bmi1, an epigenetic regulator that is involved in chromosome silencing, has been shown to be at the regulating center of EMT-transcription factors (EMT-TF). In pancreatic cancer, research showed that EMT-TF Zeb 1 binds to the upstream promoter of miRNAs from the miR200 family to repress their expression. Consequentially, this repression resulted in the removal of Bmi1 inhibition, which enables Bmi1 to execute its function in maintaining stem cell function.[49,50] In addition to Zeb1, others have reported that another EMT-TF, Twist1,

directly upregulates Bmi1 expression by binding to the regulatory region of its promoter. The overexpression of Bmi1 induced EMT and resulted in an increase in tumor-initiating abilities in head and neck squamous cell carcinoma cells. Mechanistic studies using quantitative ChIP revealed that Bmi1 and Twsit1 participate in Bmi1-containing polycomb repressive complex to bind to the promoter regions of *E-cadherin* and *p16INK4a* (a cyclin-dependent kinase inhibitor associated with senescence)[51] and further inhibit their expression.[52] Collectively, these studies suggest that chromatin modification seems to be the main mechanism in which transcription factors (Snail,[53] Zeb1 and Twist 1) affect EMT. These mechanistic studies open the possibility of targeting epigenetic regulators as an alternative way of treating CSCs.

1.3.4 Differentiation therapy to combat CSCs

When EMT occurs in carcinoma cells rather than normal cells, tumor cells become more aggressive and acquire resistance to chemotherapies and radiotherapies. Therefore, direct elimination of CSCs is challenging. Based on the observation of CSC plasticity, forcing CSCs to differentiation should diminish the frequency of CSCs, rendering tumors less aggressive and more responsive to conventional therapy. This strategy is known as differentiation therapy. Supported by the successful example of all-trans retinoid acid in treating acute promyelocytic leukemia,[54] differentiation therapy presents an effective treatment to overcome drug resistance in cancer.

There has been a widespread interest in identifying molecules that selectively target CSCs or promote their differentiation. Recently, many high-throughput screenings have reported promising small molecules that target specific signaling pathways involved in cell differentiation. In 2016, Fang *et al.* screened a library of 16,000 synthetic compounds and

identified LF3 as an efficient inhibitor that disrupts the interaction between β-catenin and the transcription factor T-cell factor 4. Since the Wnt/ β-catenin pathway is deregulated in CSCs, such disruption resulted in overexpression of Wnt target genes.[55] Another screen conducted in 2009 revealed Salinomycin as a potent molecule that selectively targets breast cancer stem cells.[56] In addition to small molecules, microRNA interference[57] and epigenetic modifications[58]have also demonstrated their ability to act on CSCs and induce differentiation.

Despite the progress in identifying novel differentiation therapeutics, the discovery process is slow and inefficient. Among thousands of screened compounds, only a few of them showed promising activities.[59,60] The inefficiency in these screenings is likely due to the hypothesis-driven design. Only well-understood molecular pathways are being used to design the screening assays. However, the detailed biological mechanisms in cancer stem cell biology remain to be elucidated.[61] More significantly, hypothesis-driven strategies limit detection to a pre-defined phenotype, potentially failing to detect other differentiated phenotypes.

Based on the limitations in current knowledge of CSC biology, it is less ideal to employ the specific target interaction approach to identify CSC differentiation inducers. Instead, the array-based sensing approach described in this dissertation does not require any prior-knowledge of target analytes. The signature generated from the sensor can be used to rapidly screen compounds that induce CSCs to a phenotypic state that is more susceptible for conventional treatment. In the following chapters, I will describe how we used array-based sensors as a high-throughput and high-content screening tool to identify

molecules that promoted the differentiation of CSCs. It is our hope that differentiation therapy will bring promises to combat cancer.

1.4 Array-based sensing in high-content screening and drug discovery

A very different application of array-based cell sensing from diagnostics is to monitor the response of cells when exposed to an environmental stimulus such as a drug. High-throughput screening (HTS) and high-content screening (HCS) using cell-based assays are increasingly integrated in various aspects of the drug discovery pipeline.[62,63] HCS aims to measure multiparameter change of cells caused by screening compounds. It is highly utilized in the phenotypic drug discovery approach to identify potential drug hits. Unlike target-based approach, it first subjects cells to a library of screening compounds and uses phenotypic assays to help identify lead compounds that induce cells to a disease state (Figure 1.4).[64] Imaging-based HCS is a powerful tool in evaluating cell status by collecting multiple cell features such as transcriptional,[65] genomic,[66] proteomic, [67] and metabolomic[68] information. However, many of the cell-based assays in HCS are limited by multi-step processing of cells prior to analyses (e.g. staining, fixing and imaging), and an incomplete understanding of biomolecular pathways for correlating drug and response.[66,69] In addition, because most HCS assays require microscopic instrumentation and extensive imaging data extraction, they usually have a low throughput.

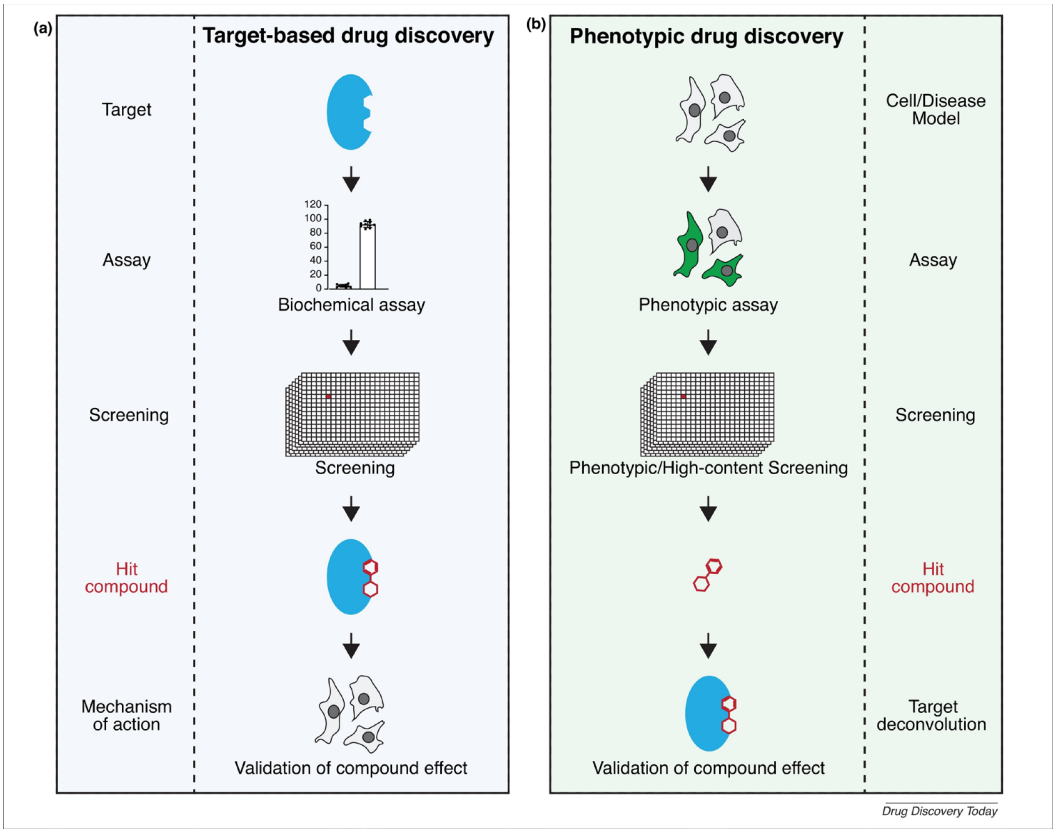

Figure 1.4. Target-based versus phenotypic drug discovery approach. Adapted from reference 54.

The goal of phenotypic-based HCS is to create a unique fingerprint of cell states and use it as a reference. As discussed in section 1.2, array-based sensing works through selective interactions between the sensor elements and cell surface functionalities to generate a signature for each cell state. Under external stimuli, such as drug candidates, any changes on the cell surface (glycoproteins, lipids, proteins etc.) could interact with the sensor array generating a detectable signal, which makes this method hypothesis-free and non-bias. By comparing the signature of cells under treatment with that of untreated cells, one can quickly distinguish if the screened compounds have any significant impacts and would be interesting targets for downstream evaluations. The hypothesis-free feature enables such sensing strategy to be particularly powerful in distinguishing subtle changes

in complex bioanalytes (e.g. cells), rather than identifying specific elements within them. To demonstrate the utility of array-based sensors HCS, Rana *et. al.* developed a gold nanoparticle-fluorescent protein sensor array and applied it to cells exposed to one of fifteen different anti-cancer drugs featuring seven different drug mechanisms. The sensing results showed distinct patterns for each treated cell line, which could be further clustered into the hypothesized drug mechanism, and novel drugging routes were also elucidated.[70]

Another advantage of utilizing array-based sensing in HCS is that the synthetic design space allows one to quickly obtain a high-content information of the target analyte. It is possible to engineer multiple different recognition elements so that different types of cell functionalities can interact with the sensor.[71] In addition, more output channels can be obtained by modifying the sensor design. For instance, using host-guest interaction between benzylammonium-functionalized nanoparticle and cucurbit[7]uril moiety, Ngoc *et. al.* doubled the output channels from three to six. The increased amount of information gathered from the sensor array allowed successful discrimination of cells by their tumorigenicity.[72]

1.5 Dissertation overview

In this dissertation, I investigate different ways that array-based sensing can be applied in drug discovery with a particular focus on cancer stem cell therapy and immunotherapy. In Chapter 2, I describe a turn-on sensing system composed of gold nanoparticles and three different fluorescent proteins through supramolecular interactions. Using this sensor array, we were able to rapidly profile phenotypically distinct CSC states and monitor their fate as CSC differentiate. This sensor platform provides a tool in screening applications for better therapeutic design. Next, we combined array-based

sensing strategy with nanoparticle surface engineering to screen a library of nanoparticles with varying degrees of hydrophobicity (Chapter 3). This is a proof of principle that array-based sensing can be adapted in high-content screenings to facilitate the drug discovery process. Through the screen, one nanoparticle was identified as a potential drug candidate that not only promoted CSCs to differentiate but also sensitized cells for therapeutic treatment. Further mechanistic studies suggested that such differentiation was induced by altering the splicing variant of α6 integrin subunit through up-regulation of reactive oxygen species in CSCs. In the last part of the thesis, we expanded and applied array-based sensing to a different class of cell analytes, immune cells. Specifically, we developed a novel sensor platform that gives out high-content information regarding macrophage polarization states. By successfully discriminating among different subtypes of M1 and M2 states, we not only validated the potentials of array-based sensing in immunotherapy but also the generalization of this approach to other phenotypically plastic cells.

1.6 References

1. S. Sharma, H. Byrne, R. J. O'Kennedy, *Essays Biochem.* **2016**, *60*, 9–18.

2. M. L. S. Silva, *Cancer Lett.* **2018**, *436*, 63–74.

3. H. M. Meng, H. Liu, H. Kuai, R. Peng, L. Mo, X. B. Zhang, *Chem. Soc. Rev.* **2016**, *45*, 2583–2602.

4. El Harrad, I. Bourais, H. Mohammadi, A. Amine, *Sensors* **2018**, *18*, 164.

5. L. Wide, C. A. Gemzell, *Acta Endocrinol. (Copenh).* **1960**, *35*, 261−267.

6. A. Heller, B. Feldman, *Chem. Rev.* **2008**, *108*, 2482–2505.

7. A. Turdo, V. Veschi, M. Gaggianesi, A. Chinnici, P. Bianca, M. Todaro, G. Stassi, *Front. Cell Dev. Biol.* **2019**, *7*, 16.

8. W. T. Kim, C. J. Ryu, *BMB Rep.* **2017**, *50*, 285–298.

9. T. S. Gerashchenko, N. M. Novikov, N. V. Krakhmal, S. Y. Zolotaryova, M. V. Zavyalova, N. V. Cherdyntseva, E. V. Denisov, V. M. Perelmuter, *J. Clin. Med.* **2019**, *8*, 1092.

10. A. M. Hassan, M. El-Shenawee, *IEEE Rev. Biomed. Eng.* **2011**, *4*, 103–118.

11. R. Buttner, J. R. Gosney, B. G. Skov, J. Adam, N. Motoi, K. J. Bloom, M. Dietel, J. W. Longshore, F. Lopez-Ríos, F. Penault-Llorca, et al., *J. Clin. Oncol.* **2017**, *35*, 3867–3876.

12. M. Doan, I. Vorobjev, P. Rees, A. Filby, O. Wolkenhauer, A. E. Goldfeld, J. Lieberman, N. Barteneva, A. E. Carpenter, H. Hennig, *Trends Biotechnol.* **2018**, *36*, 649–652.

13. A. Rahikkala, S. A. P. Pereira, P. Figueiredo, M. L. C. Passos, A. R. T. S. Araújo, M. L. M. F. S. Saraiva, H. A. Santos, *Adv. Biosyst.* **2018**, *2*, 1800020.

14. M. Srinivasarao, P. S. Low, *Chem. Rev.* **2017**, *117*, 12133–12164.

15. H. Sugai, S. Tomita, R. Kurita, *Anal. Sci.* **2020**, *36*, 923–934.

16. W. J. Peveler, M. Yazdani, V. M. Rotello, *ACS Sensors* **2016**, *1*, 1282–1285.

17. Z. Pode, R. Peri-Naor, J. M. Georgeson, T. Ilani, V. Kiss, T. Unger, B. Markus, H. M. Barr, L. Motiei, D. Margulies, *Nat. Nanotechnol.* **2017**, *12*, 1161–1168.

18. X. Li, H. Kong, R. Mout, K. Saha, D. F. Moyano, S. M. Robinson, S. Rana, X. Zhang, M. A. Riley, V. M. Rotello, *ACS Nano* **2014**, *8*, 12014–12019.

19. H. Bai, Z. Liu, T. Zhang, J. Du, C. Zhou, W. He, J. H. C. Chau, R. T. K. Kwok, J. W. Y. Lam, B. Z. Tang, *ACS Nano* **2020**, *14*, 7552–7563.

20. K. Ohtsubo, J. D. Marth, *Cell* **2006**, *126*, 855–867.

21. M. D. Mager, V. Lapointe, M. M. Stevens, *Nat. Chem.* **2011**, *3*, 582–589.

22. M. Hu, Y. Lan, A. Lu, X. Ma, L. Zhang, in *Prog. Mol. Biol. Transl. Sci.* **2019**, *162*, 1–24.

23. C. Ragulan, K. Eason, E. Fontana, G. Nyamundanda, N. Tarazona, Y. Patil, P. Poudel, R. T. Lawlor, M. Del Rio, S. L. Koo, et al., *Sci. Rep.* **2019**, *9*, 1–12.

24. K. L. M. Boylan, K. Geschwind, J. S. Koopmeiners, M. A. Geller, T. K. Starr, A. P. N. Skubitz, *Clin. Proteomics* **2017**, *14*, 34.

25. S. Katada, T. Hirokawa, Y. Oka, M. Suwa, K. Touhara, *J. Neurosci.* **2005**, *25*, 1806–1815.
26. A. P. F. Turner, N. Magan, *Nat. Rev. Microbiol.* **2004**, *2*, 160–166.

27. Y. Tao, M. Li, D. T. Auguste, *Biomaterials* **2017**, *116*, 21–33.

28. S. Rana, N. D. B. Le, R. Mout, B. Duncan, S. G. Elci, K. Saha, V. M. Rotello, *ACS Cent. Sci.* **2015**, *1*, 191–197.

29. Y. Geng, W. J. Peveler, V. M. Rotello, *Angew. Chem. Int. Ed.* **2019**, *58*, 5190–5200.

30. M. Jurcic, W. J. Peveler, C. N. Savory, D. K. Bučar, A. J. Kenyon, D. O. Scanlon, I. P. Parkin, *ACS Appl. Mater. Interfaces* **2019**, *11*, 11618–11628.

31. S. H. Lim, L. Feng, J. W. Kemling, C. J. Musto, K. S. Suslick, *Nat. Chem.* **2009**, *1*, 562–567.

32. Z. Wang, C. Xu, Y. Lu, X. Chen, H. Yuan, G. Wei, G. Ye, J. Chen, *Sensors Actuators, B Chem.* **2017**, *241*, 1324–1330.

33. J. Han, M. Bender, S. Hahn, K. Seehafer, U. H. F. Bunz, *Chem. - A Eur. J.* **2016**, *22*, 3230–3233.

34. N. D. B. Le, M. Yazdani, V. M. Rotello, *Nanomedicine* **2014**, *9*, 1487–1498.

35. H. Sugai, S. Tomita, S. Ishihara, R. Kurita, *ACS Sensors* **2019**, *4*, 827–831.

36. S. A. Mani, W. Guo, M.-J. Liao, E. N. Eaton, A. Ayyanan, A. Y. Zhou, M. Brooks, F. Reinhard, C. C. Zhang, M. Shipitsin, et al., *Cell* **2008**, *133*, 704–715.

37. A. Dongre, R. A. Weinberg, *Nat. Rev. Mol. Cell Biol.* **2019**, *20*, 69–84.

38. K. Polyak, R. A. Weinberg, *Nat. Rev. Cancer* **2009**, *9*, 265–273.

39. M. F. Clarke, J. E. Dick, P. B. Dirks, C. J. Eaves, C. H. M. Jamieson, D. L. Jones, J. Visvader, I. L. Weissman, G. M. Wahl, in *Cancer Res.*, Cancer Res, **2006**, pp. 9339–9344.

40. C. L. Chaffer, B. P. San Juan, E. Lim, R. A. Weinberg, *Cancer Metastasis Rev.* **2016**, *35*, 645–654.

41. M. H. Yang, D. S. S. Hsu, H. W. Wang, H. J. Wang, H. Y. Lan, W. H. Yang, C. H. Huang, S. Y. Kao, C. H. Tzeng, S. K. Tai, et al., *Nat. Cell Biol.* **2010**, *12*, 982–992.

42. F. Andriani, G. Bertolini, F. Facchinetti, E. Baldoli, M. Moro, P. Casalini, R. Caserini, M. Milione, G. Leone, G. Pelosi, et al., *Mol. Oncol.* **2016**, *10*, 253–271.

43. M. K. Jolly, S. C. Tripathi, D. Jia, S. M. Mooney, M. Celiktas, S. M. Hanash, S. A. Mani, K. J. Pienta, E. Ben-Jacob, H. Levine, *Oncotarget* **2016**, *7*, 27067–27084.

44. H. L. Goel, T. Gritsko, B. Pursell, C. Chang, L. D. Shultz, D. L. Greiner, J. H. Norum, R. Toftgard, L. M. Shaw, A. M. Mercurio, *Cell Rep.* **2014**, *7*, 747–761.

45. B. Bierie, S. E. Pierce, C. Kroeger, D. G. Stover, D. R. Pattabiraman, P. Thiru, J. L. Donaher, F. Reinhardt, C. L. Chaffer, Z. Keckesova, et al., *Proc. Natl. Acad. Sci. U. S. A.* **2017**, *114*, E2337–E2346.

46. Y. Katsuno, D. S. Meyer, Z. Zhang, K. M. Shokat, R. J. Akhurst, K. Miyazono, R. Derynck, *Sci. Signal.* **2019**, *12*, DOI 10.1126/scisignal.aau8544.

47. M. A. Nieto, R. Y.-J. Huang, R. A. Jackson, J. P. Thiery, *Cell* **2016**, *166*, 21–45.

48. R. Derynck, R. A. Weinberg, *Dev. Cell* **2019**, *49*, 313–316.

49. U. Wellner, J. Schubert, U. C. Burk, O. Schmalhofer, F. Zhu, A. Sonntag, B. Waldvogel, C. Vannier, D. Darling, A. Zur Hausen, et al., *Nat. Cell Biol.* **2009**, *11*, 1487–1495.

50. Y. Shimono, M. Zabala, R. W. Cho, N. Lobo, P. Dalerba, D. Qian, M. Diehn, H. Liu, S. P. Panula, E. Chiao, et al., *Cell* **2009**, *138*, 592–603.

51. J. Y. Liu, G. P. Souroullas, B. O. Diekman, J. Krishnamurthy, B. M. Hall, J. A. Sorrentino, J. S. Parker, G. A. Sessions, A. V. Gudkov, N. E. Sharpless, *Proc. Natl. Acad. Sci. U. S. A.* **2019**, *116*, 2603–2611.

52. M. H. Yang, D. S. S. Hsu, H. W. Wang, H. J. Wang, H. Y. Lan, W. H. Yang, C. H. Huang, S. Y. Kao, C. H. Tzeng, S. K. Tai, et al., *Nat. Cell Biol.* **2010**, *12*, 982–992.

53. Z. Hou, H. Peng, K. Ayyanathan, K.-P. Yan, E. M. Langer, G. D. Longmore, F. J. Rauscher, *Mol. Cell. Biol.* **2008**, *28*, 3198–3207.

54. H. de Thé, *Nat. Rev. Cancer* **2018**, *18*, 117-127

55. L. Fang, Q. Zhu, M. Neuenschwander, E. Specker, A. Wulf-Goldenberg, W. I. Weis, J. P. Von Kries, W. Birchmeier, *Cancer Res.* **2016**, *76*, 891–901.

56. P. B. Gupta, T. T. Onder, G. Jiang, K. Tao, C. Kuperwasser, R. A. Weinberg, E. S. Lander, *Cell* **2009**, *138*, 645–659.

57. A. Petrelli, R. Carollo, M. Cargnelutti, F. Iovino, M. Callari, D. Cimino, M. Todaro, L. R. Mangiapane, A. Giammona, A. Cordova, et al., *Oncotarget* **2015**, *6*, 2315–30.

58. M. T. Chiao, W. Y. Cheng, Y. C. Yang, C. C. Shen, J. L. Ko, *Autophagy* **2013**, *9*, 1509-1526.

59. K. H. Emami, C. Nguyen, H. Ma, D. H. Kim, K. W. Jeong, M. Eguchi, R. T. Moon, J-L Teo, S. W. Oh, H. Y. Kim, S. H. Moon, J. R. Ha, M. Kahn, *Proc. Natl. Acad. Sci. U. S. A.* **2004**, *101*, 12682-12687.

60. S. Chung, H. Suzuki, T. Miyamoto, N. Takamatsu, A. Tatsuguchi, K. Ueda, K. Kijima, Y. Nakamura, Y. Matsuo, *Oncotarget* **2012**, *3*, 1629-1640.

61. C. Maucort, A. Di Giorgio, S. Azoulay, M. Duca, *ChemMedChem* **2021**, *16*, 14–29.

62. M. C. Fishman, J. A. Porter, *Nature* **2005**, *437*, 491–493.

63. F. Zanella, J. B. Lorens, W. Link, *Trends Biotechnol.* **2010**, *28*, 237–245.

64. S. Lin, K. Schorpp, I. Rothenaigner, K. Hadian, *Drug Discov. Today* **2020**, *25*, 1348–1361.

65. R. A. Butcher, S. L. Schreiber, *Curr. Opin. Chem. Biol.* **2005**, *9*, 25–30.

66. H. Jiang, J. R. Pritchard, R. T. Williams, D. A. Lauffenburger, M. T. Hemann, *Nat. Chem. Biol.* **2011**, *7*, 92–100.

67. M. Schirle, M. Bantscheff, B. Kuster, *Chem. Biol.* **2012**, *19*, 72–84.

68. J. K. Nicholson, J. Connelly, J. C. Lindon, E. Holmes, *Nat. Rev. Drug Discov.* **2002**, *1*, 153–161.
69. P. J. O'Brien, *Basic Clin. Pharmacol. Toxicol.* **2014**, *115*, 4–17

70. S. Rana, N. D. B. Le, R. Mout, K. Saha, G. Y. Tonga, R. E. S. Bain, O. R. Miranda, C. M. Rotello, V. M. Rotello, *Nat. Nanotechnol.* **2015**, *10*, 65–69.

71. S. Ngernpimai, Y. Geng, J. M. Makabenta, R. F. Landis, P. Keshri, A. Gupta, C. H. Li, A. Chompoosor, V. M. Rotello, *ACS Appl. Mater. Interfaces* **2019**, *11*, 11202–11208.

72. N. D. B. Le, G. Yesilbag Tonga, R. Mout, S. T. Kim, M. E. Wille, S. Rana, K. A. Dunphy, D. J. Jerry, M. Yazdani, R. Ramanathan, et al., *J. Am. Chem. Soc.* **2017**, *139*, 8008–8012.

CHAPTER 2

RAPID PHENOTYPING OF CANCER STEM CELLS USING MULTICHANNEL NANOSENSOR ARRAYS

2.1 Abstract

Cancer stem cells (CSCs) contribute to multidrug resistance, tumor recurrence and metastasis, making them prime therapeutic targets. Their ability to differentiate and lose stem cell properties makes them challenging to study. Currently, there is no simple assay that can capture and trace the dynamic phenotypic changes on the CSC surface. Here, we report rapid discrimination of breast CSCs from non-CSCs using a nanoparticle-fluorescent-protein based sensor. This nanosensor was employed to discriminate CSCs from non-CSCs, as well as CSCs that had differentiated *in vitro* in two breast cancer models. Importantly, the sensor platform could also discriminate CSCs from the bulk population of cells in patient-derived xenografts of human breast cancer. Taken together, the results obtained demonstrate the feasibility of using the nanosensor to phenotype CSCs and monitor their fate. Furthermore, this approach provides a novel area for therapeutic interventions against these challenging targets.

2.2 Introduction

The complex geno- and phenotypic heterogeneity of tumors is reflected in the observation that tumor cells within a given cancer differ in their morphology, proliferative capacity, sensitivity to therapeutic agents and metastatic potential. Although quantitative analysis of phenotypic markers is an essential tool for drug discovery,[1] it can be challenging because of tumor heterogeneity. One of the most telling aspects of such nature is that only

a subset of cells within a tumor are capable of initiating a new primary tumor or metastasis.[2] These cells are referred to as cancer stem cells (CSCs). They have the ability to self-renew and differentiate into multiple lineages, metastasizing and populating new tumors.[3] CSCs are highly resistant to standard chemotherapeutic strategies and are considered prime drivers of tumor recurrence and metastasis, making them important therapeutic targets.[4,5]

CSCs present in solid tumors are often de-differentiated and exhibit properties of an epithelial-to-mesenchymal transition (EMT).[6,7] In fact, EMT can enrich a CSC population, a process associated with cancer progression and metastasis.[8,9] CSCs are also inherently plastic and they can differentiate i.e., undergo a mesenchymal-epithelial transition (MET), in response to stimuli from the microenvironment and other factors.[10,11] This process results in loss of stem cell properties, which make them even more difficult to detect and monitor. Interestingly, however, the EMT and MET may not be all-or-none responses, but rather multi-stage and reversible processes involving intermediate states.[12,13] During each transition state, both genomic and phenotypic changes can occur, with concomitant alterations in their behavior and response to drugs.[14] This complexity of CSC phenotypes even within the same cancer creates a challenge when profiling CSCs from individual tumors.

Current methods of phenotyping cells are mainly through fluorescent imaging and flow cytometry.[15,16] While providing useful information, these methods are limited in a few aspects: expensive instrumentation, specific antibodies, and burdensome data collection and analysis. Moreover, current strategies rely heavily on cell surface markers.[17,18,-19] Such biomarker-based approaches, however, are hindered by ambiguity and end-point evaluation. For instance, CD133 was thought to be a suitable marker for

colon CSCs, but alternative sensing modalities show this biomarker to be unreliable.[20,21] In addition, evidence has shown that a partial EMT gives rise to hybrid cells expressing both epithelial and mesenchymal markers.[13,22] Since end-point biomarker evaluation only targets one phenotype, using this approach is likely to miss any intermediate states. Thus, there is an urgent need for a simple and general method to phenotype and trace the dynamic changes that occur within populations of CSCs.

Nanotechnology in combination with natural science has emerged to become a powerful tool for investigating challenging biological questions.[23,24] Inspired by the human olfactory system, chemical nose sensing was developed as a hypothesis-free, signature-based tool to identify complex bioanalytes.[25,26,-27] Gold nanoparticles (AuNPs) with tunable surface functionality and strong quenching ability[28] are ideal for constructing nanosensors. Nanoparticle-based sensor arrays can be engineered to selectively interact with a target analyte, generating a unique response signature. Since no specific recognition is involved in the process, extensive pre-knowledge of analytes is not required, making it a hypothesis-free approach. Once trained, nanosensors can quickly identify target analytes through pattern recognition and results can be obtained within minutes. Successful implementation has been shown in a wide range of biomolecules including proteins,[29] bacteria,[30] and mammalian cells.[25]

In this paper, we employ an array-based strategy to profile CSCs and monitor their phenotypic alterations (Figure 2.1). The nanosensor used here is composed of a functionalized gold nanoparticle (AuNP) and three fluorescent proteins (FP) of which the fluorescence is initially quenched by AuNP but restored upon addition of cells. We tested our sensor against CSC models created both *in vitro* and *in vivo*, demonstrating a feasible

approach to detect differentiation and other phenotypic changes for both screening applications and personalized diagnostics.

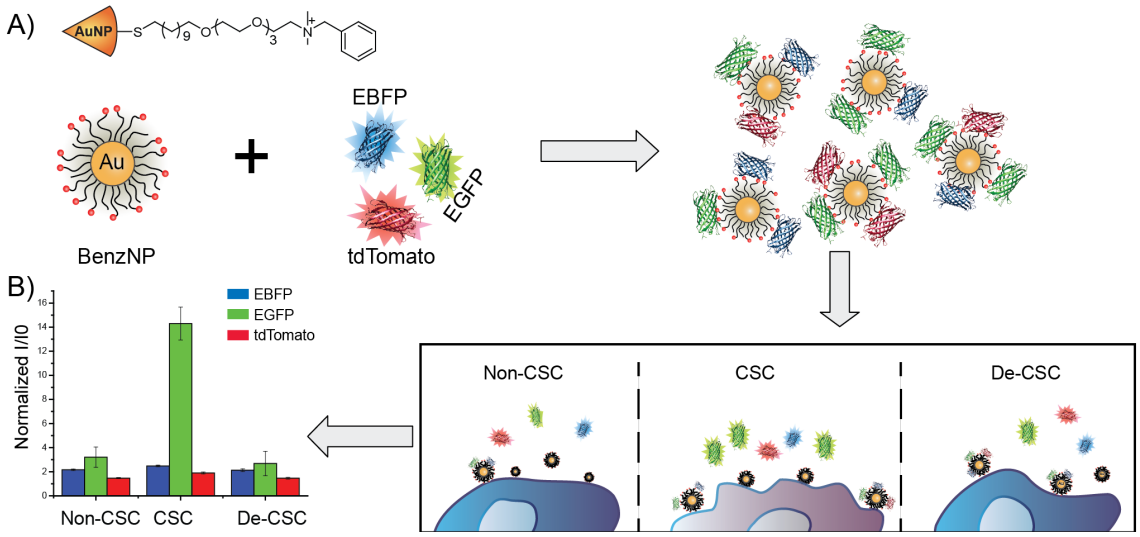

Figure 2.1. Schematic illustration of signature-based sensing of CSCs. (A) Equimolar amount of three fluorescent proteins are incubated with Benzyl-AuNP forming BenzNP-FP complexes. (B) Upon the additional of cells, fluorescent proteins are displaced and turned on by cell surface. Populations of CSCs, non-CSCs and CSCs that have differentiated and lost stem cell properties (de-CSCs) interact differentially with sensor elements, resulting in unique fluorescent patterns.

2.3 Results

2.3.1 Complexation of nanosensor. The sensor array used here is composed of a benzyl headgroup-terminated AuNP (BenzNP) and three types of fluorescent proteins (EGFP, EBFP, and tdTomato) as shown in Figure 2.1A. The cationic BenzNP binds strongly with anionic fluorescent proteins, resulting in fluorescence quenching. Upon incubation with cells, cell surface functionalities compete with fluorescent proteins for AuNP binding. The released fluorescent proteins can then freely emit light, simultaneously giving out three-channel information in one well from the microplate. We hypothesized that CSCs and non-CSCs would interact differently with the BenzNP-FP supramolecular

complexes, resulting in the generation of unique fluorescence patterns that could be used to profile CSC states (Figure 2.1B).

2.3.2 Sensing of established CSC model. We first used a system that involves Src-transformation of mammary epithelial (MCF10A) cells to test our hypothesis. Upon transformation, the frequency of CSCs ($CD44^{high}/CD24^{low}$) increases significantly.[31] Interestingly, though, this $CD44^{high}/CD24^{low}$ population is comprised of two distinct populations that differ in their differentiation status and stem cell properties.[32] The epithelial population (EPTH) is comprised of differentiated cells and lacks stem cell properties. The mesenchymal population (MES) is comprised of de-differentiated cells and exhibits stem cell properties (self-renewal, expression of stem cell genes, mammosphere formation and tumor initiation). The two subpopulations were isolated using previously reported procedures[32] and seeded at a density of 10^4 cells/well in a 96-well microplate for 24 hours. Subsequently, an equimolar amount of BenzNP and three FPs were mixed at room temperature to form the nanosensor. Cells were washed once with phosphate buffered saline (PBS) and incubated with the nanosensor for 30 minutes before fluorescent measurement. The changes in fluorescence responses were statistically analyzed using linear discriminate analysis (LDA).

As shown in Figure 2.2, the MES population that harbors CSC properties was completely discriminated from the EPTH population that lacks CSC properties with 100% correct classification (two shaded ellipses). An important issue is whether our nanosensor could detect CSCs in a heterogeneous population of cells. To address this question, MES and EPTH cells, which had been cultured either separately or as a mixture, were incubated with the nanosensor. We found that the nanosensor could discriminate the relative

proportion of CSCs with a high level of confidence (Figure 2.2). Significantly, the sensor detected a corresponding trend across all the heterogeneous populations. Cross-validation among 0%, 50% and 100% CSC groups showed 100% correct classification. Blinded cell mixture samples were tested for unknown identification among the three groups. 96% accurate unknown identification was achieved with only one case of 0% CSC misclassified as 50% CSC. To further evaluate the importance of each FP channel in our sensor, identification of unknowns using individual FP were carried out. As shown in Figure 2.3, each channel contributes to the identification to certain extent. However, when combined all together, it reaches the highest identification accuracy.

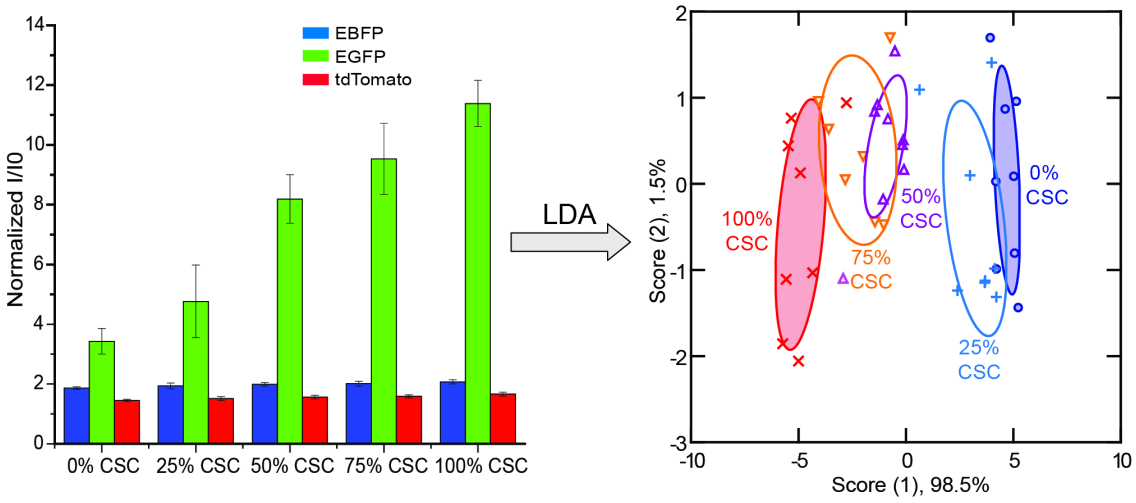

Figure 2.2. Discrimination of CSCs from the MCF-10A ER-Src system using BenzNP-FP nanosensor. Normalized fluorescent intensities against sensor only (I/I0) were obtained with nanosensor against different ratios of the MES (harboring CSCs) and EPTH subpopulations isolated from MCF-10A Src-transformed cells. Canonical scores for the first two factors of fluorescence patterns were generated and plotted through Linear Discriminant Analysis (LDA) with 95% confidence ellipses (n = 8).

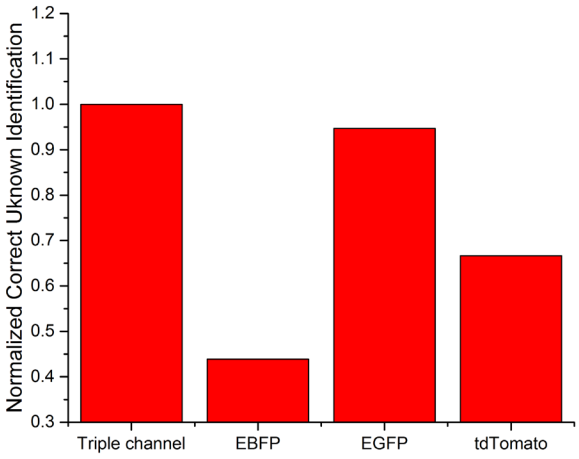

Figure 2.3. Correct unknown identification (CUI) of blinded cell mixture samples from the MCF-10A ER-Src system using either three FP or individual FP channel. Mixtures were in 0, 20, 50, 75 or 100% CSC. CUI was normalized to the percentage from the triple channel, which provides the highest identification accuracy.

2.3.3 Development of a phenotypic plastic CSC model. Although the MCF-10A ER-Src system provides a way to enrich CSCs, it does not reflect their dynamic plasticity. For this reason, we developed a second model system to monitor the CSC plasticity using a diploid, non-tumorigenic cell line (S1 cells).[33] These cells are highly differentiated and polarized. Expression of the Hippo transducer TAZ in these cells induced transformation, an EMT and the acquisition of stem cell properties (Figure 2.4A-C), consistent with previous findings.[34,35] A consequence of TAZ transformation and the EMT was loss of the integrin α6β4, and this loss had a causal role in the genesis of CSCs. Re-expression of this integrin in TAZ-transformed cells reversed the EMT and resulted in loss of stem cell properties (Figure 2.4A-C). We termed these cells de-CSCs. The identity of non-CSCs, CSCs, and de-CSCs was further verified by morphology, relative expression of epithelial and mesenchymal markers, as well as self-renewal ability (Figure 2.4A-D).

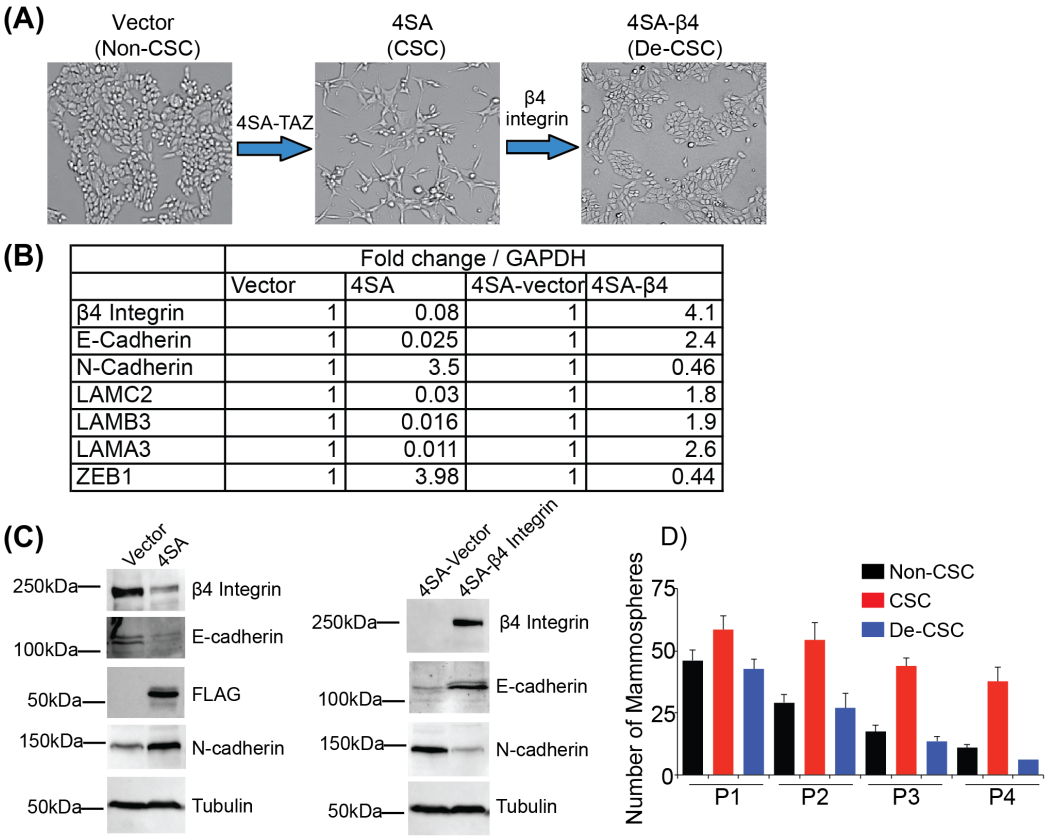

	Fold change / GAPDH			
	Vector	4SA	4SA-vector	4SA-β4
β4 Integrin	1	0.08	1	4.1
E-Cadherin	1	0.025	1	2.4
N-Cadherin	1	3.5	1	0.46
LAMC2	1	0.03	1	1.8
LAMB3	1	0.016	1	1.9
LAMA3	1	0.011	1	2.6
ZEB1	1	3.98	1	0.44

Figure 2.4. Workflow of generating reversible S1 model. Expression of active TAZ (4SA-TAZ) in S1 epithelial cells generated an EMT and CSCs. CSCs were induced to differentiate and lose stemness by overexpressing β4 integrin. (A) The morphology of each population generated was shown. (B) The expression of key EMT and epithelial genes was quantified by qPCR. Fold changes in mRNA level were shown in the table. (C) Immunoblots of the S1 system showing the change in epithelial (β4 integrin and E-cadherin) and mesenchymal (N-cadherin) proteins. Tubulin loading control was shown in each blot. (D) Cell self-renewal ability of each population was evaluated by serial passage of mammosphere formation assay.

2.3.4 Detection of phenotypical changes on CSCs. After establishing the S1 system, each of these populations was incubated with the sensor for 30 minutes, fluorescent patterns were obtained and analyzed. Consistent discrimination between the CSC and non-CSC groups was observed (Figure 2.5A). In addition, de-CSCs clustered closely and overlapped with non-CSCs on the LDA plot, which could be due to the fact that both groups lack stem cell phenotypes and share a similar morphology (Figure 2.4A). The nanosensor

was also able to detect different percentages of CSCs in the heterogeneous populations (Figure 2.5B). Cross-validation among 0%, 50% and 100% CSC mixtures showed 100% accurate classification. Complete correct unknown identification of the blinded cell mixtures was also achieved. To evaluate the performance of the LDA algorithm used, we employed the receiver operating characteristic (ROC) analysis on the S1 data set. As shown in Figure 2.5C, ROC results showed an area under the curve of 1.0, indicating a complete separation between CSC and non/de-CSC population.

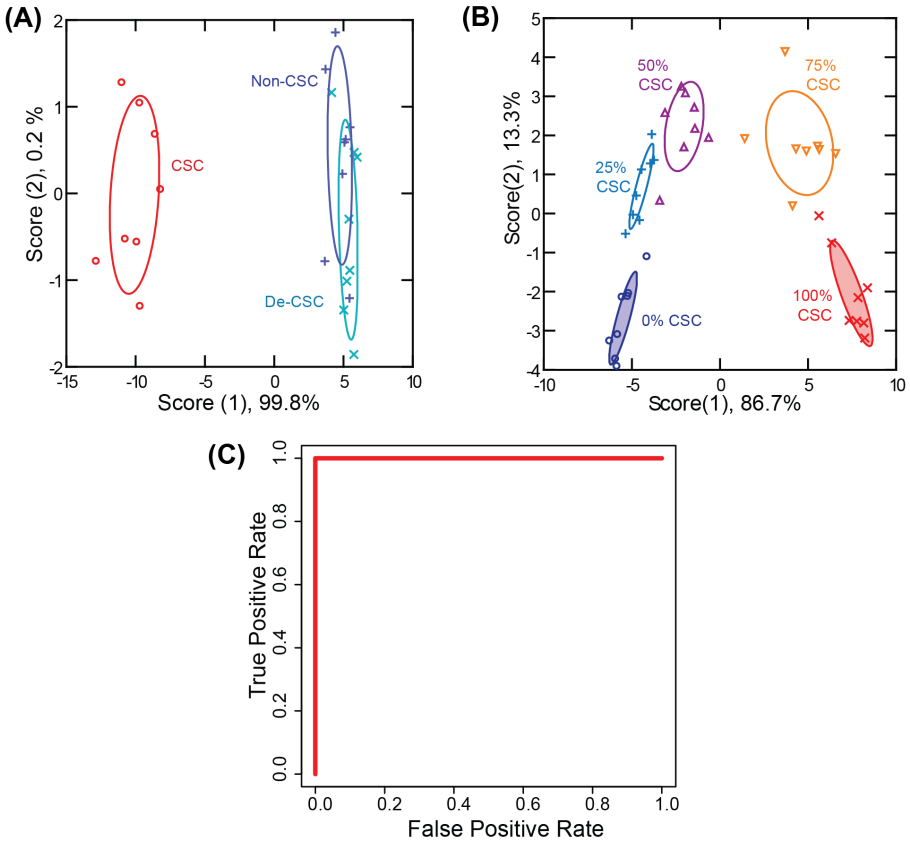

Figure 2.5. Discrimination of CSCs, non-CSCs and de-CSCs from S1 system using BenzNP-FP nanosensor. (A) A canonical score plot for the first two factors of fluorescence patterns was obtained with BenzNP-FP nanosensor against CSCs, non-CSCs, and de-CSCs from S1 cell lines. The scores were generated through LDA with 95% confidence ellipses (n = 8). (B) Similarly, a canonical score plot was derived for the classification of different ratios of CSC and non-CSC mixture. (C) Receiver operating characteristic analysis of CSCs, non-CSCs and de-CSCs from the S1 system. For analysis purpose, non-CSC and de-CSC were combined into one group and referred as non/de-CSC. The area under the curve was calculated to be 1.0 indicating complete discrimination between the two groups.

2.3.5 Sensing of patient-derived xenografts. To determine the potential utility of our sensor in human tumors, we tested the sensing system on patient-derived xenografts (PDX). PDX tumors were generated by transplanting tumor specimens from an individual breast cancer patient into immuno-compromised NSG mice. CSCs ($CD44^{high}/CD24^{low}$) and non-CSCs ($CD44^{low}/CD24^{high}$) were isolated from PDX tumors by fluorescence-activated cell sorting (FACS) (Figure 2.6A). Both populations (CSC and non-CSC) were sorted at the same time using a two-way sort to minimize the sorting effect on cell surface alterations. The identity of each population was validated by assessing their self-renewal ability in mammosphere assays (Figure 2.6B). A similar sensing strategy was performed on PDX-derived CSCs and non-CSCs. The canonical score plot obtained showed complete separation of the two groups with 100% classification accuracy (Figure 2.6C). Unknown samples from each group were tested and correctly identified into either CSCs or non-CSCs with 100% accuracy.

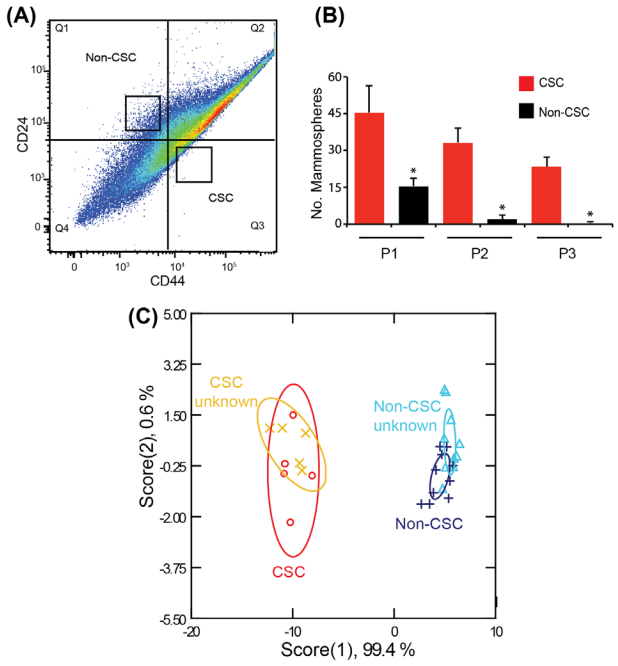

Figure 2.6. Isolation, characterization, and discrimination of primary CSCs from patient-derived xenografts. (A) CSCs and non-CSCs were isolated from PDX models of human breast cancer by FACS using CD44 and CD24 markers. (B) Self-renewal potential of these two populations was assessed by serial passage mammosphere formation assay. (C) CSC and non-CSCs from PDX were sensed with BzNP-FP nanosensor. Fluorescence patterns were analyzed through LDA. Canonical plot of the first two scores for CSC and Non-CSC samples was generated with 95% confidence ellipses. Unknown samples from each group were correctly identified based on the established training set.

2.4 Discussion

CSCs present crucial targets for breast cancer therapy.[36,37] The plastic nature of CSCs as they respond to the environment has enriched our knowledge of the EMT and MET.[10,11] Much information is harbored in the physical properties of cells, yet there are significant challenges in extracting that data in a quantitative and reliable way. In this paper, we use a nanosensor array as an alternative strategy to phenotype CSCs. The key in array-based sensing is being able to generate distinct patterns through selective interactions between sensor elements and analytes. To achieve this, the surface functionality of AuNPs is carefully considered in the sensor design. Previously, we explored a library of AuNPs with different hydrophobicity, aromaticity, and hydrogen bonding characteristics. It was discovered that benzyl-terminated AuNP contributed significantly to the differential sensor responses with cells.[25,26, 38] To ensure a high selectivity in profiling the overall physicochemical changes on cancer stem cells, we chose the Benzyl-NP as the interacting unit in this study. The successful discrimination between non-CSC and CSCs shows high accuracy of such sensing approach (Figure 2.2 & 2.5A). In the cell mixture studies for both MCF-10A ER-Src and S1 models, we observed that when CSCs were added to non-CSCs at a percentage as low as 25%, the sensor output was altered, demonstrating a high level of sensitivity of the nanosenor (Figure 2.2 & 2.5B). The reliability of our sensor strategy is further demonstrated in its ability to identify unknown samples. By computing the

Msahalanobis squared distance between the test samples and trained groups (CSCs and non-CSCs), unknown samples were clustered into the closest group. The high percentage of correct unknown identification validates the reliability of our sensor. Furthermore, all sensor elements were mixed in one well in the microplate, which reduces sensor material cost and analysis steps.

Currently, the nature of the interactions between the nanosensor and cell surface is not well understood. The sensor must interact with different components of cell membranes in order to preferentially release quenched fluorescent proteins. Carefully examining sensor composition reveals that there are potentially two places where those interactions could occur. First, the cationic amine group on the sensor could electrostatically bind with portions of cell membranes containing anionic groups, such as lipids and proteins.[39] In addition, the benzyl head group is likely to form pi-pi stacking interaction with other aromatic structures in the cell membrane, such as proteins containing tyrosine and tryptophan residues.[40] Since cell surface composition varies significantly among cell types and states,[41,42] the differential fluorescence responses of CSCs, non-CSCs, and de-CSCs observed here are likely due to a mixture of changes in the cell surface functionalities. Our previous study showed that the sensor system was highly sensitive to glycosylation patterns, providing a possible origin for the responses observed in the current study.[43] Further mechanistic studies are needed to enrich our current understanding.

Poorly differentiated tumors such as triple negative breast cancer exhibit an embryonic gene expression pattern[44] and are dependent upon developmental signaling pathways.[45 -, 46 , 47] These pathways play crucial roles initiating and maintaining the pluripotency of CSCs,[48, 49] in particular the Hippo pathway because the Hippo transducer

TAZ has a causal role in sustaining CSC function.[34,50] Our data on TAZ-mediated genesis of CSCs revealed that a key integrin, α6β4, has an important role in impeding the CSC phenotype. The restoration of α6β4 reverted stem cell properties (Figure 2.4). The results demonstrate that the S1 system has the advantage of generating CSCs from breast epithelial cells and being able to reverse stemness by expressing a single integrin. The reversible S1 system reflected the dynamic state of CSCs and the sensing results showed that the nanosensor can capture such phenotypic changes by clustering them into different groups. Taken together, the data obtained using two different *in vitro* models demonstrate the power of array-based sensing in profiling CSCs.

There has been intense interest in personalized cancer medicine based on the fact that the geno- and phenotypic properties of tumors differ significantly among patients. Interestingly, recent data revealed that CSCs isolated from patients with same cancer (colon) differ in their properties and response to chemotherapeutics.[14] This observation highlights the need to profile CSCs from individual breast cancer patients. In our study, a clear discrimination of CSCs in PDX models of human breast cancer was observed in Figure 2.6. This result is exciting because it opens the possibility of phenotyping CSCs from individual patients, though further refinement of individual samples is needed due to tumor heterogeneity. The system presents a promising future of monitoring each patient's CSCs responses to different chemotherapeutics, which could be a potential new dimension for precision medicine.

2.5 Conclusion

In summary, we report a nanoparticle-fluorescent-protein based multi-channel sensor that rapidly discriminates CSC from non-CSC phenotypes. This sensor platform

provides a tool with applications in both diagnostics and screening approaches for therapeutic design. The nanosensor is highly versatile, as demonstrated by rapid detection of CSCs in both *in vitro* and *in vivo* models. Taken together, the ability to rapidly identify and profile CSCs provides access to new strategies to combat the multidrug resistance, tumor recurrence and metastasis associated with CSCs.

2.6 Experimental Section

2.6.1 Nanoparticle Synthesis and Characterization. Benzyl gold nanoparticles with a core diameter of 2nm were synthesized according to previous reports.[51] Detailed synthesis scheme and characterization of BenzNPs can be found in the supplementary information. The characterization data corresponds well with that reported in the literature.

2.6.2 Fluorescent Proteins Expression. EGFP, EBFP, tdTomato [52] were synthesized and characterized following previously reported procedures. In brief, Escherichia coli BL21 (DE3) strain was transformed with plasmids containing recombinant proteins. Fluorescent proteins were then purified by Co^{2+} nitrilotriacetate columns and characterized by SDS-PAGE gel, absorbance and fluorescence spectra. The characterization data is similar with previous published work.[27]

2.6.3 Isolation of Mammary Epithelial Cells. MCF-10A cells that express a tamoxifen-inducible ER-SRC were provided by Dr. Kevin Struhl (Harvard Medical School, Boston, MA). Protocols for the isolation of the $CD44^{high}/CD24^{low}$ population from these Src-transformed MCF10A cells and characterization of distinct EPTH and MES sub-populations within the $CD44^{high}/CD24^{low}$ population based on the expression of the β6 integrin have been described.[32]

2.6.4 Engineering S1 Cell Lines. HMT-3522 S1 human mammary epithelial cells were obtained from Dr. Mina Bissell[53] (Lawrence Berkeley National Laboratory) and maintained as described by the Bissell laboratory.[54] These cells were transfected with either empty vector (pLVX-puro) or a constitutively active form of TAZ that contains the following S to A point mutations (S66A, S89A, S117A and S311A) and is referred to as 4SA-TAZ (pLVX-4SA-TAZ; provided by Xaralabos Varelas, Boston University).[55] Stable transfectants were selected using 2 ug/ml puromycin. To induce differentiation of S1 cells expressing 4SA-TAZ, these cells were transfected with a β4 integrin plasmid (pRC-β4) and selected with neomycin. All cell populations used were stable cell lines, which were cultured for two passages without any antibiotics to avoid potential problems related to transfection- or selection-related surface alterations. All cell populations were assessed for self-renewal ability using serial mammosphere assay as described previously.[56] The expression of key stem cell and EMT genes was quantified by qPCR.

2.6.5 Patient-derived Xenografts (PDX). PDX models of human triple-negative breast cancer were maintained in immunocompromised NOD.Cg-Prkdcscid IL2rgtm1Wjl (abbreviated as NSG) mice as described previously.[50] Tumors were harvested, minced and digested for 2-3 hours at 37°C with a mixture of collagenase (Roche, Indianapolis, IN, USA) and hyaluronidase (MP Biomedicals, Solon, OH, USA). The digested cells were passed through a cell strainer to obtain single cell suspensions and plated briefly in serum (1–2 h) to deplete mammary fibroblasts. To isolate CSCs from PDX tumors, dissociated cells were stained with antibodies for lineage markers (CD31, CD45, Ter-119), CD44 and CD24. The lineage antibodies were purchased from eBioscience. The various populations were sorted using flow cytometry [(nozzle size (mm)/pressure (psi): 85/45)]. Both

populations (CSC and non-CSC) were sorted at the same time using two-way sort to minimize the sorting effect on cell surface alterations.

2.6.6 Immunoblotting and qPCR. Cells were extracted using a Triton X-100 buffer (1% Triton X-100, 150 mM NaCl, 50 mM Tris-HCl [pH 7.5], 1 mM phenylmethanesulfonylfluoride [PMSF] and protease inhibitors), and proteins were separated by SDS-PAGE under reducing conditions. These gels were immunoblotted using the following Abs: N-Cadherin (Invitrogen); E-Cadherin (Invitrogen); β4 integrin 505;[57] c-myc (Cell Signaling); actin (Sigma); FLAG (Sigma). For qPCR, RNA was isolated using the NucleopSpin RNA kit (Macherey-Nagel) and 1 ug of total RNA was used to make cDNAs using a cDNA synthesis kit (Biorad). qPCR was performed using a SYBR green (Applied Biosystems) master mix as described by the manufacturer. qPCR primers were designed using primer bank.[58]

2.6.7 Cell Culture. MCF10A-ER-Src cells were cultured in DMEM/F12 medium containing 5% horse serum and other growth factors as described previously.[59] S1 cell lines were grown and maintained as described by the Bissell laboratory.[54] All cells were maintained at 37 °C in a humidified atmosphere containing 5% CO_2. Cells were regularly passaged by trypsinization with 0.25% trypsin with EDTA, (Invitrogen) in PBS (pH 7.2). At ~80% confluence, cells were trypsinized and plated in 96-well plates (Greiner black-and-clear bottom) and cultured for 24 hrs. Cells were washed once with PBS buffer before proceeding to the sensing studies.

2.6.8 Sensing Studies. The sensor was prepared by mixing 100nM of BenzNP with equimolar (100nM) of EBFP, EGFP and tdTomato in 5mM sodium phosphate buffer (pH7.4) for 30 minutes at room temperature. Then, 200uL of sensor solution was incubated

with and without the cell populations (washed once with PBS) in 96-well microplates for 30 minutes. The change of fluorescence intensity in each channel was recorded at its respective wavelength (EBFP: 380/450nm, EGFP: 475/510nm, tdTomato: 550/585nm) on a Molecular Devices SpectraMax M2 microplate reader using appropriate filters.

2.6.9 Linear Discriminant Analysis. The raw fluorescence data was processed by classical linear discriminant analysis using SYSTAT software (version 11.0, SystatSoftware, Richmond, CA, USA). In LDA, all variables were used in the model (complete mode) and the tolerance was set as 0.001. The raw fluorescence response patterns were transformed to canonical patterns where the ratio of between-class variance to the within-class variance was maximized according to the preassigned grouping. To identify the unknown samples, the fluorescence response patterns of each new case was first converted to canonical scores using the discriminant functions established on the training cases. Then, Mahalanobis distance[60] was computed. Blinded cases were predicted to belong to the closest group, defined by the shortest Mahalanobis distance.

2.6.10 Receiver Operating Characteristic Analysis. Receiver operating characteristic (ROC) analysis was used to evaluate the performacne of LDA algorithm. ROC analysis calcualtes the true and fales postive rate of a given binary sample set. By ploting the two rates, an area under the curve can be derived, which indicates the ability of the test to discriminate the desired two populations. ROC analysis was done using Rstudio (version 1.0.143, Integrated Development for R. RStudio, Inc., Boston, MA).

2.7 References

1. J. G. Moffat, J. Rudolph, D. Bailey, *Nat. Rev. Drug Discov.* **2014**, *13*, 588–602.

2. J. E. Dick, *Blood* **2008**, *112*, 4793–4807.

3. C. E. Meacham, S. J. Morrison, *Nature* **2013**, *501*, 328–337.

4. M. Dean, T. Fojo, S. Bates, *Nat. Rev. Cancer* **2005**, *5*, 275–284.

5. S. Vinogradov, X. Wei, *Nanomedicine* **2012**, *7*, 597–615.

6. S. A. Mani, W. Guo, M.-J. Liao, E. N. Eaton, A. Ayyanan, A. Y. Zhou, M. Brooks, F. Reinhard, C. C. Zhang, M. Shipitsin, et al., *Cell* **2008**, *133*, 704–715.

7. C. Scheel, R. A. Weinberg, *Semin. Cancer Biol.* **2012**, *22*, 396–403.

8. J. Yang, R. A. Weinberg, *Dev. Cell* **2008**, *14*, 818–829.

9. A. Singh, J. Settleman, *Oncogene* **2010**, *29*, 4741–4751.

10. K. Polyak, R. A. Weinberg, *Nat. Rev. Cancer* **2009**, *9*, 265–273.

11. J. H. Tsai, J. L. Donaher, D. A. Murphy, S. Chau, J. Yang, *Cancer Cell* **2012**, *22*, 725–736.

12. F. Andriani, G. Bertolini, F. Facchinetti, E. Baldoli, M. Moro, P. Casalini, R. Caserini, M. Milione, G. Leone, G. Pelosi, et al., *Mol. Oncol.* **2016**, *10*, 253–271.

13. M. K. Jolly, S. C. Tripathi, D. Jia, S. M. Mooney, M. Celiktas, S. M. Hanash, S. A. Mani, K. J. Pienta, E. Ben-Jacob, H. Levine, *Oncotarget* **2016**, *7*, 27067–27084.

14. M. R. Carstens, R. C. Fisher, A. P. Acharya, E. A. Butterworth, E. Scott, E. H. Huang, B. G. Keselowsky, *Proc. Natl. Acad. Sci.* **2015**, *112*, 8732–8737.

15. B. Yang, J. B. Treweek, R. P. Kulkarni, B. E. Deverman, C. K. Chen, E. Lubeck, S. Shah, L. Cai, V. Gradinaru, *Cell* **2014**, *158*, 945–958.

16. A. G. Pockley, G. A. Foulds, J. A. Oughton, N. I. Kerkvliet, G. Multhoff, *Curr. Protoc. Toxicol.* **2015**, *66*, 18.8.1-18.8.34.

17. M. Al-Hajj, M. S. Wicha, A. Benito-Hernandez, S. J. Morrison, M. F. Clarke, *Proc. Natl. Acad. Sci. U. S. A.* **2003**, *100*, 3983–3988.

18. C. Ginestier, M. H. Hur, E. Charafe-Jauffret, F. Monville, J. Dutcher, M. Brown, J. Jacquemier, P. Viens, C. G. Kleer, S. Liu, et al., *Cell Stem Cell* **2007**, *1*, 555–567.

19.G. Dontu, W. M. Abdallah, J. M. Foley, K. W. Jackson, M. F. Clarke, M. J. Kawamura, M. S. Wicha, *Genes Dev.* **2003**, *17*, 1253–1270.

20. K. Kemper, M. R. Sprick, M. De Bree, A. Scopelliti, L. Vermeulen, M. Hoek, J. Zeilstra, S. T. Pals, H. Mehmet, G. Stassi, et al., *Cancer Res.* **2010**, *70*, 719–729.

21. A. B. Mak, K. M. Blakely, R. A. Williams, P. A. Penttila, A. I. Shukalyuk, K. T. Osman, D. Kasimer, T. Ketela, J. Moffat, *J. Biol. Chem.* **2011**, *286*, 41046–41056.

22. R. Strauss, Z. Y. Li, Y. Liu, I. Beyer, J. Persson, P. Sova, T. Möller, S. Pesonen, A. Hemminki, P. Hamerlik, et al., *PLoS One* **2011**, *6*, e16186.

23. N. Barkalina, C. Charalambous, C. Jones, K. Coward, *Nanomedicine: N.B.M.* **2014**, *10*, e921–e938.

24. A. Sobczak-Kupiec, J. Venkatesan, A. Alhathal AlAnezi, D. Walczyk, A. Farooqi, D. Malina, S. H. Hosseini, B. Tyliszczak, *Nanomedicine: N.B.M.* **2016**, *12*, 2459–2473.

25. A. Bajaj, O. R. Miranda, I.-B. Kim, R. L. Phillips, D. J. Jerry, U. H. F. Bunz, V. M. Rotello, *Proc. Natl. Acad. Sci. U. S. A.* **2009**, *106*, 10912–10916.

26. S. Rana, A. K. Singla, A. Bajaj, S. G. Elci, O. R. Miranda, R. Mout, B. Yan, F. R. Jirik, V. M. Rotello, *ACS Nano* **2012**, *6*, 8233–8240.

27. S. Rana, N. D. B. Le, R. Mout, K. Saha, G. Y. Tonga, R. E. S. Bain, O. R. Miranda, C. M. Rotello, V. M. Rotello, *Nat. Nanotechnol.* **2015**, *10*, 65–69.

28. M. De, P. S. Ghosh, V. M. Rotello, *Adv. Mater.* **2008**, *20*, 4225–4241.

29. Z. Pode, R. Peri-Naor, J. M. Georgeson, T. Ilani, V. Kiss, T. Unger, B. Markus, H. M. Barr, L. Motiei, D. Margulies, *Nat. Nanotechnol.* **2017**, *12*, 1161–1168.

30. O. R. Miranda, X. Li, L. Garcia-Gonzalez, Z. J. Zhu, B. Yan, U. H. F. Bunz, V. M. Rotello, *J. Am. Chem. Soc.* **2011**, *133*, 9650–9653.

31. D. Iliopoulos, C. Polytarchou, M. Hatziapostolou, F. Kottakis, I. G. Maroulakou, K. Struhl, P. N. Tsichlis, *Sci. Signal.* **2009**, *2*, ra62–ra62.

32. H. L. Goel, T. Gritsko, B. Pursell, C. Chang, L. D. Shultz, D. L. Greiner, J. H. Norum, R. Toftgard, L. M. Shaw, A. M. Mercurio, *Cell Rep.* **2014**, *7*, 747–761.

33. M. V. Fournier, K. J. Martin, P. A. Kenny, K. Xhaja, I. Bosch, P. Yaswen, M. J. Bissell, *Cancer Res.* **2006**, *66*, 7095–7102.

34. M. Cordenonsi, F. Zanconato, L. Azzolin, M. Forcato, A. Rosato, C. Frasson, M. Inui, M. Montagner, A. R. Parenti, A. Poletti, et al., *Cell* **2011**, *147*, 759–772.

35. F. Zanconato, M. Cordenonsi, S. Piccolo, *Cancer Cell* **2016**, *29*, 783–803.

36. P. B. Gupta, T. T. Onder, G. Jiang, K. Tao, C. Kuperwasser, R. A. Weinberg, E. S. Lander, *Cell* **2009**, *138*, 645–659.

37. H. A. Hirsch, D. Iliopoulos, P. N. Tsichlis, K. Struhl, *Cancer Res.* **2009**, *69*, 7507–7511.

38. A. Bajaj, S. Rana, O. R. Miranda, J. C. Yawe, D. J. Jerry, U. H. F. Bunz, V. M. Rotello, *Chem. Sci.* **2010**, *1*, 134.

39. P. V Escribá, J. M. González-Ros, F. M. Goñi, P. K. J. Kinnunen, L. Vigh, L. Sánchez-Magraner, A. M. Fernández, X. Busquets, I. Horváth, G. Barceló-Coblijn, *J. Cell. Mol. Med.* **2008**, *12*, 829–875.

40. G. B. McGaughey, M. Gagné, A. K. Rappé, *J. Biol. Chem.* **1998**, *273*, 15458–15463.

41. P. M. Lanctot, F. H. Gage, A. P. Varki, *Curr. Opin. Chem. Biol.* **2007**, *11*, 373–380.

42. P. R. Srinivas, B. S. Kramer, S. Srivastava, *Lancet Oncol.* **2001**, *2*, 698–704.

43. S. Rana, N. D. B. Le, R. Mout, B. Duncan, S. G. Elci, K. Saha, V. M. Rotello, *ACS Cent. Sci.* **2015**, *1*, 191–197.

44. I. Ben-Porath, M. W. Thomson, V. J. Carey, R. Ge, G. W. Bell, A. Regev, R. A. Weinberg, *Nat. Genet.* **2008**, *40*, 499–507.

45. W. Y. Cai, T. Z. Wei, Q. C. Luo, Q. W. Wu, Q. F. Liu, M. Yang, G. D. Ye, J. F. Wu, Y. Y. Chen, G. Bin Sun, et al., *J. Cell Sci.* **2013**, *126*, 2877–2889.

46. E. V. Abel, E. J. Kim, J. Wu, M. Hynes, F. Bednar, E. Proctor, L. Wang, M. L. Dziubinski, D. M. Simeone, *PLoS One* **2014**, *9*, e91983.

47. S. Liu, G. Dontu, I. D. Mantle, S. Patel, N. S. Ahn, K. W. Jackson, P. Suri, M. S. Wicha, *Cancer Res.* **2006**, *66*, 6063–6071.

48. N. Oishi, T. Yamashita, S. Kaneko, *Liver Cancer* **2014**, *3*, 71–84.

49. N. Takebe, P. J. Harris, R. Q. Warren, S. P. Ivy, *Nat. Rev. Clin. Oncol.* **2011**, *8*, 97–106.

50. C. Chang, H. L. Goel, H. Gao, B. Pursell, L. D. Shultz, D. L. Greiner, S. Ingerpuu, M. Patarroyo, S. Cao, E. Lim, et al., *Genes Dev.* **2015**, *29*, 1–6.

51. G. Y. Tonga, Y. Jeong, B. Duncan, T. Mizuhara, R. Mout, R. Das, S. T. Kim, Y.-C. Yeh, B. Yan, S. Hou, et al., *Nat. Chem.* **2015**, *7*, 597–603.

52. M. De, S. Rana, V. M. Rotello, *Macromol. Biosci.* **2009**, *9*, 174–178.

53. P. Briand, O. W. Petersen, B. Van Deurs, *In Vitro Cell. Dev. Biol.* **1987**, *23*, 181–188.

54. Bissell Laboratory Protocols. http://www2.lbl.gov/LBL-Programs/lifesciences/BissellLab/protocols.html (accessed January 26, 2017).

55. Q.-Y. Lei, H. Zhang, B. Zhao, Z.-Y. Zha, F. Bai, X.-H. Pei, S. Zhao, Y. Xiong, K.-L. Guan, *Mol. Cell. Biol.* **2008**, *28*, 2426–2436.

56. H. L. Goel, B. Pursell, C. Chang, L. M. Shaw, J. Mao, K. Simin, P. Kumar, C. W. Vander Kooi, L. D. Shultz, D. L. Greiner, et al., *EMBO Mol. Med.* **2013**, *5*, 488–508.

57. I. Rabinovitz, A. Toker, A. M. Mercurio, *J. Cell Biol.* **1999**, *146*, 1147–1160.

58. Primer Bank. https://pga.mgh.harvard.edu/primerbank (accessed January 26, 2017).

59. D. Iliopoulos, H. A. Hirsch, G. Wang, K. Struhl, *Proc. Natl. Acad. Sci. U. S. A.* **2011**, *108*, 1397–1402.

60. P. C. Mahalanobis, *Proc. Natl. Inst. Sci. India.* **1936**, *2*, 49–55.

CHAPTER 3

DIFFERENTIATION OF CANCER STEM CELLS THROUGH NANOPARTICLE SURFACE ENGINEERING

3.1 Abstract

Cancer stem cells (CSCs) are a crucial therapeutic target because of their role in resistance to chemo- and radiation therapy, metastasis, and tumor recurrence. Differentiation therapy presents a potential strategy for 'defanging' CSCs. To date, only a limited number of small molecule and nanomaterial-based differentiating agents have been identified. We report here the integrated use of nanoparticle engineering and hypothesis-free sensing to identify nanoparticles capable of efficient differentiation of CSCs into novel non-CSC phenotypes. Using this strategy, we identified a nanoparticle that induces CSC differentiation by increasing intracellular reactive oxygen species levels. Importantly, this novel phenotype is more susceptible to drug treatment than either CSCs or non-CSCs, demonstrating a potentially powerful strategy for anticancer therapeutics.

3.2 Introduction

The majority of solid tumors harbor a population of cells with stem cell characteristics, including the ability to self-renew, differentiate and populate new tumors.[1] These cells are referred to as cancer stem cells (CSCs). CSCs are resistant to standard chemotherapy and are considered responsible for tumor recurrence and metastasis, making them key therapeutic targets.[2,3] One key characteristic of CSCs is their phenotypic plasticity. Through epithelial-to-mesenchymal transition (EMT), cancer cells can gain stem cell properties to become more aggressive.[4] Conversely, CSCs can also differentiate,

undergoing mesenchymal-to-epithelial transition (MET), a process that may facilitate metastasis.[5,6] The CSC dynamic is further complicated by the emerging evidence of partial EMT, where the intermediate states express both epithelial and mesenchymal traits.[4,7,8]

Given that the EMT can promote the acquisition of stem cell properties,[4, 9] therapeutic agents that promote differentiation should diminish the frequency of CSCs, rendering tumors less aggressive and more responsive to conventional therapy. This approach is known as differentiation therapy and has considerable therapeutic potential.[10] One of the most successful examples of differentiation therapy is the use of all-trans retinoic acid in acute promyelocytic leukemia (APL). By promoting cells blocked at a distinct cellular maturation stage to differentiate, APL patients who received such treatment in combination with other chemotherapies have an overall cure rate exceeding 80%.[11-, 12, 13]

There has been a widespread interest in identifying molecules that selectively kill CSCs or promote their differentiation.[14] In 2009, Gupta *et al.* screened 16,000 compounds and found that ~only 0.2% of these compounds showed selective toxicity for breast CSCs.[15] Another screen conducted in 2012 revealed a dopamine receptor antagonist as a potent molecule that selectively targets CSCs.[16] In addition to small molecules, nanoscale materials have gained significant interest as therapeutic agents for several applications, including drug delivery, immunoregulation, and bio-orthogonal drug activation.[17-,18,19,20] Recent studies have shown that nanomaterials can either kill or alter the phenotype of CSCs. For instance, carbon materials such as metallofullerenes[21] and graphene oxide[22] can induce CSC differentiation *in vitro*. Since hydrophobicity plays crucial rules in normal

stem cell biology, [23,24] it is likely that the highly hydrophobic nature of these nanomaterials is responsible for differentiating CSCs.

Despite the progress in identifying novel differentiation therapeutics, the discovery process is slow and difficult. Two major challenges are present in the generation of nanoparticle-based therapeutics. First, most studies use hypothesis-driven approaches for CSC differentiation screening that involve the use of specific markers. Since CSCs are highly plastic[25,26] and associated with different EMT states,[7,8] utilizing one or two specific markers will likely obscure the detection of differentiated phenotypes. More significantly, hypothesis-driven strategies limit detection to a pre-defined phenotype, potentially failing to detect other differentiated phenotypes. In addition, commonly used techniques such as RT-PCR, flow cytometry and mammospheres formation assay, require special instrumentation and multi-step processing of cells, limiting their compatibility with a high-throughput platform.[27-,28,29]

A second limitation in developing nanotherapeutics for CSC differentiation is the challenge of controlling surface properties inherent to many nanomaterial platforms.[30,31] These properties are crucial, determining the therapeutic efficacy of these nanomaterials, as well as impacting parameters including pharmacokinetics and biodistribution.[32]

Taken together limitations in screening and platform design space have hindered the exploration of nanomaterial-based CSC differentiation, and as such, there is a clear need for a method that features greater control over chemical diversity and can simultaneously increase throughput.

Gold nanoparticles (AuNPs) feature facile surface functionalization, [33] biologically-favorable size, and tunable contact area.[34,35] The gold used for the core is also

essentially non-toxic.[36] These properties have led to their utilization for applications as diverse as drug delivery,[37] antifouling materials,[38] and sensing in complex matrices.[39] As such, they are also particularly promising candidates for screening CSC differentiation inducers.

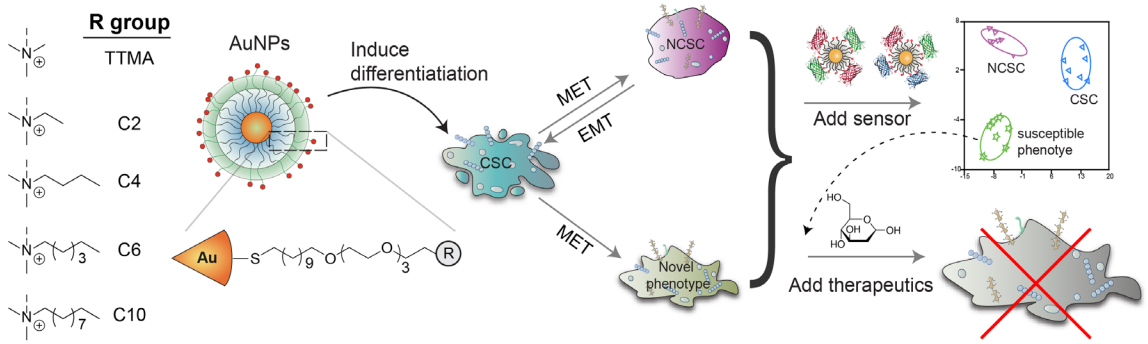

Figure 3.1. Schematic illustration of the integration of nanoparticle design and hypothesis-free sensing. Chemical structure of the 2-nm core diameter AuNPs used to stimulate CSCs are shown on the left. After AuNP treatment, cells were washed and incubated with the nanosensor to rapidly collect phenotypic information. The novel phenotype identified through the sensing screen was further subject to drug treatment to see if it was more sensitive to chemotherapy.

We report here an integrated screening/synthetic strategy for generating nanomaterial therapeutics for CSC differentiation (Figure 3.1). This approach uses the precise level of structural control afforded by AuNPs to systematically investigate the effects of NP surface chemistry on CSC differentiation. This therapeutic design capability is complemented by a hypothesis-free, array-based sensing platform for CSC screening. As opposed to the traditional biomarker-based approach, this array-based sensing uses a signature-based method to profile an entire matrix of bioanalytes, [40] effectively circumventing the bottleneck of receptor specificity as demonstrated through discrimination of CSCs from non-CSCs.[41]

In the work reported herein, a population of breast cancer cells enriched for a mesenchymal phenotype and stem cell properties was treated with cationic AuNPs capable of readily entering cells. [42] These particles bore headgroups with highly controlled hydrophobicity ranging from hydrophilic (TTMA) to highly hydrophobic (C10). [43] Screening was then performed using hypothesis-free sensing. By reading off the fluorescence patterns generated through sensor-cell interactions, we discovered that one particle (C6NP) robustly promoted CSC differentiation. Further evaluation revealed that C6NP promoted a MET, decreasing expression of key stem cell genes and mesenchymal markers. Mechanistic studies showed that this differentiation is associated with an increase in reactive oxygen species (ROS). Importantly, when CSCs were treated with C6NP in combination with mitochondrial inhibitors, a selective synergistic killing of CSCs was achieved, demonstrating the capability of this differentiation strategy for addressing CSC drug resistance (Figure 3.1).

3.3 Results and Discussion

3.3.1 AuNPs with tunable surface functionality for structure-activity studies.

We first synthesized and characterized a library of five different AuNPs [44,45] to explore the structure- activity relationship of AuNPs on CSC differentiation. The monolayer of the nanoparticle features a hydrophobic alkane chain, which provides stability in a biologically-relevant environment,[46,47] followed by a tetra(ethylene glycol) moiety that offers biocompatibility and helps to expose the terminal head-groups on the NP surface, allowing us to study the direct effects of surface chemistry on CSC differentiation. Since hydrophobicity has key implications in stem cell biology, including cell adhesion,

migration and differentiation,[23,24] we chose five functional AuNP head groups with parametrically varying degrees of hydrophobicity (Figure 3.1).

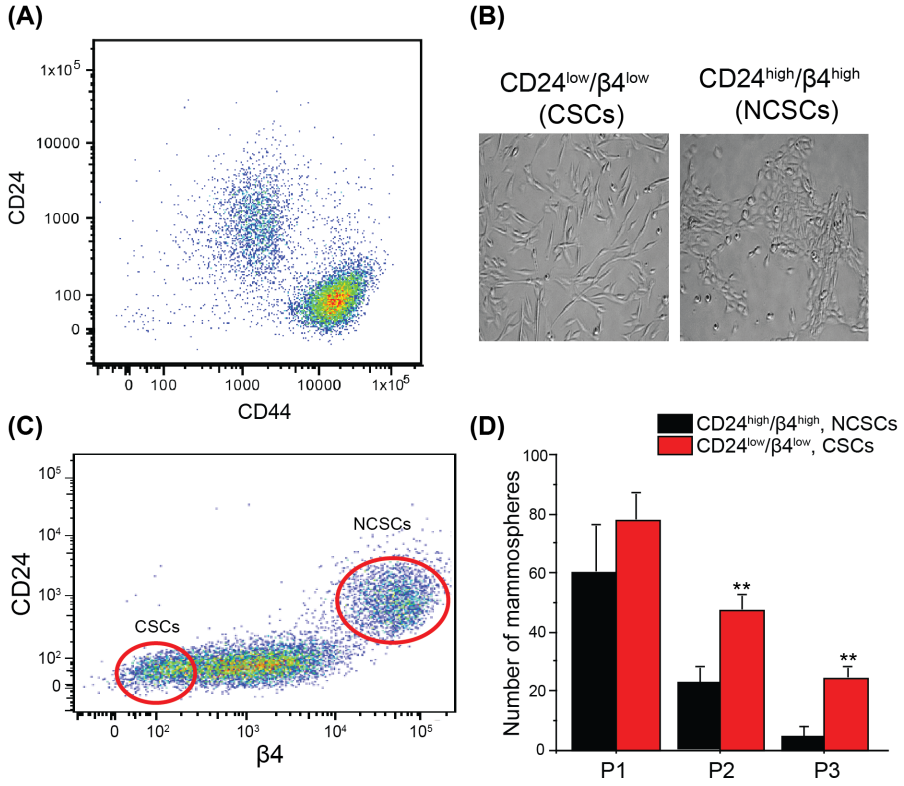

Figure 3.2. Characterization of HMLER subpopulations. (A) Morphology of HMLER $CD24^{high}/\beta4^{high}$ and $CD24^{low}/\beta4^{low}$ imaged under phase contrast microscopy at 10x magnification. (B) HMLER cells contain distinct populations of $CD44^{high}/CD24^{low}$ (CSCs) and $CD44^{low}/CD24^{high}$ (non-CSCs). (C) HMLER cells sorted based the CD24 and β4 integrin expression into CSCs and NCSCs sub-populations. (D) HMLER $CD24^{high}/\beta4^{high}$ and $CD24^{low}/\beta4^{low}$ cells were serial passaged in a mammosphere assay. $CD24^{low}/\beta4^{low}$ showed significantly more self-renewal ability than $CD24^{high}/\beta4^{high}$ over three passages. P-values for CSC population at P2 and P3 are 0.003 and 0.002, respectively.

3.3.2 Identification of two sub-populations of transformed mammary epithelial cells that differ in CSC properties. We made use of human mammary epithelial cells (HMECs) that were transformed by SV40 large-T antigen, the telomerase catalytic subunit, and H-Ras. These modified HMECs are referred to as HMLER cells.[29] Using established markers for breast CSCs (CD44 and CD24), HMLERs were sorted into

$CD44^{high}/CD24^{low}$ (CSC) and $CD44^{low}/CD24^{high}$ (non-CSC) populations (Figure 3.2A). We were also able to further sort them based on the expression of CD24 and β4 integrin to generate two sub-populations with distinct morphological differences: HMLER $CD24^{low}/\beta4^{low}$ cells are fibroblastic, mesenchymal like with a spindle-shape morphology, whereas the HMLER $CD24^{high}/\beta4^{high}$ population is more epithelial (Figure 3.2B-C). We assessed the self-renewal potential of these populations by serial mammosphere formation. The results showed that $CD24^{low}/\beta4^{low}$ cells had the ability to self-renew over several passages, while the $CD24^{high}/\beta4^{high}$ cells gradually lost their ability to form mammospheres (Figure 3.2D). Based on their morphology and self-renewal potential, we termed the HMLER $CD24^{low}/\beta4^{low}$ cells and $CD24^{high}/\beta4^{high}$ as CSCs and non-CSCs (NCSCs), respectively, for the following studies. These findings support our previous conclusion that the expression of the β4 integrin is low in breast CSCs.[48]

Sensor array design. The nanosensor employed in this work is comprised of a cationic gold nanoparticle (2nm core in diameter) bearing a benzyl terminal group (BenzNP) and three types of fluorescent proteins (FPs).[41] The nanosensor was formed by mixing equimolar of BenzNP with FPs. Due to electrostatic interactions, FPs were drawn in close proximity to the gold core and their fluorescence was quenched through energy transfer to BenzNP, resulting in a 'sensor-off' state. Upon addition of cells, cell surface functionalities compete with FPs for AuNP binding and simultaneously release FPs into solution, freely emitting light. As a result, the sensor is turned on and fluorescence signals can be collected as the signature for the target analyte. Our hypothesis is that the cell surface composition of CSCs will be altered under nanoparticle treatment, which will be captured by the nanosensor with a unique fluorescent pattern (Figure 3.3). This type of

"turn-on" sensor has successfully been employed in discriminating a range of bioanalytes including bacteria,[49] mammalian cells,[50] and patient sera.[51]

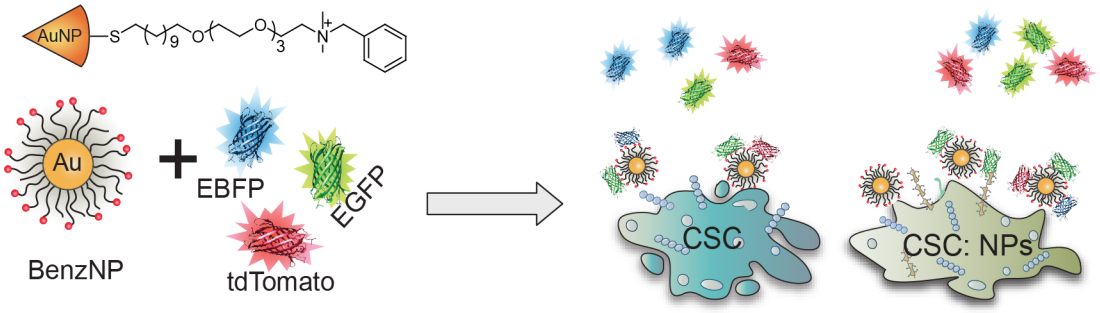

Figure 3.3. Schematic illustration of sensor composition and selective interactions with cell surfaces.

3.3.3 Screening for NP-induced CSC differentiation. The screen of the small NP library began with treating CSCs with individual AuNPs at a non-toxic concentration (Figure 3.4) for 72 hrs to allow potential differentiation effects to occur. Since the tested NPs are only 2 nm in diameter and carry positive charges, they should rapidly cross the cell membrane. Consistent with our previous work,[52] we observed intracellular uptake of these NPs in CSCs, presumably through their electrostatic interactions with cell membranes.

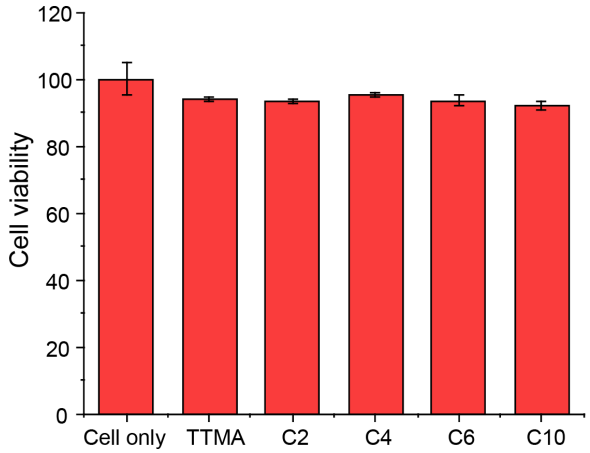

Figure 3.4. Cytotoxicity of tested NPs on HMLER-CSCs. Each NP was treated at 100 nM for 72hrs. Three biological replicates were used for each treatment group. Viability was normalized to the cell only group.

At the end of NP treatment, cells were washed with phosphate-buffered saline (PBS) to remove excess NPs, followed by a 30 min incubation with the nanosensor. The fluorescence signals of the sensor were immediately measured, and the fluorescent patterns were analyzed using linear discriminant analysis (LDA). Overall, the results can be obtained in less than an hour after sensor incubation, which is much more efficient than other screening assays. Since the cell surface composition varies significantly among cell types and states,[53,54] the resulting fluorescent pattern is unique for CSCs under each NP treatment (Figure 3.5A). LDA plot revealed that CSCs and NCSCs were well discriminated from each other. NP treatment resulted in a range of different effects on CSCs with some NPs closer to the control group (e.g. TTMA, C2 and C10) and others separated out (e.g. C4 and C6) (Figure 3.5B). Interestingly, none of the treatment groups overlapped with NCSCs, suggesting that NPs did not revert CSCs to NCSC state, rather new phenotypes were achieved. Since our sensor is highly sensitive to cell surface glycosylation,[55] it is likely that NP treatment alters glycosylation patterns and that these alterations contribute to the new phenotypes.

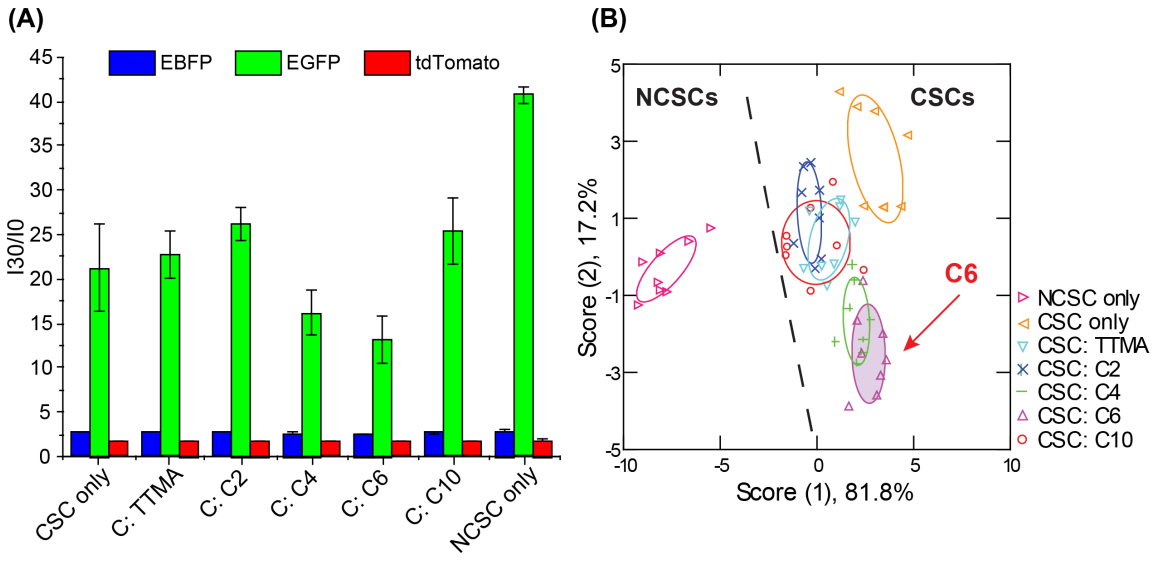

Figure 3.5. Sensing screen in capturing phenotypic changes of CSCs under different AuNP treatment. (A) Fluorescent responses of CSCs (isolated from HMLER model) under different AuNP treatment. Normalized fluorescence intensities against sensor only were obtained after 30 min of sensor incubation with cells (n=8). C: TTMA means CSCs treated with TTMA. (B) Fluorescence patterns obtained were analyzed through LDA. Canonical plot of the first two scores was generated with 95% confidence ellipses (n=8).

Next, we quantified the pairwise distance between each tested group to determine which NP treatment had the most substantial effect on CSCs. The F-index was calculated based on the within-class variance as well as between-class variance. Larger values of F-index indicated better separation or more difference between the two groups.[56,57] As shown in Table 3.1, when NP treated groups were compared with either non-treated CSCs or NCSCs, C6NP was the furthest from both control CSCs and control NCSCs with an F-index of 32.7 and 147.8 (respectively), indicating a promising hit from the sensing screen has been identified. The generality of this method was further validated on a different and more stringent CSC model system: MCF10A-ER-Src.[48] The sensing trend also suggested that C6NP is a promising hit to pursue. (Figure 3.6).

Table 3.1. Summary of the distance between any two tested groups in HMLER model.[a]

	CSC: TTMA	CSC: C2	CSC: C4	CSC: C6	CSC: C10	CSC only	NCSC only
CSC: TTMA[b]	0						
CSC: C2	1.9	0					
CSC: C4	8.2	17.0	0				
CSC: C6	16.9	29.1	1.6	0			
CSC: C10	2.9	2.4	12.3	21.9	0		
CSC only	13.6	17.2	24.3	**32.7**	19.9	0	
NCSC only	91.6	74.2	124.9	**147.8**	77.3	161.3	0

[a] Sensing results were used to compute F-index of each pair in SYSTAT software. Larger values indicated more difference between the two groups. [b] CSC treated with TTMA particle.

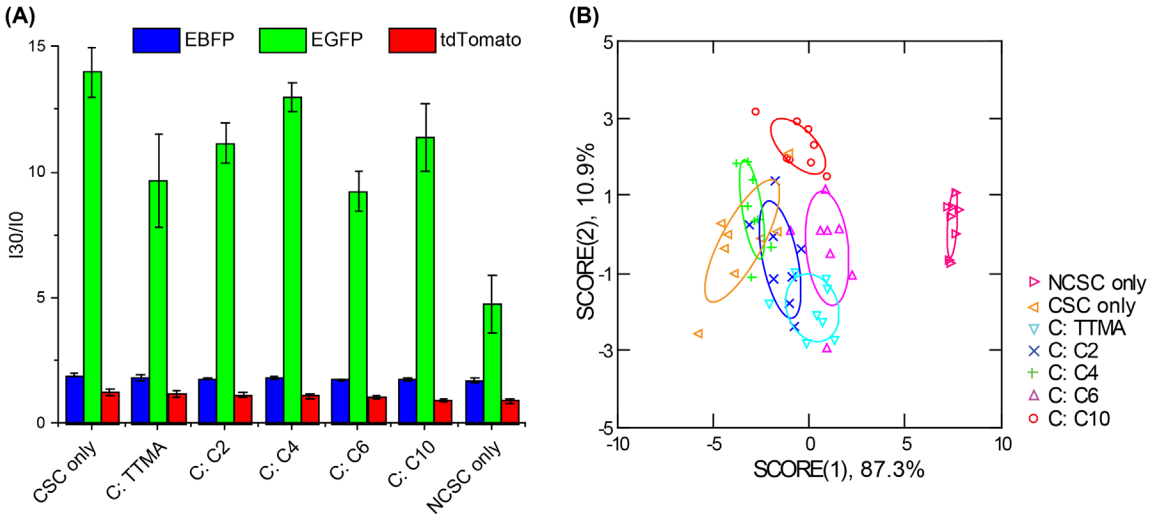

Figure 3.6. Sensing screen in capturing phenotypic changes of CSCs (from MCF10A-ER-Src system) under different AuNP treatment. (A) Normalized fluorescence intensities against sensor only group. (B) LDA canonical plot of the first two scores was generated with 95% confidence ellipses (n=8). C: TTMA means CSCs treated with TTMA.

3.3.4 Identifying phenotypic alterations from C6NP treatment. Based on the strong difference in cell nanosensor response for C6NP, we performed phenotypic and mechanistic studies on the cells. In response to C6NP treatment, we observed that cells lost their mesenchymal, spindle shape and became more epithelial in morphology. The mRNA levels of key stem cell genes (Oct4 and Zeb 1) and mesenchymal markers (CDH2 and fibronectin) were significantly reduced, while epithelial differentiation related genes (CD24, integrin β4, and α6A) were increased (Figure 3.7A), suggesting a MET had occurred. The phenotypic alterations were further evident in the decreased protein expression level of Zeb 1 and N-cadherin (Figure 3.7B). Furthermore, C6NP diminished CSC properties as evidenced by a decrease in mammosphere formation (Figure 3.7C). We also observed a significant decrease in the ability of C6NP-treated cells to adhere to laminin 511, which we have reported is a preferred extracellular matrix for CSCs (Figure 3.7D).[58] These data demonstrate that C6NP impacts CSC properties. Taken together, these data demonstrate that C6NP promotes epithelial differentiation and loss of CSC properties.

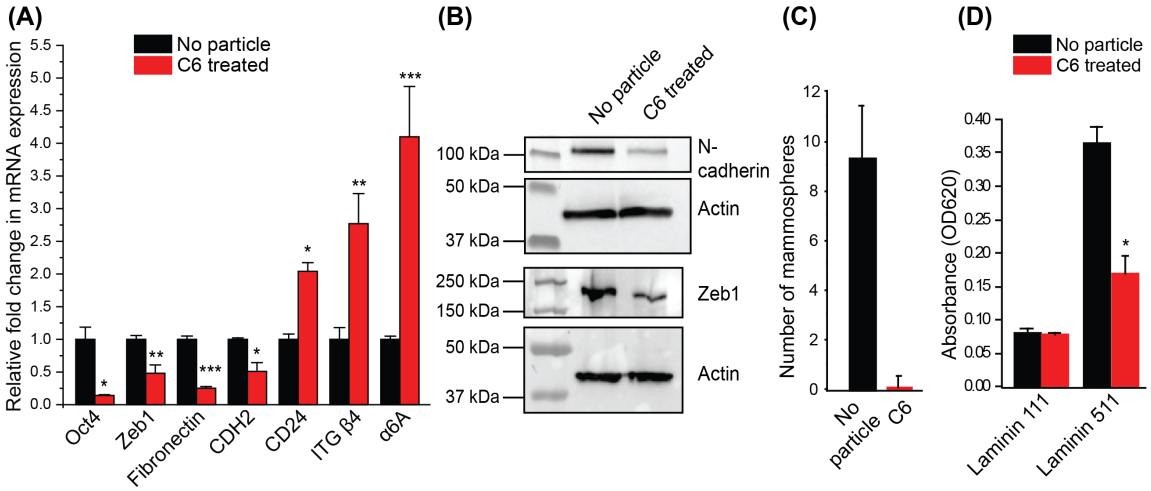

Figure 3.7. MET evaluation of HMLER-CSCs treated with 100 nM C6NP for 72 hrs. (A) mRNA quantification of key stem (Oct4 and Zeb 1), mesenchymal (CDH2 and Fibronectin) and epithelial differentiation related genes (CD24, integrin β4, and α6A) in response to C6NP treatment using qRT-PCR. Fold changes in mRNA level were normalized to GAPDH and compared with no particle treated control. (B) Immunoblot of

mesenchymal (N-cadherin) and stem cell marker (Zeb 1) expression level of CSCs under C6NP treatment. Actin is used as a loading control. (C) Significant reduction in mammosphere formation ability in C6NP treated CSCs was observed. (D) C6NP treated CSCs show decreased adhesion to laminin 511, a preferred CSC substrate (p-value of 0.016). Laminin 111 is used as a control substrate. Statistical significance was determined by two-tailed student t-test. *= $p < 0.05$, **= $p < 0.01$, ***= $p < 0.001$.

3.3.5 Increased ROS levels are a consequence of C6NP treatment. Based on the observation that CSCs have a lower level of intracellular reactive oxygen species (ROS) than their non-tumorigenic cell partners,[59,60] we investigated whether C6NP treatment impacted ROS levels. Exposure of CSCs with C6NP resulted in a significant increase in ROS (Figure 3.8). When the ROS scavenger N-acetyl-L-cysteine (NAC) was applied in combination with C6NP, ROS levels were reduced, demonstrating that C6NP increases ROS in CSCs. Although other NPs induced an initial burst of ROS at 30 minutes, only the C6NP was able to sustain this burst for 4 hrs (Figure 3.9). The initial burst of ROS is likely induced by the nature of nanoparticles[61] and elevated oxidative stress could activate the innate cellular defense mechanism to clear out foreign particles.[62]

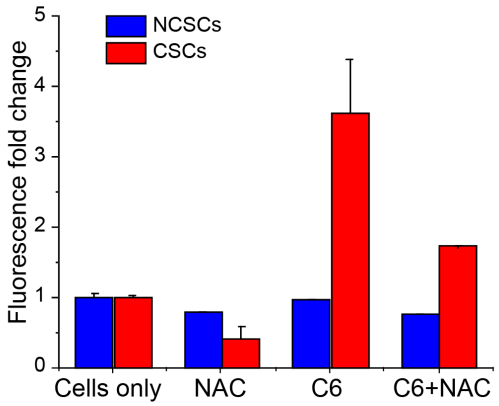

Figure 3.8. ROS production of CSCs and NCSCs treated with C6NP. The ROS level in each treatment group was normalized to its respective cell only control group (NCSCs and CSCs). Only CSCs treated with C6NP showed an increase in ROS level as compared to its control group (p value of 0.027). Treatment with NAC reduced ROS expression in C6 treated CSCs.

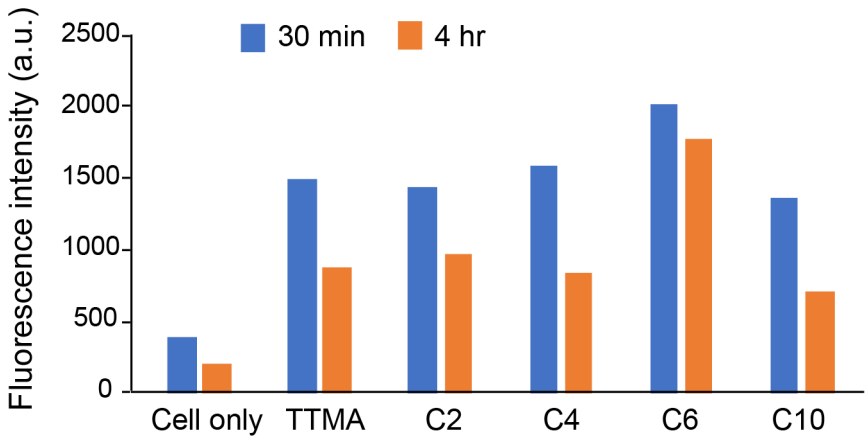

Figure 3.9. ROS production of CSCs treated with different types of NPs for either 30 min (blue) or 4 hrs (orange). All other NPs induced increased ROS production relative to the cell only control, however substantially higher levels of ROS were observed with C6, in particular after 4 hrs incubation.

We next sought to understand how the sustained induction of ROS by the C6NP could promote CSC differentiation. Our hypothesis is based on our previous work on the importance of mRNA splicing in controlling the expression of key genes that promote a CSC phenotype,[48,63] most notably, the α6β1 integrin. There are two splice variants of the a6 integrin subunit (α6A and α6B). Previous studies demonstrated that the α6Bβ1 integrin promotes a CSC phenotype while α6Aβ1 promotes a more differentiated, non-CSC phenotype.[48] Based on these data, we observed that C6NP induced expression of the α6A splice variant. Importantly, this induction of α6A is ROS-dependent, supporting an ROS-dependent mechanism for how C6NP promotes differentiation (Figure 3.10).

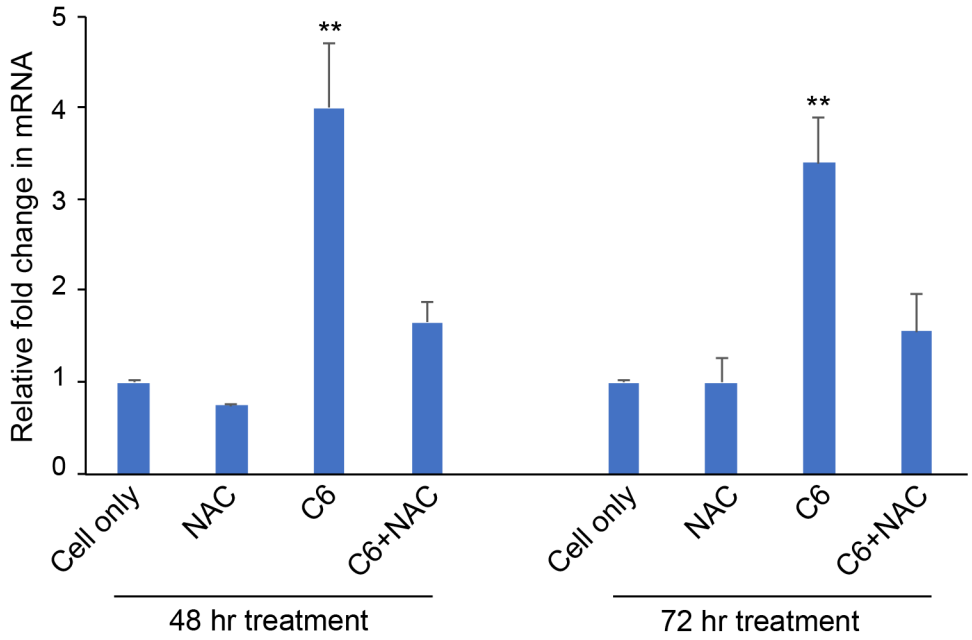

Figure 3.10. mRNA quantification of α6A splicing gene when CSCs were treated with 100 nM C6NP with or without ROS inhibitor NAC. Fold changes in mRNA level were normalized to GAPDH and compared with cell only control. Statistical significance was determined by two-tailed student t-test. *= $p < 0.05$, **= $p < 0.01$, ***= $p < 0.001$.

Normal stem cells produce a lower amount of ROS in order to maintain their quiescent state and self-renewal capabilities.[64] During differentiation, cells can adjust their metabolic system to generate enough energy for this cellular process. Evidence has shown that increased ROS levels can promote the differentiation of embryonic stem cells.[65-,66,67] This finding is consistent with our results that implicate ROS in an mRNA splicing program that promotes epithelial differentiation.

The ability of C6NP to promote the epithelial differentiation of CSCs was further investigated in a patient-derived xenograft, where CSCs and NCSCs were isolated using CD24 and CD44 markers. As evident in Figure 3.11A, CSCs under C6NP treatment showed a diminished ability to form mammospheres. An increase of ROS was also observed in CSCs treated with C6NP (Figure 3.11B). This data shows promising

generalization of our nanoparticle approach, and the integration of AuNPs-based hypothesis-free sensing and functional NP design could be applied in clinically relevant settings.

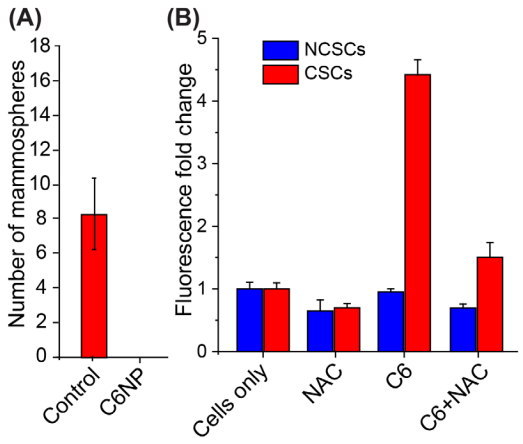

Figure 3.11. Validation of C6NP on CSCs and NCSCs isolated from a patient-derived xenograft using CD24 and CD44 markers. (A) Mammosphere formation assay of CSCs under 100 nM C6NP treatment for 48 hrs. (B) ROS production of CSCs and CSCs un-der 100 nM C6NP treatment. Fluorescence fold change of each treatment group was normalized to its respective cell only control group (NCSCs and CSCs). Only CSCs show an increase in ROS levels (p value of 0.00016) upon receiving C6NP treatment.

3.3.6 Sensitization of CSCs for drug treatment. Direct elimination of CSCs as a therapeutic approach is challenged by the chemo- and radiation resistant nature of these cells.[68] In contrast, differentiation therapy aims to induce CSCs to a less aggressive state, consequentially becoming more susceptible to existing therapies. To evaluate whether epithelial differentiation caused by C6NP has any therapeutic relevance, we assessed the efficacy of a metabolic inhibitor, 2-deoxy-D-glucose (2DG) on CSCs, either alone or in combination with C6NP. Indeed, a non-toxic dose (100 nM) of C6NP significantly potentiated the ability of 2DG to kill CSCs (Figure 3.12A). Furthermore, the combination index (CI) was calculated to quantitatively determine if the cotreatment of C6NP and 2DG had any synergistic effects on CSCs. CI < 1 indicates synergism, while CI = 1 indicates

additivity, and CI > 1 indicates antagonism.[69] Surprisingly, synergy was observed at all tested combinations with CI values ranging from 0.66 to 0.25 (Table 3.2). Interestingly, when tested against NCSCs, no significant change in cell death was seen at the dosages where synergistic elimination of CSCs was observed, suggesting the synergistic killing was specific to CSCs (Figure 3.12B). This finding not only supports the idea of differentiation therapy in solid tumors, but also opens the potential therapeutic applications of nanomaterials in combating CSCs.

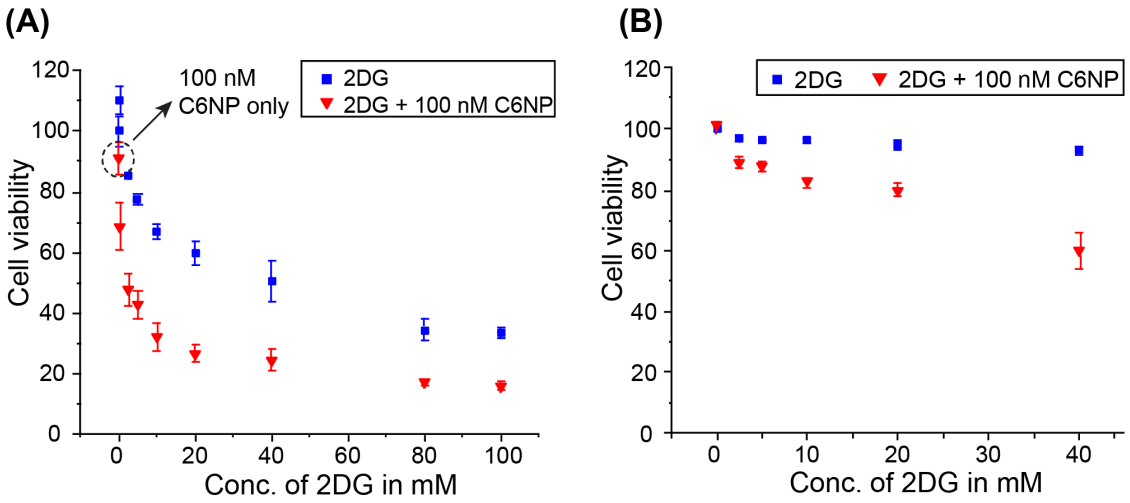

Figure 3.12. IC_{50} of 2DG alone or in combination with C6NP on HMLER-CSCs (A) or NCSCs (B). CSCs or NCSCs were treated with either 2DG or in combination of 100 nM C6NP for 48 hrs. Cells viability was normalized to cell only group without any treatment (n=3). 100 nM C6NP is circled to indicate the non-toxic dosage of C6NP used.

Table 3.2. Quantification of synergy for combination therapy on HMLER-CSCs.

[C6NP] in mM	[2DG] in mM	Killing Effect	Combination Index (CI)
10^{-4}	0.25	0.31	0.66
10^{-4}	2.5	0.52	0.46
10^{-4}	5	0.57	0.45
10^{-4}	10	0.68	0.35
10^{-4}	20	0.73	0.32
10^{-4}	40	0.76	0.33
10^{-4}	80	0.83	0.25
10^{-4}	100	0.84	0.25

3.4 Conclusion

In summary, we report the dual use of AuNPs as therapeutics and as sensors for effecting CSCs differentiation. The precise level of control afforded over nanoparticle structure allows us to systematically investigate the effects of surface chemistry on CSC differentiation. Through coupling with the nanosensor platform, the resulting cell phenotype can be accessed in a matter of minutes, a feature highly desirable for high-throughput and high-content screening. By combining NP engineering and hypothesis-free sensing, we successfully identified a novel phenotype that is more susceptible to traditional chemotherapeutic treatment. The resulting cells presented an increased level of ROS which could be responsible for sensitizing CSCs to drug treatment. Overall, this work comprehensively demonstrates the application of functionalized AuNPs in multiple aspects of screening nanomaterials for CSC differentiation, with significant potential in addressing a key issue in cancer therapy.

3.5 Experimental Section

3.5.1 Nanoparticle Synthesis and Characterization. Gold nanoparticles with a core diameter of 2 nm and ligands were synthesized according to previous reports.[70] In brief, 2 nm AuNPs were synthesized by Brust-Schiffrin two-phase method to obtain pentanethiol covered gold core. Functionalized AuNPs were synthesized through ligand exchange reactions in nitrogen atmosphere followed by multiple washing and dialysis.[42] Detailed characterization can be found in the supporting information.

3.5.2 Fluorescent Protein Expression. EGFP, EBFP, and tdTomato were synthesized and characterized according to reported protocols.[71] In short, Escherichia coli strain BL21 was transformed with plasmids containing corresponding recombinant

proteins. After growth in 2X YT media and induction, cells were lysed and purified by Co^{2+} nitrilotriacetate columns. Fluorescent proteins were further characterized by 12% SDS-PAGE gel, scanning absorbance and emission spectrum. The results are consistent with previously reported work.[37]

3.5.3 Nanoparticle Treatment. CSCs and NCSCs were seeded at a density of 10^4 cells per well on a 96-well microplate for overnight attachment. Before treatment, cells were washed once with phosphate-buffered saline (PBS). 150 μL of media containing 100 nM of each NP were added to cells. After 72 hrs treatment, cells were washed once with PBS before proceeding to sensing studies.

3.5.4 Sensing Studies. Nanosensor was formed by mixing equal molar of BenzNP and FPs (100 nM) in 5mM phosphate buffer for 30 min in dark at room temperature. After sensor was formed, 150 μL of sensor solution was incubated with or without cells in a 96-well plate. The plate was kept in the dark. Fluorescent reading was recorded every 15 min until 45 min, using a SpectraMax M2 plate reader (Molecular Devices, San Jose, CA). The excitation/emission wavelength for each channel is the following: EBFP: 380/450 nm, EGFP: 475/510 nm, tdTomato:550/585 nm.

3.5.5 Linear Discriminant Analysis. Linear discriminant analysis (LDA) was applied on raw fluorescence data to statistically classify each group, using SYSTAT software (version 11.0, Systat Software, Richmond, CA, U.S.A.). All variables were used in the complete mode and the tolerance was set as 0.001. Input data was transformed to canonical scores to best separate each group where the between-class variance was maximized while the within-class variance was minimized. To quantify how different each nanoparticle treatment group is from the control, the F-index was computed in SYSTAT.

Larger values of F-index indicate smaller within-class variance and better between-class separation.[56]

3.5.6 Cell Culture. HMLER cells were prepared by transforming human mammary epithelial cells (HMECs) with SV40 large-T antigen, the telomerase catalytic subunit, and H-Ras and kindly provided by Dr. Weinberg.[29] HMLER cells were stained for integrin β4 and CD24. Cells were then sorted into $CD24^{low}/\beta4^{low}$ and $CD24^{high}/\beta4^{high}$. CD24 antibody was obtained from Biolegend (catalog 311104), β4 antibody was provided by the Dr Rita Falcioni.[72] HMLER, HMLER $CD24^{low}/\beta4^{low}$, and HMLER $CD24^{high}/\beta4^{high}$ were cultured in mammary epithelial cell growth basal medium with BPE, hEGF, Insulin, Hydrocortisone, and GA-1000 (components bought in a kit, Lonza, cc-3150).

3.5.7 Inductively Coupled Plasma Mass Spectrometry (ICP-MS). For ICP-MS experiments, CSCs isolated from HMLER system were seeded in 48-well plate and treated with 100 nM NPs for 3 days. At the end of the treatment, cell supernatant was collected and attached cells were washed twice with PBS before subjecting to lysis buffer (Genlantis) for 30 min. Cells were then transferred into a 15-mL tube and digested with 0.5 mL of aqua regia for 24 hrs, and the sample was then diluted to 10 mL using de-ionized water. Au standard solutions (Perkin Elmer) were prepared prior to each experiment. A Perkin Elmer NEXION 300X ICP mass spectrometer was used for the analysis of samples. Prior to the analysis, daily performance measurements were done to ensure the instrument was operating under optimum conditions. Using the standard mode, ^{197}Au signals were obtained. The RF power for the ICP was 1.6 kW, and the nebulizer gas flow rate was within a range of 0.9–1 L/min. The plasma gas flow rate and auxiliary gas flow rate were 16.5 L/min and 1.4 L/min, respectively. The analog stage voltage and pulse stage for the detector

were −1600 V and 950 V, respectively. The deflector voltage was set to −12 V, and 50 ms was selected for the dwell time during the operation of the ICP-MS.

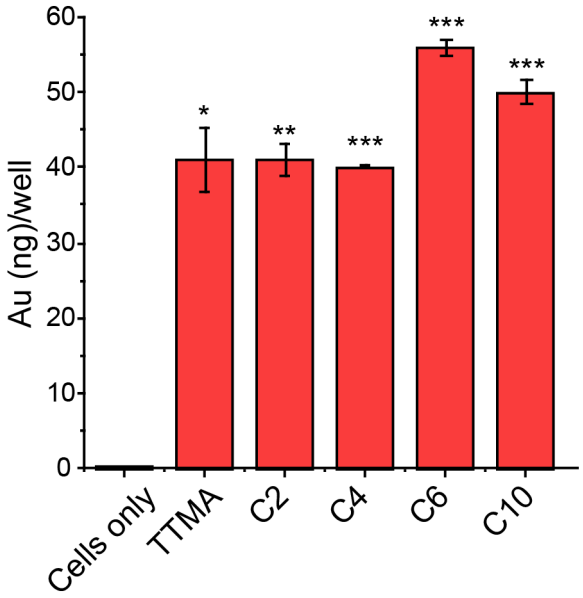

Figure 3.13. Intracellular uptake of AuNPs on HMLER-CSC quantified by ICP-MS. Three biological replicates were used for each treatment group. Gold amount was normalized to a standard calibration curve. Statistical significance was determined by two-tailed student t-test. *= $p < 0.05$, **= $p < 0.01$, ***= $p < 0.001$.

3.5.8 Mammosphere Assay. To generate mammospheres, single-cell suspensions were maintained in mammosphere media as described before[73] in Costar 3471 six-well ultra-low attachment plates at a density of 5×10^3 cells/well. Number of mammospheres were counted and plotted as an average of three independent wells.

3.5.9 Quantitative RT-PCR. mRNA was isolated from cells using the EZ-10 DNAaway RNA Miniprep kit (Biobasic, catalog BS88133-50preps) and cDNA was synthesized using a kit (Azura Genomics, Catalog AZ-1996). RT-PCR was performed in an Applied Biosystems Quantstudio 6 Flex machine. Primer sequences were obtained from the Harvard Primer Bank.[74]

3.5.10 Immunoblotting. HMLER $CD24^{low}/\beta4^{low}$ cells were either treated with 100 nM of C6NP or left untreated for 72 hrs. Cells were lysed using Ripa buffer (Boston Bioproducts BP-115). Lysates were then separated on an 8% SDS-PAGE under reducing conditions. Membrane was blocked using 5% non-fat milk in Tris-Buffered Saline Tween-20 (TBST). Primary antibody was stained overnight (N-cadherin: Abcam, AB7057, 1:1000; Actin: Invitrogen, MA5-11869, 1:1000; Zeb1: Cell Signaling, 3396, 1:1000). Blots were washed three times in TBST before staining with secondary antibody for 2 hrs (Jackson Immunoresearch). Blot was imaged using chemiluminescence.

3.5.11 Patient-derived Xenografts (PDX). PDX tumor established from triple-negative breast cancer patient was dissociated using collagenase. Dissociated cells were passed through cell strainer and washed with PBS twice. Dissociated single cells were plated in presence of FBS for 30 min to remove mouse stromal cells to ensure no cells from the host animal contaminated the PDX cells. The floating cells were immunostained using CD44 and CD24 antibodies (Biolegend, 103006 and 311118 respectively) and FACS sorted into $CD44^{high}/CD24^{low}$ (CSCs) and $CD44^{low}/CD24^{low}$ (NCSCs) sub-populations.

3.5.12 Cell Adhesion Assay. $CD24^{low}/\beta4^{low}$ (CSCs) cells were treated with 100 nM C6NP for 72 h. Treated cells and untreated cells were plated at 40,000 cells per well on laminin 111 and laminin 511 treated tissue culture wells (3 μg of laminin per well). Cells were incubated for 2 hrs, at which time the plate was washed with PBS and stained with crystal violet. Stained plate was read on a DTX880 multimode detector (Beckman Coulter).

3.5.13 ROS Detection. 10^5 cells were washed with Hanks' Balanced Salt Solution (HBSS, Gibco) and pretreated with n-acetyl cysteine (NAC, 10 mM) for 15 min. 100 nM C6NP was then added for 30 min before adding H_2DCFDA (Invitrogen) for another 20

min. After treatment, cells were washed twice with HBSS, suspended in 100 μL of HBSS and read on promega Glomax.

3.5.14 Cell Viability Assay. CSCs and NCSCs were seeded at a density of 10^4 on a 96-well microplate for overnight attachment. The next day, cells either receive 2DG or C6NP or 2DG with 100 nM C6NP. After 2-day incubation, cells were washed once with PBS before adding 150 μL of 10% AlamarBlue solution. The plate was incubated in dark at 37°C for 3 h. 130 μL of supernatant was then transferred to a black plate for fluorescent reading at 560/590 nm.

3.5.15 Synergy Computation. Synergy for each combination dose was calculated according to the Chou-Talalay synergy combination index (CI) metric.[69] Computation was done using CompuSyn software, which is published by Combosyn, Inc. (www.combosyn.com). Synergism is defined when CI is less than 1.

3.6 References

1. J. E. Dick, *Blood* **2008**, *112*, 4793–4807.

2. T. Shibue, R. A. Weinberg, *Nat. Rev. Clin. Oncol.* **2017**, *14*, 611–629.

3. J. Massagué, A. C. Obenauf, *Nature* **2016**, *529*, 298–306.

4. M. A. Nieto, R. Y.-J. Huang, R. A. Jackson, J. P. Thiery, *Cell* **2016**, *166*, 21–45.

5. J. P. Thiery, H. Acloque, R. Y. J. Huang, M. A. Nieto, *Cell* **2009**, *139*, 871–890.

6. J. H. Tsai, J. L. Donaher, D. A. Murphy, S. Chau, J. Yang, *Cancer Cell* **2012**, *22*, 725–736.

7. M. Yu, A. Bardia, B. S. Wittner, S. L. Stott, M. E. Smas, D. T. Ting, S. J. Isakoff, J. C. Ciciliano, M. N. Wells, A. M. Shah, et al., *Science* **2013**, *339*, 580–584.

8. A. Dongre, R. A. Weinberg, *Nat. Rev. Mol. Cell Biol.* **2019**, *20*, 69–84.

9. C. Scheel, R. A. Weinberg, *Semin. Cancer Biol.* **2012**, *22*, 396–403.

10. H. de Thé, *Nat. Rev. Cancer* **2018**, *18*, 117–127.

11. T. R. Breitman, S. E. Selonick, S. J. Collins, *Proc. Natl. Acad. Sci. U. S. A.* **1980**, *77*, 2936–2940.

12. A L. Ades, A. Guerci, E. Raffoux, M. Sanz, P. Chevallier, S. Lapusan, C. Recher, X. Thomas, C. Rayon, S. Castaigne, et al., *Blood* **2010**, *115*, 1690–1696.

13. F. Lo-Coco, G. Avvisati, M. Vignetti, C. Thiede, S. M. Orlando, S. Iacobelli, F. Ferrara, P. Fazi, L. Cicconi, E. Di Bona, et al., *N. Engl. J. Med.* **2013**, *369*, 111–121.

14. K. Chen, Y. Huang, J. Chen, *Acta Pharmacol. Sin.* **2013**, *34*, 732–740.

15. P. B. Gupta, T. T. Onder, G. Jiang, K. Tao, C. Kuperwasser, R. A. Weinberg, E. S. Lander, *Cell* **2009**, *138*, 645–659.

16. E. Sachlos, R. M. Risueño, S. Laronde, Z. Shapovalova, J.-H. Lee, J. Russell, M. Malig, J. D. McNicol, A. Fiebig-Comyn, M. Graham, et al., *Cell* **2012**, *149*, 1284–1297.

17. A. Rahikkala, S. A. P. Pereira, P. Figueiredo, M. L. C. Passos, A. R. T. S. Araújo, M. L. M. F. S. Saraiva, H. A. Santos, *Adv. Biosyst.* **2018**, *2*, 1800020.

18. F. Scaletti, J. Hardie, Y. W. Lee, D. C. Luther, M. Ray, V. M. Rotello, *Chem. Soc. Rev.* **2018**, *47*, 3421–3432.

19. T. Vorup-Jensen, T. Boesen, *Adv. Drug Deliv. Rev.* **2011**, *63*, 1008–1019.

20. R. Das, R. F. Landis, G. Y. Tonga, R. Cao-Milán, D. C. Luther, V. M. Rotello, *ACS Nano* **2019**, *13*, 229–235.

21. Y. Liu, C. Chen, P. Qian, X. Lu, B. Sun, X. Zhang, L. Wang, X. Gao, H. Li, Z. Chen, et al., *Nat. Commun.* **2015**, *6*, 5988.

22. M. Fiorillo, A. F. Verre, M. Iliut, M. Peiris-Pagés, B. Ozsvari, R. Gandara, A. R. Cappello, F. Sotgia, A. Vijayaraghavan, M. P. Lisanti, *Oncotarget* **2015**, *6*, 3553–3562.

23. R. Ayala, C. Zhang, D. Yang, Y. Hwang, A. Aung, S. S. Shroff, F. T. Arce, R. Lal, G. Arya, S. Varghese, *Biomaterials* **2011**, *32*, 3700–3711.

24. B. Valamehr, S. J. Jonas, J. Polleux, R. Qiao, S. Guo, E. H. Gschweng, B. Stiles, K. Kam, T.-J. M. Luo, O. N. Witte, et al., *Proc. Natl. Acad. Sci.* **2008**, *105*, 14459–14464.

25. M. C. Cabrera, R. E. Hollingsworth, E. M. Hurt, *World J. Stem Cells* **2015**, *7*, 27–36.

26. M. R. Carstens, R. C. Fisher, A. P. Acharya, E. A. Butterworth, E. Scott, E. H. Huang, B. G. Keselowsky, *Proc. Natl. Acad. Sci.* **2015**, *112*, 8732–8737.

27. S. A. Mani, W. Guo, M.-J. Liao, E. N. Eaton, A. Ayyanan, A. Y. Zhou, M. Brooks, F. Reinhard, C. C. Zhang, M. Shipitsin, et al., *Cell* **2008**, *133*, 704–715.

28. R. Strauss, J. Bartek, A. Lieber, *Methods Mol. Biol.* **2013**, *1049*, 355–368.

29. B. Elenbaas, L. Spirio, F. Koerner, M. D. Fleming, D. B. Zimonjic, J. L. Donaher, N. C. Popescu, W. C. Hahn, R. A. Weinberg, *Genes Dev.* **2001**, *15*, 50–65.

30. L. Yan, F. Zhao, S. Li, Z. Hu, Y. Zhao, *Nanoscale* **2011**, *3*, 362–382.

31. D. R. Dreyer, S. Park, C. W. Bielawski, R. S. Ruoff, *Chem. Soc. Rev.* **2010**, *39*, 228–240.

32. R. R. Arvizo, O. R. Miranda, D. F. Moyano, C. A. Walden, K. Giri, R. Bhattacharya, J. D. Robertson, V. M. Rotello, J. M. Reid, P. Mukherjee, *PLoS One* **2011**, *6*, e24374.

33. E. C. Dreaden, A. M. Alkilany, X. Huang, C. J. Murphy, M. A. El-Sayed, *Chem. Soc. Rev.* **2012**, *41*, 2740–2779.

34. L. Zhang, F. Gu, J. Chan, A. Wang, R. Langer, O. Farokhzad, *Clin. Pharmacol. Ther.* **2008**, *83*, 761–769.

35. Y. C. Yeh, B. Creran, V. M. Rotello, *Nanoscale* **2012**, *4*, 1871–1880.

36. A. M. Alkilany, C. J. Murphy, *J. Nanoparticle Res.* **2010**, *12*, 2313–2333.

37. P. Ghosh, G. Han, M. De, C. K. Kim, V. M. Rotello, *Adv. Drug Deliv. Rev.* **2008**, *60*, 1307–1315.

38. L. Guerrini, R. Alvarez-Puebla, N. Pazos-Perez, L. Guerrini, R. A. Alvarez-Puebla, N. Pazos-Perez, *Materials (Basel).* **2018**, *11*, 1154.

39. Y. Geng, W. J. Peveler, V. M. Rotello, *Angew. Chem. Int. Ed.* **2019**, *58*, 5190–5200.

40. S. Rana, N. D. B. Le, R. Mout, K. Saha, G. Y. Tonga, R. E. S. Bain, O. R. Miranda, C. M. Rotello, V. M. Rotello, *Nat. Nanotechnol.* **2015**, *10*, 65–69.

41. Y. Geng, H. L. Goel, N. B. Le, T. Yoshii, R. Mout, G. Y. Tonga, J. J. Amante, A. M. Mercurio, V. M. Rotello, *Nanomedicine N. B. M.* **2018**, *14*, 1931–1939.

42. K. Saha, M. Rahimi, M. Yazdani, S. T. Kim, D. F. Moyano, S. Hou, R. Das, R. Mout, F. Rezaee, M. Mahmoudi, et al., *ACS Nano* **2016**, *10*, 4421–4430.

43. D. F. Moyano, M. Goldsmith, D. J. Solfiell, D. Landesman-Milo, O. R. Miranda, D. Peer, V. M. Rotello, *J. Am. Chem. Soc.* **2012**, *134*, 3965–3967.

44. K. Saha, D. F. Moyano, V. M. Rotello, *Mater. Horiz.* **2014**, *1*, 102–105.

45. C.-C. You, O. R. Miranda, B. Gider, P. S. Ghosh, I.-B. Kim, B. Erdogan, S. A. Krovi, U. H. F. Bunz, V. M. Rotello, *Nat. Nanotechnol.* **2007**, *2*, 318–323.

46. Z.-J. Zhu, R. Tang, Y.-C. Yeh, O. R. Miranda, V. M. Rotello, R. W. Vachet, *Anal. Chem.* **2012**, *84*, 4321–4326.

47. T. A. Larson, P. P. Joshi, K. Sokolov, *ACS Nano* **2012**, *6*, 9182–9190.

48. H. L. Goel, T. Gritsko, B. Pursell, C. Chang, L. D. Shultz, D. L. Greiner, J. H. Norum, R. Toftgard, L. M. Shaw, A. M. Mercurio, *Cell Rep.* **2014**, *7*, 747–761.

49. X. Li, H. Kong, R. Mout, K. Saha, D. F. Moyano, S. M. Robinson, S. Rana, X. Zhang, M. A. Riley, V. M. Rotello, *ACS Nano* **2014**, *8*, 12014–12019.

50. N. D. B. Le, G. Yesilbag Tonga, R. Mout, S. T. Kim, M. E. Wille, S. Rana, K. A. Dunphy, D. J. Jerry, M. Yazdani, R. Ramanathan, et al., *J. Am. Chem. Soc.* **2017**, *139*, 8008–8012.

51. W. J. Peveler, R. F. Landis, M. Yazdani, J. W. Day, R. Modi, C. J. Carmalt, W. M. Rosenberg, V. M. Rotello, *Adv. Mater.* **2018**, *30*, 1800634.

52. Z.-J. Zhu, P. S. Ghosh, O. R. Miranda, R. W. Vachet, V. M. Rotello, *J. Am. Chem. Soc.* **2008**, *130*, 14139–14143.

53. P. M. Lanctot, F. H. Gage, A. P. Varki, *Curr. Opin. Chem. Biol.* **2007**, *11*, 373–380.

54. P. R. Srinivas, B. S. Kramer, S. Srivastava, *Lancet Oncol.* **2001**, *2*, 698–704.

55. S. Rana, N. D. B. Le, R. Mout, B. Duncan, S. G. Elci, K. Saha, V. M. Rotello, *ACS Cent. Sci.* **2015**, *1*, 191–197.

56. T. Calinski, J. Harabasz, *Commun. Stat. Theory Methods* **1974**, *3*, 1–27.

57. L. Wilkinson, L. Engelman, J. Corter, M. Coward M. In *Cluster Analysis*. 2009. I-77. Available at http://biostats.unh.edu/Statistics_I_II_III_IV.pdf.

58. C. Chang, H. L. Goel, H. Gao, B. Pursell, L. D. Shultz, D. L. Greiner, S. Ingerpuu, M. Patarroyo, S. Cao, E. Lim, et al., *Genes Dev.* **2015**, *29*, 1–6.

59. M. Diehn, R. W. Cho, N. A. Lobo, T. Kalisky, M. J. Dorie, A. N. Kulp, D. Qian, J. S. Lam, L. E. Ailles, M. Wong, et al., *Nature* **2009**, *458*, 780–783.

60. S. Ding, C. Li, N. Cheng, X. Cui, X. Xu, G. Zhou, *Oxid. Med. Cell. Longev.* **2015**, *2015*, 1–11.

61. A. Chompoosor, K. Saha, P. S. Ghosh, D. J. Macarthy, O. R. Miranda, Z.-J. Zhu, K. F. Arcaro, V. M. Rotello, *Small* **2010**, *6*, 2246–2249.

62. R. Scherz-Shouval, E. Shvets, E. Fass, H. Shorer, L. Gil, Z. Elazar, *EMBO J.* **2007**, *26*, 1749–1760.

63. H. Zhang, R. L. Brown, Y. Wei, P. Zhao, S. Liu, X. Liu, Y. Deng, X. Hu, J. Zhang, X. D. Gao, et al., *Genes Dev.* **2019**, *33*, 166–179.

64. Y. Y. Jang, S. J. Sharkis, *Blood* **2007**, *110*, 3056–3063.

65. H. Jang, J. Yang, E. Lee, J.-H. Cheong, *Arch. Pharm. Res.* **2015**, *38*, 381–388.

66. T. Ezashi, P. Das, R. M. Roberts, *Proc. Natl. Acad. Sci.* **2005**, *102*, 4783–4788.

67. A. R. Ji, S. Y. Ku, M. S. Cho, Y. Y. Kim, Y. J. Kim, S. K. Oh, S. H. Kim, S. Y. Moon, Y. M. Choi, *Exp. Mol. Med.* **2010**, *42*, 175–186.

68. T. Nunes, D. Hamdan, C. Leboeuf, M. El Bouchtaoui, G. Gapihan, T. Nguyen, S. Meles, E. Angeli, P. Ratajczak, H. Lu, et al., *Int. J. Mol. Sci.* **2018**, *19*, 4036.

69. T.-C. Chou, *Cancer Res.* **2010**, *70*, 440–446.

70. G. Y. Tonga, Y. Jeong, B. Duncan, T. Mizuhara, R. Mout, R. Das, S. T. Kim, Y.-C. Yeh, B. Yan, S. Hou, et al., *Nat. Chem.* **2015**, *7*, 597–603.

71. M. De, S. Rana, V. M. Rotello, *Macromol. Biosci.* **2009**, *9*, 174–178.

72. R. Falcioni, A. Sacchi, J. Resau, S. J. Kennel, *Cancer Res.* **1988**, *48*, 816–821.

73. H. L. Goel, B. Pursell, C. Chang, L. M. Shaw, J. Mao, K. Simin, P. Kumar, C. W. Vander Kooi, L. D. Shultz, D. L. Greiner, et al., *EMBO Mol. Med.* **2013**, *5*, 488–508.

74. PrimerBank. https://pga.mgh.harvard.edu/primerbank/ (accessed Apr 29, 2019).

CHAPTER 4

HIGH-CONTENT AND HIGH-THROUGHPUT IDENTIFICATION OF MACROPHAGE POLARIZATION PHENOTYPES

4.1 Abstract

Macrophages are plastic cells of the innate immune system that perform a wide range of immune- and homeostasis-related functions. Due to their plasticity, macrophages can polarize into a spectrum of activated phenotypes. Rapid identification of macrophage polarization states provides valuable information for drug discovery, toxicological screening, and immunotherapy evaluation. The complexity associated with macrophage activation limits the ability of current biomarker-based methods to rapidly identify unique activation states. In this study, we demonstrate the ability of a 2-element sensor array that provides an information-rich 5-channel output to successfully determine macrophage polarization phenotypes in a matter of minutes. The simple and robust sensor generates a high dimensional data array which enables accurate macrophage evaluations in standard cell lines and primary cells after cytokine treatment, as well as following exposure to a model disease environment.

4.2 Introduction

Macrophages are plastic leukocytes that perform a vast range of immune- and homeostasis-related functions, with their function and behavior dictated by environmental stimuli. Macrophages can be characterized as being activated into two major phenotypes, M1 and M2.[1] M1 macrophages are associated with inflammation, including secretion of pro-inflammatory cytokines, engulfment of foreign entities, generation of reactive oxygen

and nitrogen species, and assistance in T-helper type1 (Th1) cell responses to fight infection. Conversely, M2 macrophages perform anti-inflammatory and wound repair functions.[2,3] Disturbance of the mechanisms that govern the balance of M1 and M2 states can result in a number of health problems, including infections, cancer, pregnancy complications, and inflammatory and autoimmune diseases.[4,5] Given the significance and complexity of the roles macrophages play in biology and disease, knowledge of their activation and polarization state can provide critical information regarding the disease microenvironment, and be useful in selecting therapeutic approaches. For example, manipulation of tumor-associated macrophages (TAMs) provides a potential means to combat cancer. The tumor microenvironment releases factors that drive macrophages toward an M2-like phenotype,[6] resulting in secretion of anti-inflammatory cytokines, promotion of tumor growth and invasion, and facilitation of metastases. Therapies are being developed to "re-educate" these TAMs from this immune-suppressing state to an antitumor M1 phenotype as a more effective, less toxic cancer treatment.[7,8] The development of such entities would be facilitated by a means to evaluate macrophage characteristics in a straightforward and high-throughput manner.

Efforts to generate therapies based on macrophage phenotypic conversion (to stimulate immune activation or suppression) and evaluate macrophage immunes responses to other agents in drug discovery and toxicology are challenging due to the complexity of the polarization process. An increasing body of research reveals that macrophage polarization is more intricate than a two-state, M1/ M2 conversion; rather, a spectrum of states exists.[9-,10,11] M2 macrophages can be further subclassified into M2a, M2b, M2c, among others, depending on the activating stimulus and resulting surface markers

displayed.[12] In addition, the macrophage polarization/sub-polarization process is dynamic and can evolve based on changes in the microenvironment.[13-,14,15] Complicating the matter further, macrophages can have mixed or overlapping M1 and M2-associated indicators. For instance, macrophages isolated from patients with advanced gastric and pancreatic cancers show high levels of both pro-inflammatory and anti-inflammatory cytokines. Both sets expressed IL-10 (M2-associated), while the former also had high levels of IL-12, and the latter IL-1β and TNF-α (M1 associated).[16,17] These factors make it challenging to identify macrophage polarization states for diagnostic applications and fundamentally, to understand or identify phenotypes that are relevant to disease states.

Currently, the presence or levels of cellular and/or secreted biomarkers is most commonly used to detect and characterize macrophage polarization.[18,19,12] While providing useful information, this approach is reliant on the specificity of the markers and requires multiple assays to obtain sufficient information for cellular evaluation. Additional limitations include: expression overlap between different polarization states (as mentioned above), poor phenotypic resolution of similar stimuli, non-translatable markers between mice and humans,[12] and the fact that mRNA levels do not necessarily signal a robust difference in protein expression/at the functional level.[19] In addition, the techniques used to identify the presence of biomarkers, such as RT-PCR, Western blot, and flow cytometry, are expensive and not amenable to multiplexing or high-throughput applications. Thus, there is a strong need for a general high-throughput method that can be used to evaluate these cells and their characteristics to facilitate therapeutic design and understand phenotypic responses of macrophages to stimuli.

As an alternative to marker-specific approaches, chemical nose or array-based sensing employs and discerns selective interactions between analytes and sensor elements to generate unique patterns for each analyte. The resulting pattern can be further analyzed for quantitative classification. Once trained, the sensor can rapidly identify analytes based on pattern recognition. This approach has been successfully used in a wide range of systems including mammalian cells,[20-,21,22] bacteria,[23-,24,25] and proteins in biofluids.[26-,27,28] The strategy is ideal for cell phenotyping because changes in cellular responses yield variations in surface composition (e.g., protein, lipids, glycans, etc.) that result in different fingerprints, providing high-content information for each cellular state.[29-,30,31] Because macrophage polarization is accompanied by changes in cellular metabolism and surface protein expression,[1, 12, 32] we hypothesized that an array-based sensing strategy would provide a general platform for discriminating macrophage phenotypic and sub-phenotypic states. Incorporation of this strategy into a multi-channel format would enable multidimensional, high-content output from a single microwell, rendering this method readily applicable to high-throughput screening.[33]

In this paper, we describe the development and application of a polymer-protein supramolecular assembly as a sensor array to gather high-throughput, high-content information on macrophage polarization state. The sensor is composed of only two elements: a guanidine-functionalized cationic poly(oxanorborneneimide) (PONI) polymer, and an anionic green fluorescent protein (GFP). The two entities form a complex through electrostatic interactions, resulting in a Förster resonance energy transfer (FRET) pair. When this sensor is applied to macrophages in different polarization/sub-polarization states, it yields fluorescent signals in five channels. The multidimensional output is then

quantitatively analyzed using linear discriminant analysis (LDA) to reproducibly classify different macrophage activation states (Figure 4.1A). To the best of our knowledge, this combination of sensor elements resulting in a 5-channel output has not been reported previously. We validated the sensor with model macrophage RAW 264.7 cells and primary bone marrow-derived macrophages (BMDMs) stimulated with known M1 and M2 polarizing cytokines. The successful discrimination of M1 and M2 macrophages among the five subtypes demonstrates the ability of the sensor to accurately differentiate subtle phenotypic changes. We further evaluated the efficacy of the sensor system in a model disease environment, where macrophages were cultured in cancer cell-conditioned media, generating distinct patterns for macrophages exposed to different cancer types. Taken together, the sensor platform can classify macrophage phenotypes in a matter of minutes. Furthermore, this platform can read out the effects of subtle environmental changes on macrophages, providing a new tool for diagnostics and for fundamental studies of macrophage behavior. The information generated can provide valuable insights on macrophages in diseases, potentially improving efficiency of existing therapies and facilitating the development of new treatments.

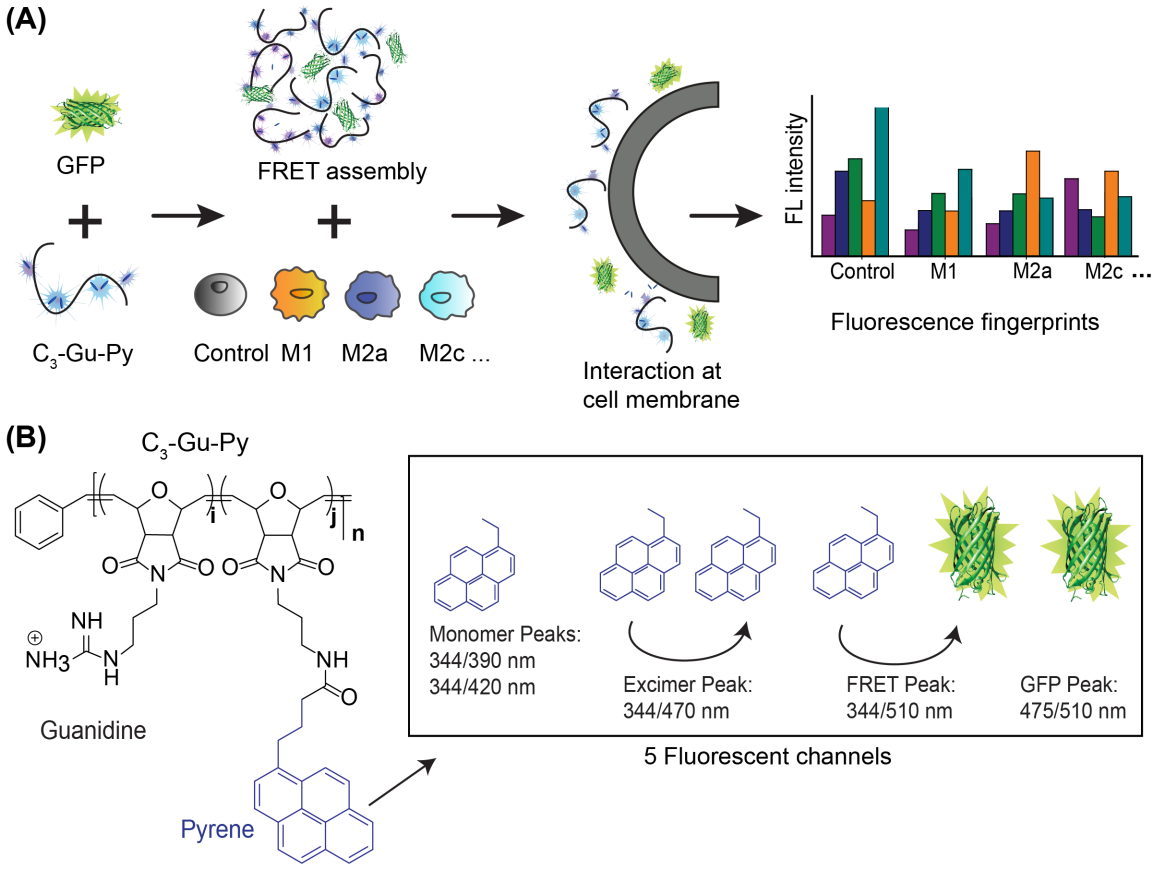

Figure 4.1. Schematic illustration of phenotyping macrophage activation states using array-based sensor. (A) FRET-based sensor assembly was formed between PONI-C_3-Guanidine-Pyrene and GFP. Selective interactions of sensor elements at cell surface membrane resulted in fluorescence changes in all five channels, generating a distinct fingerprint for each cell activation state. (B) Chemical structure of PONI-C_3-Guanidine-Pyrene and the resulting five fluorescence channels in the FRET complex.

4.3 Results

4.3.1 Supramolecular assembly of sensor. The sensor is designed to provide an information-rich, five-channel output with only two sensor elements. The first element of the sensor is a cationic poly(oxanorbornene) (PONI) random copolymer scaffold that incorporates a guanidine group and a pyrene dye molecule (C_3-Gu-Py). The positively charged guanidine group ensures that selective interactions occur only when the complex is close to negatively charged cell surface functionalities. The solvatochromic pyrene

molecule will alter its spectral properties when local environmental factors, such as polarity and hydrophobicity, change.[34] In this way, both selectivity and sensitivity of the sensor are ensured. Through electrostatic interactions, cationic C_3-Gu-Py forms a polymeric complex with an anionic GFP. In practice, the pyrene unit provides three signals, two corresponding to the free pyrene and one to the excimer form. The GFP then adds two channels: free GFP fluorescence and FRET with the two pyrene channels (Figure 4.1B).

Initial studies focused on the optical characterization of the C_3-Gu-Py/GFP supramolecular assembly. Polymer C_3-Gu-Py was titrated with increasing concentrations of GFP. After 30 min of incubation, a simultaneous decrease in pyrene emission at 470 nm and increase of GFP emission at 510 nm was observed upon irradiation with 344 nm light (Figure 4.2A). Efficient fluorescence quenching of C_3-Gu-Py was observed at higher concentrations of assembly (Figure 4.2B). The association constant Ka of 7.17×10^5 M^{-1} was derived by fitting the fluorescent titration curve.

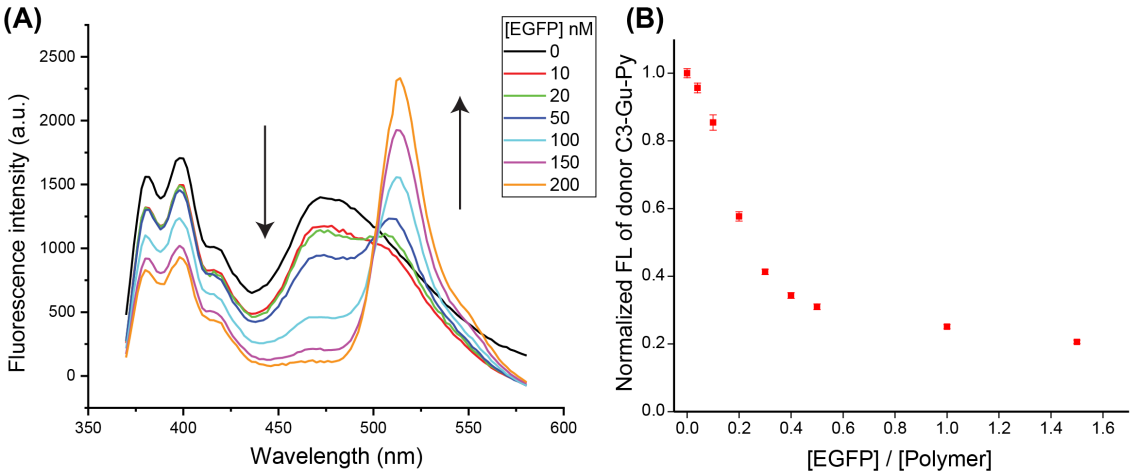

Figure 4.2. Fluorescence titrations (A) and quenching (B) between C_3-Gu-Py and EGFP**.** 0.5 µM C_3-Gu-Py was titrated with varying concentrations of EGFP in 10 mM HEPEs buffer. Fluorescence spectrum was recorded at pyrene excitation of 344 nm. A decrease in pyrene emission at 470 nm and increase of EGFP emission at 510 nm was observed. Each value is the average of three independent measurements.

The overall spectrum featured five distinguished output peaks that can be recorded from the sensor: pyrene monomers at 344/390 and 344/420, pyrene excimer at 344/470, GFP at 475/510, and FRET signal at 344/510. Based on the spectral flexibility, a concentration of 0.5 μM C_3-Gu-Py and 50 nM GFP was selected for the following experiments. Dynamic light scattering data revealed the polymer assembly was ~ 230 nm in diameter and the size slightly increased to ~237 nm when GFP was added. Transmission electron microscopy images confirmed these results, indicating that a supramolecular assembly was formed between C_3-Gu-Py and GFP.

4.3.2 Discrimination of M1 and M2 subtypes using RAW 264.7 cells. We first tested the ability of the sensor system to distinguish among macrophage phenotypes using the RAW 264.7 macrophage cell line. Established cytokines were used to stimulate the cells, with each activating macrophage through a different mechanism (Table 4.1), generating a distinct phenotypic state. RT-PCR results assessing standard M1 and M2 markers confirmed that cells were polarized into corresponding states after 48 h activation (Figure 4.3). LPS and IFN-γ treated cells (M1 stimulation) showed significant increases in TNF-α and iNOS mRNA expression whereas the IL-4 (M2a stimulation) group had an increase in EGR2 and mannose receptor (MR) expression. Similar TNF-α level observed between the combination treatment and the control group could be explained by the prolonged 48 hr activation time, negative regulators such as NFκB and nuclear factor activated T cells,[35,36] greater production of nitric oxide, and the fast turn-over rate of TNF-α.[37] Although the IL-10 group (M2c stimulation) was tested against multiple M2 markers, including EGR2, MR, and TGF-β, as well as the reduction of M1 marker iNOS, no

significant changes in the levels of expression of any associated genes were observed (Figure 4.3B & 4.4).

Table 4.1. Mechanisms and effects of in vitro macrophage polarization of macrophages via different cytokines

Polarization stimulus	Mechanism	Surface marker change	Resulting phenotype
Lipopolysaccharide (LPS)	Binds TLR 4, induces secretion of pro-inflammatory cytokines[38]	Increased expression levels of MHC-II, CD80, CD86; decreased levels of MRC1 or Fc-γ RII[39]	M1
Interferon-γ (IFN-γ)	Binds IFN-γ receptor[40]		
Combo (LPS + IFN-γ)	Synergizes LPS and IFN-γ		
Interleukin 4 (IL-4)	Binds IL-4Rα and IL-2R, down-regulates proinflammatory mediators[1,32]	Decreased expression of CD14 and CCR5;[41] regulation of MHC-II, β2 integrins, chemokine CCL22/MDC[42]	M2a
Interleukin 10 (IL-10)	Deactivates macrophages by inhibiting production of pro-inflammatory cytokines[1]	Down-regulation of MHC II and co-stimulatory molecules[1]	M2c

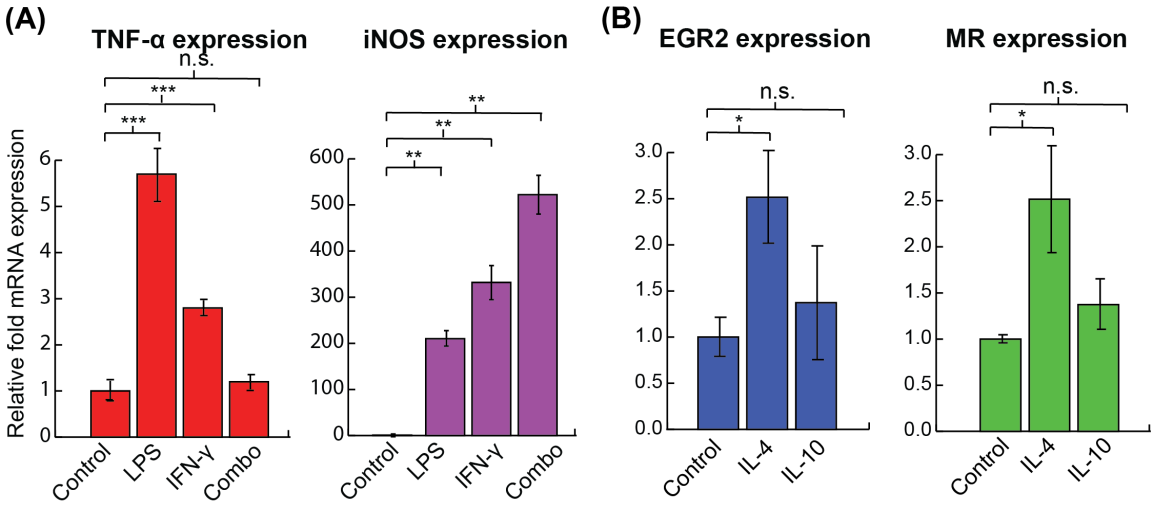

Figure 4.3. RAW 264.7 macrophage activation confirmed by RT-PCR. (A) mRNA quantification of M1-associated genes, TNF-α and iNOS. (B) mRNA quantification of M2-associated genes, EGR2 and MR, according to treatment group. Control = non-treated cells,

combo = LPS + IFN-γ treated. Fold changes in mRNA level were normalized to β-actin. Statistical significance was determined by two-tailed student t-test. *= $p < 0.1$, **= $p < 0.05$, ***= $p < 0.005$, n = 3 biological replicates. n.s. = not significant.

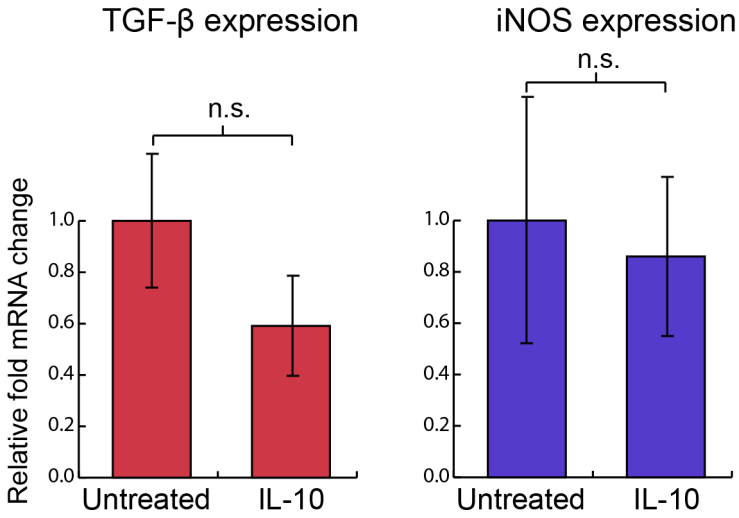

Figure 4.4. RT-PCR quantification of M2 state in IL-10 activated RAW 264.7 macrophages. TGF-β is M2-associated gene. Reduction of M1-associated gene iNOS is used to evaluate M2 state. Control = non-treated cells. Fold changes in mRNA level were normalized to β- actin. Statistical significance was determined by two-tailed student t-test. *= $p < 0.1$, **= $p < 0.05$, ***= $p < 0.005$, n = 3 biological replicates (3 technical replicates were used each). n.s. = not significant.

Having confirmed that polarization had occurred, cells from each treatment group were plated on a 96-well microplate for overnight attachment. Equivalent cell numbers (10,000 per sample) were used to ensure that changes in sensor response were due to alterations in cell surface functionalities, not density. For the sensing process, C_3-Gu-Py and GFP were premixed for 30 min to allow formation of stable FRET complexes. Subsequently, cells were washed once with phosphate buffered saline (PBS) and incubated with the sensor complex in the dark. Fluorescence signals were recorded every 15 min until equilibrium was reached. The 5-channel readout generated a distinct fluorescence pattern for each treatment group (Figure 4.5A). We further utilized linear discriminate analysis

(LDA) to test whether the six cell phenotypes could be robustly discriminated based upon their fluorescent signatures. As shown in Figure 4.5B, the LDA plot revealed six distinct clusters for M1 and M2 subtypes with a correct classification of 100%, demonstrating that each activation pathway resulted in a distinct cellular response. We further validated the reliability of the sensor by performing unknown sample identification and comparing the results against the training set. Among the 45 tested unknowns, 41 samples were predicted correctly into their corresponding group, giving a high percentage of correct unknown identification of 91%. The accuracy of unknown identification can be further improved by increasing the size and complexity of the training set. Next, we investigated the necessity of having 5 channels of information from the sensor by comparing the performance of classification and unknown identification using either an individual sensor element or different combinations. The highest percentage of accuracy was achieved when all 5 channels were used, demonstrating the importance of multidimensional data in discriminating complex cell phenotypes (Figure 4.5C).

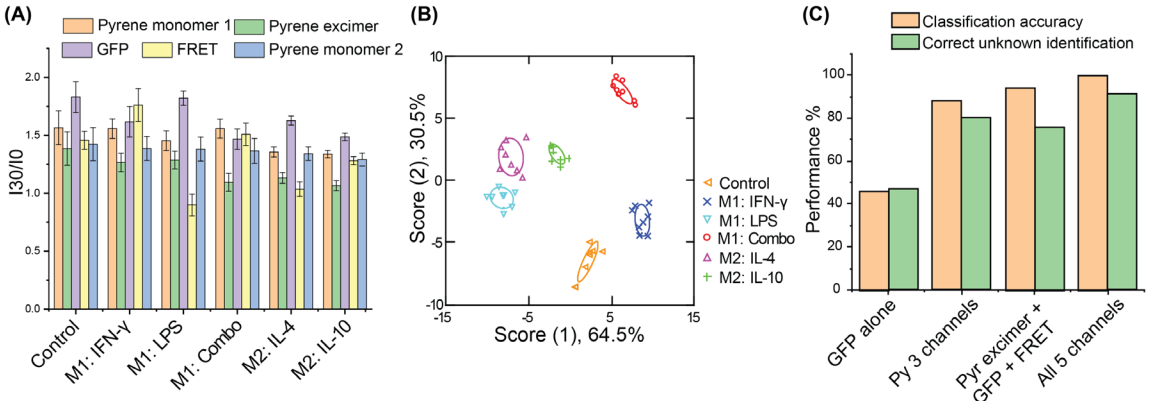

Figure 4.5. Discrimination of RAW 264.7 macrophages activated by M1 or M2 subtype stimuli using sensor complexes. (A) Fluorescence intensities of each treatment group were obtained at 30 min and normalized against sensor only. n = 8 biological replicates. (B) The fluorescence patterns were analyzed through linear discriminant analysis (LDA) and the first two canonical scores were plot-ted with 95% confidence ellipse (n=8). (C) Correct classification percentage and unknown identification of M1 and M2 sub-types using different combinations of sensor channels.

4.3.3 Discrimination of M1 and M2 subtypes with primary macrophages. Immortalized macrophage cell lines provide a useful tool for assessing sensor response, however, these models differ in multiple aspects from their primary cell analogs. We next tested the sensor using physiologically relevant primary bone marrow-derived macrophages (BMDM). Progenitor cells were isolated from C57/B6 mice and induced to differentiate into macrophages using previously reported procedures.[43] Once macrophage cells were obtained, we exposed them to M1 and M2 subtype polarization stimuli for 48 h as used above for RAW 264.7 cells. RT-PCR results confirmed appropriate activations in each case, with increases in TNF-α and iNOS mRNA expression for M1 related stimuli (LPS and/or IFN-γ) and EGR2 and MR mRNA levels for IL-4 stimulated M2 cells. Although IL-10 activation did not show substantial enhancement in EGR2 level, a nearly 6-fold increase in MR expression was observed (Figure 4.6). Following macrophage polarization, similar sensor procedure was performed. The fluorescence patterns observed were distinct from those of the RAW cells, suggesting differences exist in the two cell models. Complete discrimination among the five assessed groups of M1 and M2 phenotypes was achieved with 96% correct classification (Figure 4.7). 92% of correct unknown identification confirmed the high reliability of our sensor.

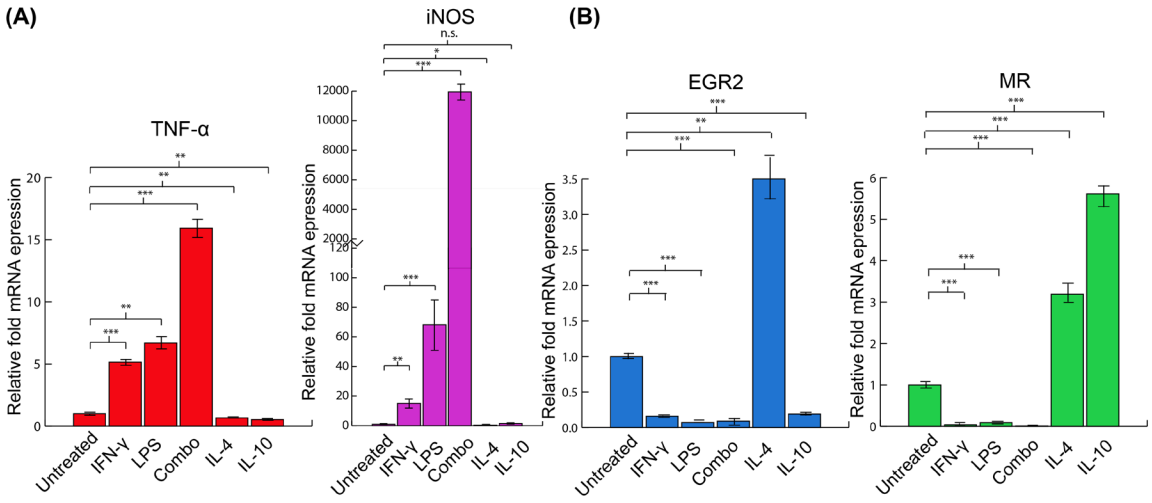

Figure 4.6. RT-PCR quantification activated primary bone marrow-derived macrophages. (A) mRNA quantification of M1-associated genes, TNF-α and iNOS. (B) mRNA quantification of M2-associated genes, EGR2 and MR, according to treatment group. Control = non-treated cells; combo = cells treated with both IFN-γ and LPS. Fold changes in mRNA level were normalized to β-actin. *= $p < 0.1$, **= $p < 0.05$, ***= $p < 0.005$, n = 3 biological replicates (3 technical replicates were used each). n.s. = not significant.

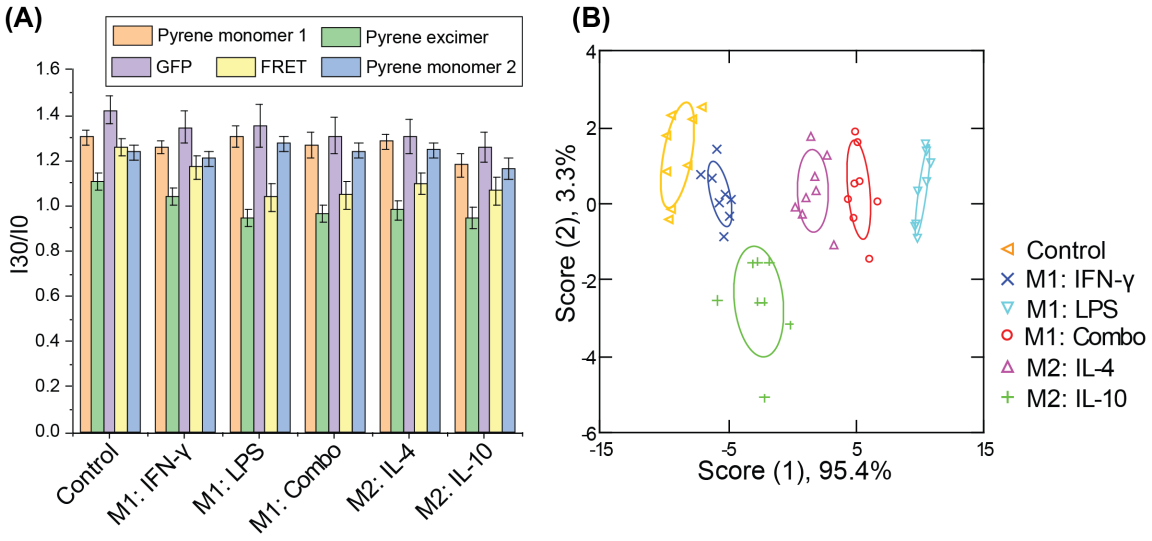

Figure 4.7. Discrimination of M1 and M2 subtypes of bone marrow-derived macrophages. (A) Fluorescence signals of the five sensor channels were obtained and normalized to sensor only. n = 8 biological replicates. (B) LDA plot of the first two canonical scores was plotted with 95% confidence ellipse (n=8).

When the sensor complex interacts with cells, in most cases, all monitored fluorescence channels showed an increase in signal intensity. This suggests that upon interacting with macrophages, the sensor complex disaggregates, exposing its individual components to interact with the cell surface. Depending upon the local environment, the fluorescence intensities for individual molecules (pyrene, GFP, and FRET) also change. Since distinct fluorescence patterns were consistently observed for each stimulus, we believe this disruption process is modulated by cell surface functionalities and composition. Our previous studies have indicated that the sensor complex is highly sensitive to glycosylation patterns on cell surfaces.[30] However, more mechanistic studies are needed in order to elucidate which other cell components are also interacting with sensor elements.

4.3.4 Discrimination of macrophages exposed to conditioned media from different cancer cells. The above studies demonstrate that our sensor array was able to discriminate macrophages polarized with specific cytokines. However, biological microenvironments are often far more complex and have multiple stimuli. Hence, we assessed whether the sensor could discern macrophage phenotype in a model disease environment to address this issue. First, conditioned media was generated by culturing different types of cancer cells (HeLa, cervical carcinoma, and MCF7, mammary carcinoma) until ~80% confluency was reached. Then, the culture media was extracted and used to stimulate macrophages for 48 h. RT-PCR results revealed different activation patterns for macrophages activated with media conditioned from different cell lines (Figure 4.8). C_3-Gu-Py and GFP complexes were added to cells and the 5-channel fluorescence readouts were collected.

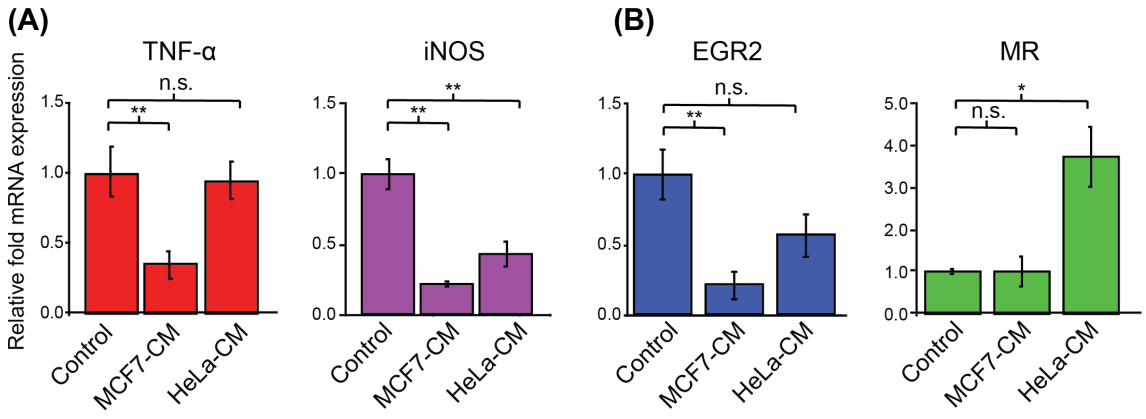

Figure 4.8. RT-PCR quantification macrophages exposed to conditioned media from different cancer cells. (A) mRNA quantification of M1-associated genes, TNF-α and iNOS. (B) mRNA quantification of M2-associated genes, EGR2 and MR. Control = non-treated cells. MCF7-M and HeLa-M = conditioned media from MCF7 and HeLa cells, respectively. Fold changes in mRNA level were normalized to β-actin. *= $p < 0.1$, **= $p < 0.05$, ***= $p < 0.005$, n = 3 biological replicates (3 technical replicates were used each). n.s. = not significant.

Distinct fluorescence signals were obtained for macrophages subjected to each of the conditioned media types. An LDA plot showed three well-separated clusters with 100% classification accuracy (Figure 4.9). When macrophages were exposed to cultured media conditioned by cervical cancer versus breast cancer cells, the sensing readout was dramatically different, indicating that a unique state of activation was present following each type of stimulation. A high percentage (96%) of correct unknown identification was also achieved. These results are exciting because it demonstrates that this method not only functions following single cytokine stimulation, but also in more complex environments. This is promising evidence that with careful evaluation, this sensing method could be applied to profile macrophages from individual patients, offering insights for precision medicine.

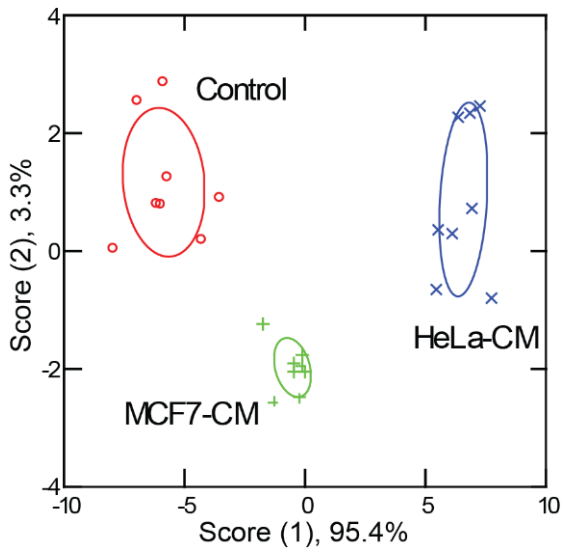

Figure 4.9. Discrimination of macrophage cells cultured under exposure to conditioned media from different cancer cell types for 48 h. The LDA plot of the first two canonical scores was obtained and plotted with 95% confidence ellipses (n=8). CM is cancer cell conditioned medium, with the cell line type preceding it, control represent macrophages cultured using standard growth media.

4.4 Discussion

The Macrophage polarization is a complex and dynamic process. With its roles in homeostasis and disease, it is important to be able to discern macrophages characteristics in a rapid and straight-forward manner. Compared with current methods of characterizing macrophage polarization, the sensor reported in this study has advantages of generating a multidimensional and high-content chemical readout regarding the cell surface in a high-throughput matter. Standard methods, such as RT-PCR and ELISA, can only capture a limited number of well-established markers for each cell activation state, and are independent (not multiplexed) assays, requiring a separate analysis for each. Considering the heterogeneity of macrophage polarization and the overlapping nature of M1 and M2 markers,[11,12] it is also difficult to elucidate and differentiate activation states with standard

methods. For instance, the multiple IL-10 markers used in our RT-PCR studies did not reveal significant changes. The ambiguity of a less-well characterized sub-phenotype could be because the end-point evaluation missed the dynamic changes on the macrophage marker expression during the 48 h activation.

In contrast, the array-based sensor utilizes selective interactions between sensor elements and the entire analyte surface to generate high-content fingerprints for each activation state. Once trained, the sensor can rapidly identify target analytes through pattern recognition. Although the C_3-Gu-Py moiety has been utilized for bacterial sensing,[44] its capability in mammalian cell sensing has not been investigated. By coupling the polymer with simple GFP through supramolecular interactions, sensor can discern less-characterized sub-phenotypes, such as IL-10 stimulated macrophages, which are challenging to identify using traditional methods like RT-PCR (Figure 4.5 & 4.7). The 5-channel, high-content information gathered from the sensor is crucial in achieving a high level of classification accuracy and it allows us to address challenging biological questions from a chemical perspective. In addition, running assays like RT-PCR and ELISA can be time-consuming and error prone, with relatively high costs for thorough characterizations consisting of multiple markers. In contrast, the sensor material used here is synthetically easy to generate, and all components can be mixed in one microplate well, which not only reduces sensor material but is also compatible for high-throughput screening applications. What is more, accurate phenotyping can be obtained in less than an hour, making this method simple, robust, and rapid.

Due to the robust and facile nature of the system, there are many potential applications for the array-based sensing strategy. Altered immune states are a major factor

in diseases including cancer, atherosclerosis, and auto-immune disorders.[45 -, 46 , 47] Macrophage polarization states are key in driving forward disease progression. Rapid assessment of their activation states can provide valuable information in selecting appropriate therapeutic strategies.[48,49] Notably, the high-throughput nature of the method would facilitate the rapid screening of immune states for individual patients, enabling personalized medicinal approaches in tackling these immune-driven diseases. Furthermore, this strategy could be applied to other plastic immune cells, such as dendritic cells and T cells.[50,51] By extending this sensor to other cell types, the status of major components of the immune system could be rapidly determined. This strategy can also greatly improve the drug discovery process, by allowing for rapid identification of altered cell states, and/or evaluation of immunogenicity following agent treatment.[52] Potential immune adjuvants or anti-inflammatory entities could be screened together by using the sensor on immune cells in a multi-well plate format. With these capabilities, the sensor system not only has utility as a fundamental research tool, but as a high-throughput, high-content means for therapeutic screening against general plastic cell types.

4.5 Conclusion

In summary, we demonstrate the use of a simple and robust chemical system that can quickly capture the overall responses of activated macrophages in a high-throughput format, which is challenging with biomolecular tools. Through the supramolecular assembly of only two elements, a 5-channel output is achieved. The high level of information density enables us to accurately profile a spectrum of activation state of macrophages. The ability to use chemical entities to answer biological questions opens the doors for sensing and beyond.

4.6 Experimental Section

4.6.1 PONI-C$_3$-guanidine polymer synthesis. Monomers and polymers were synthesized according to previous reports.[53] Detailed synthetic scheme can be found in the supporting information.

4.6.2 Dynamic light scattering (DLS). The hydrodynamic diameter of polymer and polymer-GFP complex were measured at 25 °C in 10 mM HEPEs buffer using a Malvern Zetasizer Nano ZS instrument. The measurement angle was 173° (backscatter). All samples were pre-incubated in DLS/zeta cuvette for 30 seconds at room temperature. The plots showed below were the average of three individual measurements.

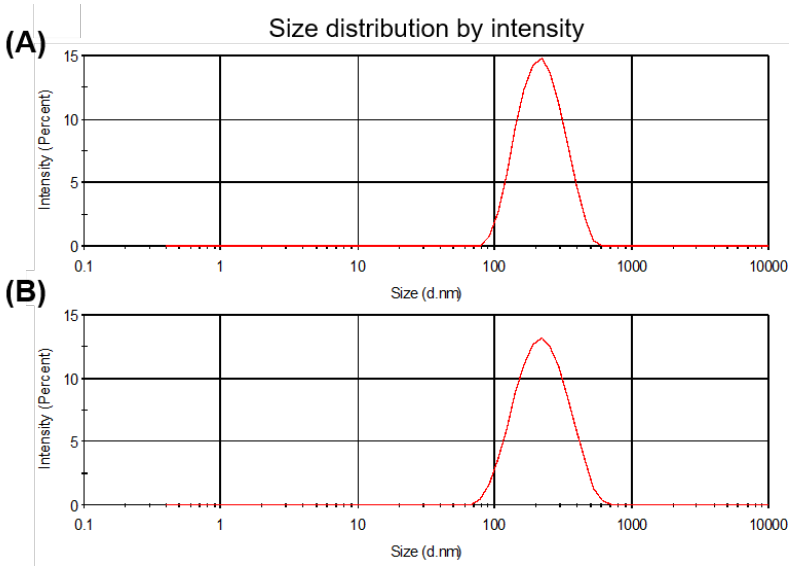

Figure 4.10. Hydrodynamic size of PONI-C$_3$-Gu-Py polymer (A) and polymer-GFP assembly (B) in 10mM HEPEs buffer. C$_3$-Gu-Py polymer formed a complex with an average diameter of 230 ± 84.4 nm. With the addition of EGFP, the size of polymer-EGFP assembly is approximately 237 ± 97.7 nm in diameter.

4.6.3 Transmission electron microscopy (TEM). TEM samples were prepared by either 0.5 μM of C3-Gu-Py only or mixing 0.5 μM of C3-Gu-Py with 50 nM of GFP in 10 mM HEPES buffer for 30 min in dark at room temperature. 5 μL of the solutions were then

placed on 300 mesh Copper grids (with formvar films) obtained from Electron Microscopy Sciences (EMS FF300-Cu) and allowed to dry overnight. The samples were analyzed using a TEM JOEL 2000FX at an acceleration voltage of 200kV.

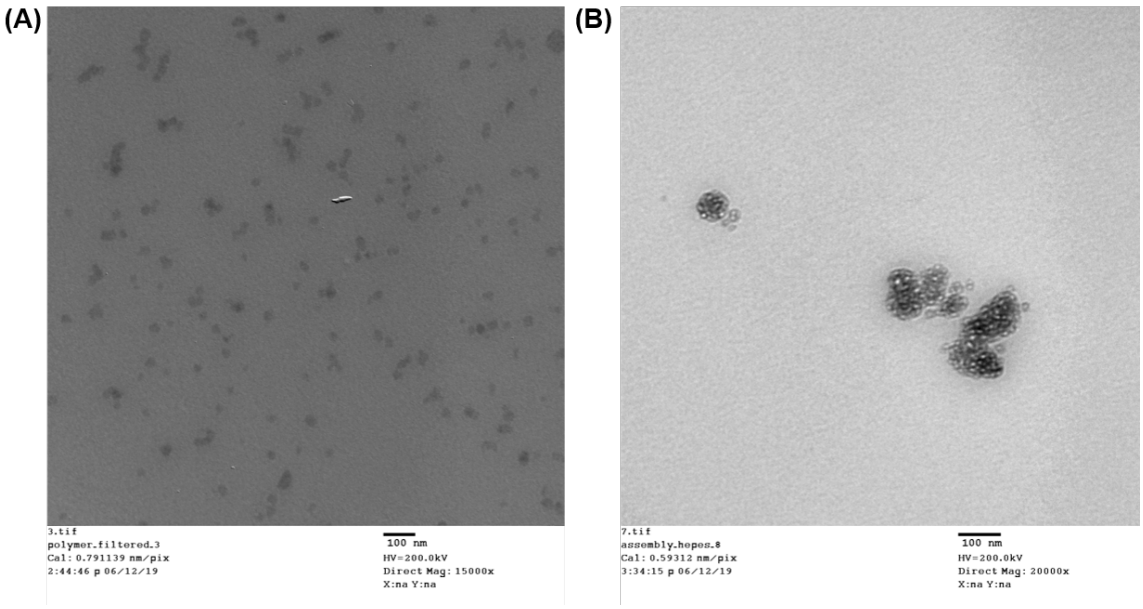

Figure 4.11. TEM image of PONI-C_3-Gu-Py polymer (A) and polymer-EGFP assembly (B) in 10 mM HEPEs buffer. C3-Gu-Py polymer formed a complex of size ~25 nm. The difference in sizes measured by DLS and TEM can be attributed to the drying process during TEM sample preparation as well as the high vacuum conditions in the TEM chamber. Upon the addition of EGFP, larger complexes were observed.

4.6.4 Green fluorescent protein expression. GFP was constructed and characterized according to reported protocols.[54] In short, Escherichia coli strain BL21 was transformed with plasmids containing GFP recombinant protein. After transformation and induction with IPTG, cells were lysed and purified by Co^{2+} nitrilotriacetate columns. Fluorescent proteins were further characterized by SDS-PAGE gel, scanning absorbance and emission spectrum. The results are consistent with previously reported work.[30]

4.6.5 Fluorescent titration. 0.5 μM C_3-Gu-Py polymer was titrated with GFP at a concentration range from 0 to 200 μM in a black 96 well-microplate. The solution was

mixed in 10 mM HEPEs buffer. After 30 min incubation at room temperature in dark, the fluorescence spectrum was measured at an excitation wavelength of 344 nm.

4.6.6 Binding affinity calculation. Fluorescence titration was utilized to calculate the binding affinity of the C_3-Gu-Py polymer with GFP. The fluorescence decay of the C_3-Gu-Py excimer as a function of GFP concentration was fitted to a one-site binding equation,[55] which is:

$$I = I_0 + (\frac{I_{lim} - I_0}{2C_0}) \times \left[(C_0 + C + \frac{1}{K}) - \sqrt{(C_0 + C + \frac{1}{K})^2 - 4CC_0} \right]$$

where I is the fluorescence intensity of C3-Gu-Py excimer at a given concentration of GFP, I0 is the fluorescence intensity of C_3-Gu-Py in the absence of GFP, I_{lim} is the fluorescence intensity when the quenching reaches a plateau, C0 refers to the concentration of C_3-Gu-Py, and C is the concentration of GFP. Based on the equation, microscopic binding constant K was determined by using the non-linear least-squares curve fitting analysis in OriginPro (OriginLab Co., Northampton, USA).

4.6.7 Linear discriminant analysis (LDA). LDA was applied on normalized fluorescence data to statistically classify each group, using SYSTAT software (version 11.0, SystatSoftware, Richmond, CA, U.S.A.). All variables were used in the complete mode and the tolerance was set as 0.001. Input data was transformed to canonical scores to best separate each group where the between-class variance was maximized while the within-class variance was minimized. After transformation, LDA reduces the high dimension data to a lower dimension. The 2D plot pictorially shows where each data point lies in the new dimensional space. Therefore, the positive and negative values on the axis do not have any physiologically meaning other than a set of axes that separate out the input data.

4.6.8 Unknown identification. The identity of unknown samples was predicted by computing the Mahalanobis distance of the unknown data to the training groups using LDA. [56] First, the normalized fluorescence responses of the unknown samples were converted to canonical scores in LDA, using the discriminant functions established from the reference set. Next, Mahalanobis distance of that case to the centroid of each training cluster in the LDA space was computed.[56,57] The unknown sample was predicted to belong to the closest group, defined by the shortest Mahalanobis distance.

4.6.9 Cell culture. RAW 264.7 cells, HeLa and MCF7 cell lines were purchased from American Type Culture Collection (ATCC, Manassas, VA). Primary bone marrow derived macrophages (BMDMs) were isolated from freshly euthanized C57/B6 mice, donated generously by Dr. Jessie Mager, Department of Veterinary and Animal Science, University of Massachusetts Amherst. The BMDMs were isolated, differentiated and cultured according to previously reported methods.[43] All cells were cultured at 37 °C under a humidified atmosphere containing 5% CO_2. Standard growth media consisted of high glucose Dulbecco's Modified Eagle Medium (DMEM) supplemented with 10% fetal bovine serum (FBS) and 1% antibiotics (100 µg/ml penicillin and 100 µg/ml streptomycin). Under the above culture conditions, the cells were sub-cultured approximately once every two to five days.

4.6.10 Macrophage polarization via activation agents. Both RAW 264.7 cells and BMDMs were treated with the following polarization stimuli for 48 hours to induce the desired polarization state. LPS group: 50 ng/mL, IFN-γ group: 50 ng/mL, Combo group: 50 ng/mL LPS and IFN-γ, IL-4 group: 30 ng/mL, and IL-10 group: 30 ng/mL. After

2-day polarization, cells were washed with PBS, trypsinized, and plated as 10,000 cells per well on a 96-well plate overnight before proceeding to sensing studies.

4.6.11 Macrophage polarization via cancer cell conditioned media. HeLa and MCF7 cell lines were cultured under DMEM medium supplemented with 10% FBS and 1% antibiotics for 2 days to reach above 90% confluency. The supernatant from each cell line was then collected and centrifuged for 5 minutes. Subsequently, 5 mL of the supernatant was transferred into a T25 culture flask containing RAW cells. After 48 hours of culture, RAW 264.7 cells were washed with PBS, trypsinized and plated as 10,000 cells per well on a 96-well plate for overnight attachment.

4.6.12 Sensing studies. The sensor was prepared by mixing 0.5 μM of C_3-Gu-Py with 50 nM of GFP in 10 mM HEPES buffer for 30 minutes in dark at room temperature. Subsequently, 150 μL of sensor solution was incubated with and without the cell populations (washed once with PBS) in 96-well microplates. The change in fluorescence intensity for each channel was recorded every 15 minutes at its respective wavelength (pyrene monomer: 344/390 nm and 344/420 nm, pyrene excimer: 344/470 nm, GFP: 475/510 nm, FRET: 344/510 nm) on a Molecular Devices SpectraMax M2 microplate reader using appropriate filters.

4.6.13 RT-PCR preparation. Cells were plated in 24-well plates at a density of 50,000 cells/well. Cells were treated with the appropriate polarization stimulus for 48 h. Following treatments, RNA was extracted following the procedure below.

4.6.14 RNA extraction and cDNA conversion. Approximately 1.5 μg RNA was harvested using the PureLink RNA Mini Kit (Ambion) following the manufacturer's instructions. SuperScript IV Reverse Transcriptase was used for the conversion of

approximately 150 ng of RNA to cDNA, along with RNaseOut, 10 mM dNTPs, and 50 μM Random Hexamers (ThermoFisher, Pittsburgh, PA), also following the manufacturer's instructions.

4.6.15 RT-PCR Preparation. Cells were plated in 24-well plates at a density of 50,000 cells/well. Cells were treated with the appropriate polarization stimulus for 48 hr. Following treatments, RNA was extracted following the procedure below.

4.6.16 Quantitative RT-PCR. RT-PCR was performed on cDNA as prepared above using a CFX Connect real-time system with iTaq Universal SYBR Green Supermix (Biorad, Hercules, CA). All DNA primers were purchased from Integrated DNA Technologies (Caralville, Iowa). The following primer sequences were used:

β-actin (forward) GATCAGCAAGCAGGAGTACGA,

β-actin (reverse) AAAACGCAGCGCAGTAACAGT;

iNOS (forward) GTTCTCAGCCCAACAATACAAGA,

iNOS (reverse) GTGGACGGGTCGATGTCAC;

TNF-α (forward) CCTGTAGCCCACGTCGTAG,

TNF-α (reverse) GGGAGTCAAGGTACAACCC;

EGR2 (forward) TGAGAGAGCAGCGATTGATT,

EGR2 (reverse) ATAACAGTCAGTGTGTCCCC;

Mannose Receptor (forward) GGATGTTGATGGCTACTGGA,

Mannose Receptor (reverse) AGTAGCAGGGATTTCGTCTG;

TGF-β (forward) GCGGACTACTATGCTAAAGA,

TGF-β (reverse) TTCTCATAGATGGCGTTGTT.

Analyses were performed as follows: the samples were first activated at 50 °C for 2 min, then 95 °C for 2 min. Then denaturing occurred at 95 °C for 30 s followed by annealing at 57 °C; the denature/anneal process was repeated over 40 cycles. Relative gene expression was determined by comparing the C_t value of the gene of interest to that of the β-actin housekeeping gene, by the $2^{\Delta\Delta Ct}$ method.[58] Three biological replicates were performed for each control group and three technical replicates were used for each biological replicate.

4.7 References

1. F. O. Martinez, A. Sica, A. Mantovani, M. Locati, *Front. Biosci.* **2008**, *13*, 453–461.

2. P. J. Murray, J. E. Allen, S. K. Biswas, E. A. Fisher, D. W. Gilroy, S. Goerdt, S. Gordon, J. A. Hamilton, L. B. Ivashkiv, T. Lawrence, et al., *Immunity* **2014**, *41*, 14–20.

3. F. O. Martinez, S. Gordon, *F1000Prime Rep.* **2014**, *6*, 13.

4. A. Shapouri-Moghaddam, S. Mohammadian, H. Vazini, M. Taghadosi, S.-A. Esmaeili, F. Mardani, B. Seifi, A. Mohammadi, J. T. Afshari, A. Sahebkar, *J. Cell. Physiol.* **2018**, *233*, 6425–6440.

5. Y.-C. Liu, X.-B. Zou, Y.-F. Chai, Y.-M. Yao, *Int. J. Biol. Sci.* **2014**, *10*, 520–529.

6. R. Ostuni, F. Kratochvill, P. J. Murray, G. Natoli, *Trends Immunol.* **2015**, *36*, 229–239.

7. C. Belgiovine, M. D'Incalci, P. Allavena, R. Frapolli, *Cell. Mol. Life Sci.* **2016**, *73*, 2411–2424.

8. M. Wenes, M. Shang, M. Di Matteo, J. Goveia, R. Martín-Pérez, J. Serneels, H. Prenen, B. Ghesquière, P. Carmeliet, M. Mazzone, *Cell Metab.* **2016**, *24*, 701–715.

9. J. Xue, S. V. Schmidt, J. Sander, A. Draffehn, W. Krebs, I. Quester, D. De Nardo, T. D. Gohel, M. Emde, L. Schmidleithner, et al., *Immunity* **2014**, *40*, 274–288.

10. R. M. Ransohoff, *Nat. Neurosci.* **2016**, *19*, 987–991.

11. B.-Z. Qian, J. W. Pollard, *Cell* **2010**, *141*, 39–51.

12. A. Mantovani, A. Sica, S. Sozzani, P. Allavena, A. Vecchi and M. Locati, *Trends Immunol.* **2004**, *25*, 677–686.

13. E. Mathew, A. L. Brannon, A. C. Del Vecchio, P. E. Garcia, M. K. Penny, K. T. Kane, A. Vinta, R. J. Buckanovich, M. P. di Magliano, *Neoplasia* **2016**, *18*, 142–151.

14. C. Auffray, D. Fogg, M. Garfa, G. Elain, O. Join-Lambert, S. Kayal, S. Sarnacki, A. Cumano, G. Lauvau, F. Geissmann, *Science (80-.).* **2007**, *317*, 666–670.

15. A. Fernandez, M. Vermeren, D. Humphries, R. Subiros-Funosas, N. Barth, L. Campana, A. MacKinnon, Y. Feng, M. Vendrell, *ACS Cent. Sci.* **2017**, *3*, 995–1005.

16. H. Sugai, K. Kono, A. Takahashi, F. Ichihara, H. Kawaida, H. Fujii, Y. Matsumoto, *J. Surg. Res.* **2004**, *116*, 277–287.

17. O. Helm, J. Held-Feindt, E. Grage-Griebenow, N. Reiling, H. Ungefroren, I. Vogel, U. Krüger, T. Becker, M. Ebsen, C. Röcken, et al., *Int. J. Cancer* **2014**, *135*, 843–861.

18. G. A. Duque and A. Descoteaux, *Front. Immunol.* 2014, **5**.

19. C. A. Ambarus, S. Krausz, M. van Eijk, J. Hamann, T. R. D. J. Radstake, K. A. Reedquist, P. P. Tak, D. L. P. Baeten, *J. Immunol. Methods* **2012**, *375*, 196–206.

20. Y. Geng, H. L. Goel, N. B. Le, T. Yoshii, R. Mout, G. Y. Tonga, J. J. Amante, A. M. Mercurio and V. M. Rotello, *Nanomedicine N. B. M.* **2018**, *14*, 1931-1939.

21. L. Wu, H. Ji, Y. Guan, X. Ran, J. Ren, X. Qu, *NPG Asia Mater.* **2017**, *9*, e356–e356.

22. X. Yang, J. Li, H. Pei, Y. Zhao, X. Zuo, C. Fan, Q. Huang, *Anal. Chem.* **2014**, *86*, 3227–3231.

23. X. Li, H. Kong, R. Mout, K. Saha, D. F. Moyano, S. M. Robinson, S. Rana, X. Zhang, M. A. Riley and V. M. Rotello, *ACS Nano* **2014**, *8*, 12014–12019.

24. J. R. Carey, K. S. Suslick, K. I. Hulkower, J. A. Imlay, K. R. C. Imlay, C. K. Ingison, J. B. Ponder, A. Sen, A. E. Wittrig, *J. Am. Chem. Soc.* **2011**, *133*, 7571–7576.

25. Y. Tao, X. Ran, J. Ren, X. Qu, *Small* **2014**, *10*, 3667–3671.

26. Z. Pode, R. Peri-Naor, J. M. Georgeson, T. Ilani, V. Kiss, T. Unger, B. Markus, H. M. Barr, L. Motiei, D. Margulies, *Nat. Nanotechnol.* **2017**, *12*, 1161–1168.

27. D. Zamora-Olivares, T. S. Kaoud, K. N. Dalby, E. V. Anslyn, *J. Am. Chem. Soc.* **2013**, *135*, 14814–14820.

28. L. Motiei, Z. Pode, A. Koganitsky, D. Margulies, *Angew. Chemie Int. Ed.* **2014**, *53*, 9289–9293.

29. Y. Tao, M. Li, D. T. Auguste, *Biomaterials* **2017**, *116*, 21–33.

30. S. Rana, N. D. B. Le, R. Mout, B. Duncan, S. G. Elci, K. Saha and V. M. Rotello, *ACS Cent. Sci.* **2015**, *1*, 191–197.

31. Y. Geng, W. J. Peveler and V. M. Rotello*, Angew. Chemie Int. Ed.* **2019**, *58*, 5190–5200.

32. F. O. Martinez, L. Helming, S. Gordon, *Annu. Rev. Immunol.* **2009**, *27*, 451–483.

33. S. Rana, N. D. B. Le, R. Mout, K. Saha, G. Y. Tonga, R. E. S. Bain, O. R. Miranda, C. M. Rotello and V. M. Rotello, *Nat. Nanotechnol.* **2015**, *10*, 65–69.

34. A. S. Klymchenko, *Acc. Chem. Res.* **2017**, *50*, 366–375.

35. H. T. Idriss and J. H. Naismith, *Microsc. Res. Tech.* **2000**, *50*, 184–195.

36. N. Parameswaran and S. Patial, *Crit. Rev. Eukaryot. Gene Expr.* **2010**, *20*, 87–103.

37. F. Held, E. Hoppe, M. Cvijovic, M. Jirstrand and J. Gabrielsson, *J. Pharmacokinet. Pharmacodyn.* **2019**, *46*, 223–240.

38. Wan, Y. Shan, Y. Fan, C. Fan, S. Chen, J. Sun, L. Zhu, L. Qin, M. Yu and Z. Lin, *Mol. Med. Rep.* **2016**, *14*, 4505–4510.

39. U. Boehm, T. Klamp, M. Groot, J. C. Howard, *Annu. Rev. Immunol.* **1997**, *15*, 749–795.

40. K. Schroder, P. J. Hertzog, T. Ravasi, D. A. Hume, *J. Leukoc. Biol.* **2004**, *75*, 163–189.

41. J. Wang, G. Roderiquez, T. Oravecz, M. A. Norcross, *J. Virol.* **1998**, *72*, 7642–7647.

42. A A. Mantovani, S. Sozzani, M. Locati, P. Allavena, A. Sica, *Trends Immunol.* **2002**, *23*, 549–555.

43. J. Weischenfeldt, B. Porse, *Cold Spring Harb. Protoc.* **2008**, *3*, pdb.prot5080.

44. S. Ngernpimai, Y. Geng, J. M. Makabenta, R. F. Landis, P. Keshri, A. Gupta, C. H. Li, A. Chompoosor and V. M. Rotello, *ACS Appl. Mater. Interfaces*, **2019**, *11*, 11202–11208.

45. E. Elinav, R. Nowarski, C. A. Thaiss, B. Hu, C. Jin, R. A. Flavell, *Nat. Rev. Cancer* **2013**, *13*, 759–771.

46. A. Gisterå, G. K. Hansson, *Nat. Rev. Nephrol.* **2017**, *13*, 368–380.

47. I. B. McInnes, C. D. Buckley, J. D. Isaacs, *Nat. Rev. Rheumatol.* **2016**, *12*, 63–68.

48. M. Benoit, B. Desnues, J.-L. Mege, *J. Immunol.* **2008**, *181*, 3733–9.

49. C. N. Lumeng, J. L. Bodzin, A. R. Saltiel, C. N. Lumeng, J. L. Bodzin, A. R. Saltiel, *J Clin Invest* **2007**, *117*, 175–184.

50. L. Zhou, M. M. W. Chong, D. R. Littman, *Immunity* **2009**, *30*, 646–655.

51. S. J. Galli, N. Borregaard, T. A. Wynn, *Nat. Immunol.* **2011**, *12*, 1035–1044.

52. Q. Xu, J. T. Norman, S. Shrivastav, J. Lucio-Cazana, J. B. Kopp, *Am. J. Physiol. Physiol.* **2007**, *293*, F631–F640.

53. R. F. Landis, A. Gupta, Y. W. Lee, L. S. Wang, B. Golba, B. Couillaud, R. Ridolfo, R. Das, V. M. Rotello, *ACS Nano* **2017**, *11*, 946–952.

54. M. De, S. Rana and V. M. Rotello, *Macromol. Biosci.* **2009**, *9*, 174–178.

55. B. Valeur, J. Pouget, J. Bourson, M. Kaschke, N. P. Ernsting, *J. Phys. Chem.* **1992**, *96*, 6545–6549.

56. P. C. Mahalanobis, *Proc. Natl. Inst. Sci. India.* **1936**, *2*, 49–55.

57. R. Gnanadesikan, J. R. Kettenring, *Biometrics* **2006**, *28*, 81.

58. T. D. Schmittgen, K. J. Livak, *Nat. Protoc.* **2008**, *3*, 1101–1108.

CHAPTER 5

CONCLUSION AND OUTLOOK

5.1 Potentials of array-based sensing in biomedical research

Over the past decade, numerus amount of research works has demonstrated array-based sensing to be an effective strategy in extracting valuable information from challenging biological analytes. In this dissertation, I have developed and applied multi-channel sensor arrays to profile phenotypically plastic cells including cancer stem cells and macrophages. Being able to quickly identify different cell states is an essential step for disease diagnosis. In addition, I have demonstrated the power of array-based sensing in high-content screenings with the example of how we identified a potential CSC differentiation inducer. Furthermore, the high-content information collected from macrophage polarization states can be applied in multiple areas of immunology including screening of immune states for individual patients, evaluating immunogenicity following agent treatment, and identifying the status of major components of the immune system. Taken together, array-based sensing strategy provides a simple and robust tool for cell phenotyping and holds promises in biomedical research.

Despite the comprehensive information that array-based sensing can offer, there are still challenges that need to be addressed before translating the method into the real-world applications. One challenge that array-based sensing strategy faces in HCS and HTS is that the sensor needs to be synthetically easy to make and scale to a large quantity. The platform described in Chapter 4 is appealing, however, considering the storage condition and expression efficiency, the use of fluorescent protein still limits its application in large scale screenings. Materials such as polymers are a great choice if one can retain the sensitivity in an all-polymeric platform. In addition, due to the cross-reactivity among sensor

elements, not all sensor arrays reported are in a single-microwell, which is less ideal for HTS. Designing sensor arrays that can be mixed in one well not only reduces sensor material cost but also simplifies data collection and analysis steps.

There has always been interests in understanding what the sensor arrays are responding to. As discussed in this thesis, the nature of the interactions between the sensor and cell surface is not well-understood. We have demonstrated in the past that the sensor arrays are sensitive to the glycosylation patterns on the cell surface, but other types of interactions are also possible. Combining the output of sensor arrays with advances in highly specific sensors will lead to better sensor design and expedite the biomarker discovery process. It is our hope that array-based sensing will offer a different perspective in studying challenging biological questions and open a new avenue for anticancer therapies.

5.2 The role of α6β4 integrin in CSC differentiation

Integrins are αβ heterodimeric transmembrane proteins that interact with the extracellular matrix and transduce signals. They play essential roles in communicating cells with their microenvironments. Integrins have been found to be involved in a variety of cell signaling events including migration, invasion, proliferation, survival under both physiological and pathological conditions.[1,2] Among the 24 different integrin receptors discovered (paired α and β subunits), β4 integrin subunit forms a heterodimer with α6 subunit to bind with laminins in the extracellular matrix and facilitate the formation of hemidesmosomes. Previous research has reported that high β4 expression level is correlated with poor patient survival in many cancer types.[3,4,5] In this thesis, we showed that upon EMT induction, β4 integrin expression was significantly decreased. Interestingly,

the restoration of α6β4 reverted stem cell properties (Chapter 2). This result is further validated in the nanoparticle screening studies, where an increase in α6β4 integrin expression level was observed when CSCs were induced by the C6 nanoparticle to undergo differentiation (Chapter 3). These findings are consistent with the previous work that the expression of β4 subunit is low in CSCs as compared to non-CSCs.[6] In sum, α6β4 coherently shows its importance in destemming CSCs/promote differentiation.

However, conflicting data on the function of β4 integrin in CSCs has been reported. In 2017, Bierie *et al.* discovered that the mesenchymal cell population could be further stratified into two sub-populations based on integrin β4 expression level. Although $\beta4^{hi}$ cells have more epithelial traits and $\beta4^{lo}$ fraction has more mesenchymal traits, both populations showed equivalent mammosphere formation ability. Interestingly, we observed that $\beta4^{lo}$ cells retained their self-renewal abilities over a few passages, whereas $\beta4^{hi}$ cells gradually lost this ability (Chapter 3). In addition, their results demonstrated that although $\beta4^{lo}$ cells are more mesenchymal in morphology and have higher EMT-associated gene expressions, they are actually less tumorigenic than $\beta4^{hi}$ cells.

The conflicting results could be due to the different methods used for enriching mesenchymal cells. As shown in Figure 5.1, the results from Bierie *et al.* were obtained using naturally arising mesenchymal cells (NAMEC) derived from immortalized, non-tumorigenic human mammary epithelial (HMLE) cells, whereas we used HMLE cells transformed with H-Ras oncogene (HMLER). The different enrichment methods could result in different EMT states. Since it is rare for cells to reside in a fully mesenchymal state via an EMT,[7] it is likely that the NAMEC and HMLER cells were at different partial EMT states with heterogeneous cell dynamics before integrin sorting. Even though these

cells were sorted based on the same set of surface markers (CD24, CD44, ITGB4), the resulting subpopulations were not identical to each other in the comparison. In other words, the $CD44^{hi}CD24^{lo}\beta4^{lo}$ cells, which have the less tumor-initiating ability in Bierie *et al.* study, are not the same population with stem properties in our studies.

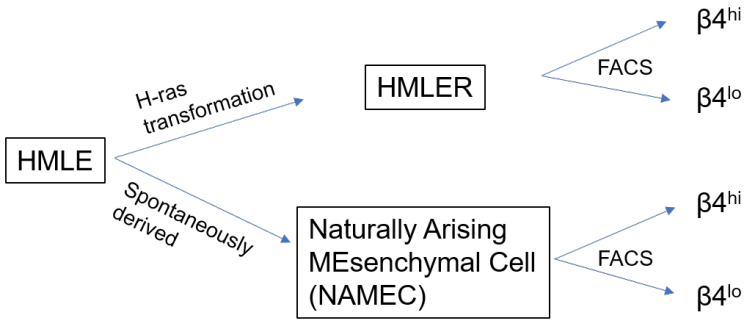

Figure 5.1. Different isolation and CSC enrichment methods. Both mesenchymal cell populations (HMLER and NAMEC) were derived from immortalized, non-tumorigenic human mammary epithelial cells (HMLE) and further sorted into two subpopulations based on integrin β4 level.

These conflicting results are interesting because they suggest that CSCs and their tumor-initiating ability is a complex property that cannot be solely determined by surface markers. This hypothesis is partially supported in the same paper, where the opposite trend of tumor-initiating abilities in integrin β4 subpopulations is observed with MDA-MB-231 cells. In fact, research in other tumor types has also shown contradictory results when using CSCs enriched from different cell lines. In glioblastoma stem cells, some reported undetectable level of β4[8] whereas others reported an elevated level of expression.[9] The difference is that the former study used CD133-enriched glioblastoma stem cell tumorspheres whereas the latter used mammospheres derived from glioma cell line LN229 to conduct CSC-related work. Therefore, consistent detection and isolation methods are needed as we gain more insights into CSC biology.

5.3 Alternative CSC detection methods and screening application

Although CSCs are typically defined and isolated by surface markers, in the past decade, there is an emerging trend of seeking alternative detection and isolation methods. In a recent study, a small population of cells with intrinsic autofluorescence was identified from freshly isolated primary epithelial tumors. These cells display functional features of CSCs including self-renewing, highly tumorigenic, and chemo-resistant. Mechanistic studies suggest that the autofluorescence comes from the membrane-bound cytoplasmic vesicles. This study proposes the intracellular auto-fluorescent vesicles to be a new functional marker for CSC isolation and detection through flow cytometry.[10] In a separate study, a group of researchers developed a microfluidic device to isolate breast CSCs utilizing the EMT property of enhanced cell migration, The trapped migratory cells were shown to have a higher tumor-initiating ability and more metastatic than the non-migratory cells.[11]

The distinct sensing patterns of subpopulations of mesenchymal cells from both S1 and HMLER CSC models (Chapter 2 and 3) suggest that array-based sensors can discriminate cells with different cell surface components. It would be interesting to test whether the sensor arrays demonstrated in this thesis would sense the above-mentioned functionally different subpopulations of CSCs, and the auto-fluorescent cell populations of CSCs. If so, the complex microfluidic device, labor-intense cell imaging, and flow cytometry could be avoided, hence increasing the throughput of detecting CSCs.

The sensing screen demonstrated in Chapter 3 has proven its application in identifying novel CSC differentiation inducers. In this thesis, we only explored the hydrophobic effect on CSC differentiation. In the future, it is promising to strategically

build the screening library to increase the likelihood of identifying compounds that induce the change in CSC phenotype. Since epigenetic regulators, such as Bmi1 and HDAC, have been shown to be important for CSCs to acquire stemness (Chapter 1.3.3), incorporating epigenetic inhibitors into the library seems promising. In addition, CSCs have been reported to contain lower levels of ROS than non-CSCs, thus, screening compounds that targets the higher expression of ROS scavengers may be an efficient way of changing CSC properties.

5.4 Tumor microenvironment

In this thesis, we demonstrated that that different tumor microenvironments could differentially activate microphages into distinct phenotypic states (Chapter 4). Such influence is complicated and being able to dissect out the key players involved in the process is a fundamental question to be addressed. Cancer-associated fibroblasts (CAFs) are a major component of the tumor microenvironment. Increasing amount of evidence have shown the crucial roles that CAFs play in modulating the immune system and influencing the tumor microenvironment, including polarizing T cells and macrophages, and recruiting B cells.[12] It is interesting to explore how CAFs synergize with tumor associated microphages (TAMs) and influence microphage polarization. Although CAFs can induce M1 to M2 trans-differentiation, specific communication cues remain to be elucidated. Identifying key factors that are involved in such process will help develop strategies to re-educate TAMs from this immune-suppressing state to an antitumor M1 phenotype.

5.5 References

1. C. Margadant, E. Frijns, K. Wilhelmsen, A. Sonnenberg, *Curr. Opin. Cell Biol.* **2008**, *20*, 589–596.

2. P. Moreno-Layseca, C. H. Streuli, *Matrix Biol.* **2014**, *34*, 144–153.

3. L. K. Diaz, M. Cristofanilli, X. Zhou, K. L. Welch, T. L. Smith, Y. Yang, N. Sneige, A. A. Sahin, M. Z. Gilcrease, *Mod. Pathol.* **2005**, *18*, 1165–1175.

4. A. Kurokawa, M. Nagata, N. Kitamura, A. A. Noman, M. Ohnishi, T. Ohyama, T. Kobayashi, S. Shingaki, R. Takagi, *Cancer* **2008**, *112*, 1272–1281.

5. M. Li, X. Jiang, G. Wang, C. Zhai, Y. Liu, H. Li, Y. Zhang, W. Yu, Z. Zhao, *J. Cancer* **2019**, *10*, 5223–5233.

6. H. L. Goel, T. Gritsko, B. Pursell, C. Chang, L. D. Shultz, D. L. Greiner, J. H. Norum, R. Toftgard, L. M. Shaw, A. M. Mercurio, *Cell Rep.* **2014**, *7*, 747–761.

7. R. Derynck, R. A. Weinberg, *Dev. Cell* **2019**, *49*, 313–316.

8. J. D. Lathia, J. Gallagher, J. M. Heddleston, J. Wang, C. E. Eyler, J. MacSwords, Q. Wu, A. Vasanji, R. E. McLendon, A. B. Hjelmeland, et al., *Cell Stem Cell* **2010**, *6*, 421–432.

9. B. Ma, L. Zhang, Y. Zou, R. He, Q. Wu, C. Han, B. Zhang, *J. Exp. Clin. Cancer Res.* **2019**, *38*, 23.

10. I. Miranda-Lorenzo, J. Dorado, E. Lonardo, S. Alcala, A. G. Serrano, J. Clausell-Tormos, M. Cioffi, D. Megias, S. Zagorac, A. Balic, et al., *Nat. Methods* **2014**, *11*, 1161–1169.

11. Y. C. Chen, B. Humphries, R. Brien, A. E. Gibbons, Y. T. Chen, T. Qyli, H. R. Haley, M. E. Pirone, B. Chiang, A. Xiao, et al., *Sci. Rep.* **2018**, *8*, 244.

12. E. Sahai, I. Astsaturov, E. Cukierman, D. G. DeNardo, M. Egeblad, R. M. Evans, D. Fearon, F. R. Greten, S. R. Hingorani, T. Hunter, et al., *Nat. Rev. Cancer* **2020**, *20*, 174–186.

BIBLIOGRAPHY

A. A. Mantovani, S. Sozzani, M. Locati, P. Allavena, A. Sica, *Trends Immunol.* **2002**, *23*, 549–555.

A. L. Ades, A. Guerci, E. Raffoux, M. Sanz, P. Chevallier, S. Lapusan, C. Recher, X. Thomas, C. Rayon, S. Castaigne, et al., *Blood* **2010**, *115*, 1690–1696.

A. B. Mak, K. M. Blakely, R. A. Williams, P. A. Penttila, A. I. Shukalyuk, K. T. Osman, D. Kasimer, T. Ketela, J. Moffat, *J. Biol. Chem.* **2011**, *286*, 41046–41056.

A. Bajaj, O. R. Miranda, I.-B. Kim, R. L. Phillips, D. J. Jerry, U. H. F. Bunz, V. M. Rotello, *Proc. Natl. Acad. Sci. U. S. A.* **2009**, *106*, 10912–10916.

A. Bajaj, S. Rana, O. R. Miranda, J. C. Yawe, D. J. Jerry, U. H. F. Bunz, V. M. Rotello, *Chem. Sci.* **2010**, *1*, 134.

A. Chompoosor, K. Saha, P. S. Ghosh, D. J. Macarthy, O. R. Miranda, Z.-J. Zhu, K. F. Arcaro, V. M. Rotello, *Small* **2010**, *6*, 2246–2249.

A. Dongre, R. A. Weinberg, N*at. Rev. Mol. Cell Biol.* **2019**, *20*, 69–84.

A. Dongre, R. A. Weinberg, *Nat. Rev. Mol. Cell Biol.* **2019**, *20*, 69–84.

A. Fernandez, M. Vermeren, D. Humphries, R. Subiros-Funosas, N. Barth, L. Campana, A. MacKinnon, Y. Feng, M. Vendrell, *ACS Cent. Sci.* **2017**, *3*, 995–1005.

A. G. Pockley, G. A. Foulds, J. A. Oughton, N. I. Kerkvliet, G. Multhoff, *Curr. Protoc. Toxicol.* **2015**, *66*, 18.8.1-18.8.34.

A. Gisterå, G. K. Hansson, *Nat. Rev. Nephrol.* **2017**, *13*, 368–380.

A. Heller, B. Feldman, *Chem. Rev.* **2008**, *108*, 2482–2505.

A. Kurokawa, M. Nagata, N. Kitamura, A. A. Noman, M. Ohnishi, T. Ohyama, T. Kobayashi, S. Shingaki, R. Takagi, *Cancer* **2008**, *112*, 1272–1281.

A. M. Alkilany, C. J. Murphy, *J. Nanoparticle Res.* **2010**, *12*, 2313–2333.

A. M. Hassan, M. El-Shenawee, *IEEE Rev. Biomed. Eng.* **2011**, *4*, 103–118.

A. Mantovani, A. Sica, S. Sozzani, P. Allavena, A. Vecchi and M. Locati, *Trends Immunol.* **2004**, *25*, 677–686.

A. P. F. Turner, N. Magan, *Nat. Rev. Microbiol.* **2004**, *2*, 160–166.

A. Petrelli, R. Carollo, M. Cargnelutti, F. Iovino, M. Callari, D. Cimino, M. Todaro, L. R. Mangiapane, A. Giammona, A. Cordova, et al., *Oncotarget* **2015**, *6*, 2315–30.

A. R. Ji, S. Y. Ku, M. S. Cho, Y. Y. Kim, Y. J. Kim, S. K. Oh, S. H. Kim, S. Y. Moon, Y. M. Choi, *Exp. Mol. Med.* **2010**, *42*, 175–186.

A. Rahikkala, S. A. P. Pereira, P. Figueiredo, M. L. C. Passos, A. R. T. S. Araújo, M. L. M. F. S. Saraiva, H. A. Santos, *Adv. Biosyst.* **2018**, *2*, 1800020.

A. Rahikkala, S. A. P. Pereira, P. Figueiredo, M. L. C. Passos, A. R. T. S. Araújo, M. L. M. F. S. Saraiva, H. A. Santos, *Adv. Biosyst.* **2018**, *2*, 1800020.

A. S. Klymchenko, *Acc. Chem. Res.* **2017**, *50*, 366–375.

A. Shapouri-Moghaddam, S. Mohammadian, H. Vazini, M. Taghadosi, S.-A. Esmaeili, F. Mardani, B. Seifi, A. Mohammadi, J. T. Afshari, A. Sahebkar, *J. Cell. Physiol.* **2018**, *233*, 6425–6440.

A. Singh, J. Settleman, *Oncogene* **2010**, *29*, 4741–4751.

A. Sobczak-Kupiec, J. Venkatesan, A. Alhathal AlAnezi, D. Walczyk, A. Farooqi, D. Malina, S. H. Hosseini, B. Tyliszczak, *Nanomedicine: N.B.M.* **2016**, *12*, 2459–2473.

A. Turdo, V. Veschi, M. Gaggianesi, A. Chinnici, P. Bianca, M. Todaro, G. Stassi, *Front. Cell Dev. Biol.* **2019**, *7*, 16.

B. Bierie, S. E. Pierce, C. Kroeger, D. G. Stover, D. R. Pattabiraman, P. Thiru, J. L. Donaher, F. Reinhardt, C. L. Chaffer, Z. Keckesova, et al., *Proc. Natl. Acad. Sci. U. S. A.* **2017**, *114*, E2337–E2346.

B. Elenbaas, L. Spirio, F. Koerner, M. D. Fleming, D. B. Zimonjic, J. L. Donaher, N. C. Popescu, W. C. Hahn, R. A. Weinberg, *Genes Dev.* **2001**, *15*, 50–65.

B. Ma, L. Zhang, Y. Zou, R. He, Q. Wu, C. Han, B. Zhang, *J. Exp. Clin. Cancer Res.* **2019**, *38*, 23.

B. Valamehr, S. J. Jonas, J. Polleux, R. Qiao, S. Guo, E. H. Gschweng, B. Stiles, K. Kam, T.-J. M. Luo, O. N. Witte, et al., *Proc. Natl. Acad. Sci.* **2008**, *105*, 14459–14464.

B. Valeur, J. Pouget, J. Bourson, M. Kaschke, N. P. Ernsting, *J. Phys. Chem.* **1992**, *96*, 6545–6549.

B. Yang, J. B. Treweek, R. P. Kulkarni, B. E. Deverman, C. K. Chen, E. Lubeck, S. Shah, L. Cai, V. Gradinaru, *Cell* **2014**, *158*, 945–958.

B.-Z. Qian, J. W. Pollard, *Cell* **2010**, *141*, 39–51.

C. A. Ambarus, S. Krausz, M. van Eijk, J. Hamann, T. R. D. J. Radstake, K. A. Reedquist, P. P. Tak, D. L. P. Baeten, *J. Immunol. Methods* **2012**, *375*, 196–206.

C. Auffray, D. Fogg, M. Garfa, G. Elain, O. Join-Lambert, S. Kayal, S. Sarnacki, A. Cumano, G. Lauvau, F. Geissmann, *Science (80-.).* **2007**, *317*, 666–670.

C. Belgiovine, M. D'Incalci, P. Allavena, R. Frapolli, *Cell. Mol. Life Sci.* **2016**, *73*, 2411–2424.

C. Chang, H. L. Goel, H. Gao, B. Pursell, L. D. Shultz, D. L. Greiner, S. Ingerpuu, M. Patarroyo, S. Cao, E. Lim, et al., *Genes Dev.* **2015**, *29*, 1–6.

C. Chang, H. L. Goel, H. Gao, B. Pursell, L. D. Shultz, D. L. Greiner, S. Ingerpuu, M. Patarroyo, S. Cao, E. Lim, et al., *Genes Dev.* **2015**, *29*, 1–6.

C. E. Meacham, S. J. Morrison, *Nature* **2013**, *501*, 328–337.

C. Ginestier, M. H. Hur, E. Charafe-Jauffret, F. Monville, J. Dutcher, M. Brown, J. Jacquemier, P. Viens, C. G. Kleer, S. Liu, et al., *Cell Stem Cell* **2007**, *1*, 555–567.

C. L. Chaffer, B. P. San Juan, E. Lim, R. A. Weinberg, *Cancer Metastasis Rev.* **2016**, *35*, 645–654.

C. Margadant, E. Frijns, K. Wilhelmsen, A. Sonnenberg, *Curr. Opin. Cell Biol.* **2008**, *20*, 589–596.

C. Maucort, A. Di Giorgio, S. Azoulay, M. Duca, *ChemMedChem* **2021**, *16*, 14–29.

C. N. Lumeng, J. L. Bodzin, A. R. Saltiel, C. N. Lumeng, J. L. Bodzin, A. R. Saltiel, *J Clin Invest* **2007**, *117*, 175–184.

C. Ragulan, K. Eason, E. Fontana, G. Nyamundanda, N. Tarazona, Y. Patil, P. Poudel, R. T. Lawlor, M. Del Rio, S. L. Koo, et al., *Sci. Rep.* **2019**, *9*, 1–12.

C. Scheel, R. A. Weinberg, *Semin. Cancer Biol.* **2012**, *22*, 396–403.

C. Scheel, R. A. Weinberg, *Semin. Cancer Biol.* **2012**, *22*, 396–403.

C.-C. You, O. R. Miranda, B. Gider, P. S. Ghosh, I.-B. Kim, B. Erdogan, S. A. Krovi, U. H. F. Bunz, V. M. Rotello, *Nat. Nanotechnol.* **2007**, *2*, 318–323.

D. F. Moyano, M. Goldsmith, D. J. Solfiell, D. Landesman-Milo, O. R. Miranda, D. Peer, V. M. Rotello, *J. Am. Chem. Soc.* **2012**, *134*, 3965–3967.

D. Iliopoulos, C. Polytarchou, M. Hatziapostolou, F. Kottakis, I. G. Maroulakou, K. Struhl, P. N. Tsichlis, *Sci. Signal.* **2009**, *2*, ra62–ra62.

D. Iliopoulos, H. A. Hirsch, G. Wang, K. Struhl, *Proc. Natl. Acad. Sci. U. S. A.* **2011**, *108*, 1397–1402.

D. R. Dreyer, S. Park, C. W. Bielawski, R. S. Ruoff, *Chem. Soc. Rev.* **2010**, *39*, 228–240.

D. Zamora-Olivares, T. S. Kaoud, K. N. Dalby, E. V. Anslyn, *J. Am. Chem. Soc.* **2013**, *135*, 14814–14820.

E. C. Dreaden, A. M. Alkilany, X. Huang, C. J. Murphy, M. A. El-Sayed, *Chem. Soc. Rev.* **2012**, *41*, 2740–2779.

E. Elinav, R. Nowarski, C. A. Thaiss, B. Hu, C. Jin, R. A. Flavell, *Nat. Rev. Cancer* **2013**, *13*, 759–771.

E. Mathew, A. L. Brannon, A. C. Del Vecchio, P. E. Garcia, M. K. Penny, K. T. Kane, A. Vinta, R. J. Buckanovich, M. P. di Magliano, *Neoplasia* **2016**, *18*, 142–151.

E. Sachlos, R. M. Risueño, S. Laronde, Z. Shapovalova, J.-H. Lee, J. Russell, M. Malig, J. D. McNicol, A. Fiebig-Comyn, M. Graham, et al., *Cell* **2012**, *149*, 1284–1297.

E. Sahai, I. Astsaturov, E. Cukierman, D. G. DeNardo, M. Egeblad, R. M. Evans, D. Fearon, F. R. Greten, S. R. Hingorani, T. Hunter, et al., *Nat. Rev. Cancer* **2020**, *20*, 174–186.

E. V. Abel, E. J. Kim, J. Wu, M. Hynes, F. Bednar, E. Proctor, L. Wang, M. L. Dziubinski, D. M. Simeone, *PLoS One* **2014**, *9*, e91983.

El Harrad, I. Bourais, H. Mohammadi, A. Amine, *Sensors* **2018**, *18*, 164.

F. Andriani, G. Bertolini, F. Facchinetti, E. Baldoli, M. Moro, P. Casalini, R. Caserini, M. Milione, G. Leone, G. Pelosi, et al., *Mol. Oncol.* **2016**, *10*, 253–271.

F. Andriani, G. Bertolini, F. Facchinetti, E. Baldoli, M. Moro, P. Casalini, R. Caserini, M. Milione, G. Leone, G. Pelosi, et al., *Mol. Oncol.* **2016**, *10*, 253–271.

F. Held, E. Hoppe, M. Cvijovic, M. Jirstrand and J. Gabrielsson, *J. Pharmacokinet. Pharmacodyn.* **2019**, *46*, 223–240.

F. Lo-Coco, G. Avvisati, M. Vignetti, C. Thiede, S. M. Orlando, S. Iacobelli, F. Ferrara, P. Fazi, L. Cicconi, E. Di Bona, et al., *N. Engl. J. Med.* **2013**, *369*, 111–121.

F. O. Martinez, A. Sica, A. Mantovani, M. Locati, *Front. Biosci.* **2008**, *13*, 453–461.

F. O. Martinez, L. Helming, S. Gordon, *Annu. Rev. Immunol.* **2009**, *27*, 451–483.

F. O. Martinez, S. Gordon, *F1000Prime Rep.* **2014**, *6*, 13.

F. Scaletti, J. Hardie, Y. W. Lee, D. C. Luther, M. Ray, V. M. Rotello, *Chem. Soc. Rev.* **2018**, *47*, 3421–3432.

F. Zanconato, M. Cordenonsi, S. Piccolo, *Cancer Cell* **2016**, *29*, 783–803.

F. Zanella, J. B. Lorens, W. Link, *Trends Biotechnol.* **2010**, *28*, 237–245.

G. A. Duque and A. Descoteaux, *Front. Immunol.* 2014, **5**.

G. B. McGaughey, M. Gagné, A. K. Rappé, *J. Biol. Chem.* **1998**, *273*, 15458–15463.

G. Dontu, W. M. Abdallah, J. M. Foley, K. W. Jackson, M. F. Clarke, M. J. Kawamura, M. S. Wicha, *Genes Dev.* **2003**, *17*, 1253–1270.

G. Y. Tonga, Y. Jeong, B. Duncan, T. Mizuhara, R. Mout, R. Das, S. T. Kim, Y.-C. Yeh, B. Yan, S. Hou, et al., *Nat. Chem.* **2015**, *7*, 597–603.

G. Y. Tonga, Y. Jeong, B. Duncan, T. Mizuhara, R. Mout, R. Das, S. T. Kim, Y.-C. Yeh, B. Yan, S. Hou, et al., *Nat. Chem.* **2015**, *7*, 597–603.

H. A. Hirsch, D. Iliopoulos, P. N. Tsichlis, K. Struhl, *Cancer Res.* **2009**, *69*, 7507–7511.

H. Bai, Z. Liu, T. Zhang, J. Du, C. Zhou, W. He, J. H. C. Chau, R. T. K. Kwok, J. W. Y. Lam, B. Z. Tang, *ACS Nano* **2020**, *14*, 7552–7563.

H. de Thé, *Nat. Rev. Cancer* **2018**, *18*, 117-127

H. de Thé, *Nat. Rev. Cancer* **2018**, *18*, 117–127.

H. Jang, J. Yang, E. Lee, J.-H. Cheong, *Arch. Pharm. Res.* **2015**, *38*, 381–388.

H. Jiang, J. R. Pritchard, R. T. Williams, D. A. Lauffenburger, M. T. Hemann, *Nat. Chem. Biol.* **2011**, *7*, 92–100.

H. L. Goel, B. Pursell, C. Chang, L. M. Shaw, J. Mao, K. Simin, P. Kumar, C. W. Vander Kooi, L. D. Shultz, D. L. Greiner, et al., *EMBO Mol. Med.* **2013**, *5*, 488–508.

H. L. Goel, T. Gritsko, B. Pursell, C. Chang, L. D. Shultz, D. L. Greiner, J. H. Norum, R. Toftgard, L. M. Shaw, A. M. Mercurio, *Cell Rep.* **2014**, *7*, 747–761.

H. M. Meng, H. Liu, H. Kuai, R. Peng, L. Mo, X. B. Zhang, *Chem. Soc. Rev.* **2016**, *45*, 2583–2602.

H. Sugai, K. Kono, A. Takahashi, F. Ichihara, H. Kawaida, H. Fujii, Y. Matsumoto, *J. Surg. Res.* **2004**, *116*, 277–287.

H. Sugai, S. Tomita, R. Kurita, *Anal. Sci.* **2020**, *36*, 923–934.

H. Sugai, S. Tomita, S. Ishihara, R. Kurita, *ACS Sensors* **2019**, *4*, 827–831.

H. T. Idriss and J. H. Naismith, *Microsc. Res. Tech.* **2000**, *50*, 184–195.

H. Zhang, R. L. Brown, Y. Wei, P. Zhao, S. Liu, X. Liu, Y. Deng, X. Hu, J. Zhang, X. D. Gao, et al., *Genes Dev.* **2019**, *33*, 166–179.

I. B. McInnes, C. D. Buckley, J. D. Isaacs, *Nat. Rev. Rheumatol.* **2016**, *12*, 63–68.

I. Ben-Porath, M. W. Thomson, V. J. Carey, R. Ge, G. W. Bell, A. Regev, R. A. Weinberg, *Nat. Genet.* **2008**, *40*, 499–507.

I. Miranda-Lorenzo, J. Dorado, E. Lonardo, S. Alcala, A. G. Serrano, J. Clausell-Tormos, M. Cioffi, D. Megias, S. Zagorac, A. Balic, et al., *Nat. Methods* **2014**, *11*, 1161–1169.

I. Rabinovitz, A. Toker, A. M. Mercurio, *J. Cell Biol.* **1999**, *146*, 1147–1160.

J. D. Lathia, J. Gallagher, J. M. Heddleston, J. Wang, C. E. Eyler, J. MacSwords, Q. Wu, A. Vasanji, R. E. McLendon, A. B. Hjelmeland, et al., *Cell Stem Cell* **2010**, *6*, 421–432.

J. E. Dick, *Blood* **2008**, *112*, 4793–4807.

J. G. Moffat, J. Rudolph, D. Bailey, *Nat. Rev. Drug Discov.* **2014**, *13*, 588–602.

J. H. Tsai, J. L. Donaher, D. A. Murphy, S. Chau, J. Yang, *Cancer Cell* **2012**, *22*, 725–736.

J. Han, M. Bender, S. Hahn, K. Seehafer, U. H. F. Bunz, *Chem. - A Eur. J.* **2016**, *22*, 3230–3233.

J. K. Nicholson, J. Connelly, J. C. Lindon, E. Holmes, *Nat. Rev. Drug Discov.* **2002**, *1*, 153–161.

J. Massagué, A. C. Obenauf, *Nature* **2016**, *529*, 298–306.

J. P. Thiery, H. Acloque, R. Y. J. Huang, M. A. Nieto, *Cell* **2009**, *139*, 871–890.

J. R. Carey, K. S. Suslick, K. I. Hulkower, J. A. Imlay, K. R. C. Imlay, C. K. Ingison, J. B. Ponder, A. Sen, A. E. Wittrig, *J. Am. Chem. Soc.* **2011**, *133*, 7571–7576.

J. Wang, G. Roderiquez, T. Oravecz, M. A. Norcross, *J. Virol.* **1998**, *72*, 7642–7647.

J. Weischenfeldt, B. Porse, *Cold Spring Harb. Protoc.* **2008**, *3*, pdb.prot5080.

J. Xue, S. V. Schmidt, J. Sander, A. Draffehn, W. Krebs, I. Quester, D. De Nardo, T. D. Gohel, M. Emde, L. Schmidleithner, et al., *Immunity* **2014**, *40*, 274–288.

J. Yang, R. A. Weinberg, *Dev. Cell* **2008**, *14*, 818–829.

J. Y. Liu, G. P. Souroullas, B. O. Diekman, J. Krishnamurthy, B. M. Hall, J. A. Sorrentino, J. S. Parker, G. A. Sessions, A. V. Gudkov, N. E. Sharpless, *Proc. Natl. Acad. Sci. U. S. A.* **2019**, *116*, 2603–2611.

K. Chen, Y. Huang, J. Chen, *Acta Pharmacol. Sin.* **2013**, *34*, 732–740.

K. H. Emami, C. Nguyen, H. Ma, D. H. Kim, K. W. Jeong, M. Eguchi, R. T. Moon, J-L Teo, S. W. Oh, H. Y. Kim, S. H. Moon, J. R. Ha, M. Kahn, *Proc. Natl. Acad. Sci. U. S. A.* **2004**, *101*, 12682-12687.

K. Kemper, M. R. Sprick, M. De Bree, A. Scopelliti, L. Vermeulen, M. Hoek, J. Zeilstra, S. T. Pals, H. Mehmet, G. Stassi, et al., *Cancer Res.* **2010**, *70*, 719–729.

K. L. M. Boylan, K. Geschwind, J. S. Koopmeiners, M. A. Geller, T. K. Starr, A. P. N. Skubitz, *Clin. Proteomics* **2017**, *14*, 34.

K. Ohtsubo, J. D. Marth, *Cell* **2006**, *126*, 855–867.

K. Polyak, R. A. Weinberg, *Nat. Rev. Cancer* **2009**, *9*, 265–273.

K. Saha, D. F. Moyano, V. M. Rotello, *Mater. Horiz.* **2014**, *1*, 102–105.

K. Saha, M. Rahimi, M. Yazdani, S. T. Kim, D. F. Moyano, S. Hou, R. Das, R. Mout, F. Rezaee, M. Mahmoudi, et al., *ACS Nano* **2016**, *10*, 4421–4430.

K. Schroder, P. J. Hertzog, T. Ravasi, D. A. Hume, *J. Leukoc. Biol.* **2004**, *75*, 163–189.

L. Fang, Q. Zhu, M. Neuenschwander, E. Specker, A. Wulf-Goldenberg, W. I. Weis, J. P. Von Kries, W. Birchmeier, *Cancer Res.* **2016**, *76*, 891–901.

L. Guerrini, R. Alvarez-Puebla, N. Pazos-Perez, L. Guerrini, R. A. Alvarez-Puebla, N. Pazos-Perez, *Materials (Basel).* **2018**, *11*, 1154.

L. K. Diaz, M. Cristofanilli, X. Zhou, K. L. Welch, T. L. Smith, Y. Yang, N. Sneige, A. A. Sahin, M. Z. Gilcrease, *Mod. Pathol.* **2005**, *18*, 1165–1175.

L. Motiei, Z. Pode, A. Koganitsky, D. Margulies, *Angew. Chemie Int. Ed.* **2014**, *53*, 9289–9293.

L. Wide, C. A. Gemzell, *Acta Endocrinol. (Copenh).* **1960**, *35*, 261−267.

L. Wilkinson, L. Engelman, J. Corter, M. Coward M. In *Cluster Analysis*. 2009. I-77. Available at http://biostats.unh.edu/Statistics_I_II_III_IV.pdf.

L. Wu, H. Ji, Y. Guan, X. Ran, J. Ren, X. Qu, *NPG Asia Mater.* **2017**, *9*, e356–e356.

L. Yan, F. Zhao, S. Li, Z. Hu, Y. Zhao, *Nanoscale* **2011**, *3*, 362–382.

L. Zhang, F. Gu, J. Chan, A. Wang, R. Langer, O. Farokhzad, *Clin. Pharmacol. Ther.* **2008**, *83*, 761–769.

L. Zhou, M. M. W. Chong, D. R. Littman, *Immunity* **2009**, *30*, 646–655.

M. A. Nieto, R. Y.-J. Huang, R. A. Jackson, J. P. Thiery, *Cell* **2016**, *166*, 21–45.

M. Al-Hajj, M. S. Wicha, A. Benito-Hernandez, S. J. Morrison, M. F. Clarke, *Proc. Natl. Acad. Sci. U. S. A.* **2003**, *100*, 3983–3988.

M. Benoit, B. Desnues, J.-L. Mege, *J. Immunol.* **2008**, *181*, 3733–9.

M. C. Cabrera, R. E. Hollingsworth, E. M. Hurt, *World J. Stem Cells* **2015**, *7*, 27–36.

M. C. Fishman, J. A. Porter, *Nature* **2005**, *437*, 491–493.

M. Cordenonsi, F. Zanconato, L. Azzolin, M. Forcato, A. Rosato, C. Frasson, M. Inui, M. Montagner, A. R. Parenti, A. Poletti, et al., *Cell* **2011**, *147*, 759–772.

M. D. Mager, V. Lapointe, M. M. Stevens, *Nat. Chem.* **2011**, *3*, 582–589.

M. De, P. S. Ghosh, V. M. Rotello, *Adv. Mater.* **2008**, *20*, 4225–4241.

M. De, S. Rana and V. M. Rotello, *Macromol. Biosci.* **2009**, *9*, 174–178.

M. Dean, T. Fojo, S. Bates, *Nat. Rev. Cancer* **2005**, *5*, 275–284.

M. Diehn, R. W. Cho, N. A. Lobo, T. Kalisky, M. J. Dorie, A. N. Kulp, D. Qian, J. S. Lam, L. E. Ailles, M. Wong, et al., *Nature* **2009**, *458*, 780–783.

M. Doan, I. Vorobjev, P. Rees, A. Filby, O. Wolkenhauer, A. E. Goldfeld, J. Lieberman,

N. Barteneva, A. E. Carpenter, H. Hennig, *Trends Biotechnol.* **2018**, *36*, 649–652.

M. F. Clarke, J. E. Dick, P. B. Dirks, C. J. Eaves, C. H. M. Jamieson, D. L. Jones, J. Visvader, I. L. Weissman, G. M. Wahl, in *Cancer Res.*, Cancer Res, **2006**, pp. 9339–9344.

M. Fiorillo, A. F. Verre, M. Iliut, M. Peiris-Pagés, B. Ozsvari, R. Gandara, A. R. Cappello, F. Sotgia, A. Vijayaraghavan, M. P. Lisanti, *Oncotarget* **2015**, *6*, 3553–3562.

M. H. Yang, D. S. S. Hsu, H. W. Wang, H. J. Wang, H. Y. Lan, W. H. Yang, C. H. Huang, S. Y. Kao, C. H. Tzeng, S. K. Tai, et al., *Nat. Cell Biol.* **2010**, *12*, 982–992.

M. Hu, Y. Lan, A. Lu, X. Ma, L. Zhang, in *Prog. Mol. Biol. Transl. Sci.* **2019**, *162*, 1–24.

M. Jurcic, W. J. Peveler, C. N. Savory, D. K. Bučar, A. J. Kenyon, D. O. Scanlon, I. P. Parkin, *ACS Appl. Mater. Interfaces* **2019**, *11*, 11618–11628.

M. K. Jolly, S. C. Tripathi, D. Jia, S. M. Mooney, M. Celiktas, S. M. Hanash, S. A. Mani, K. J. Pienta, E. Ben-Jacob, H. Levine, *Oncotarget* **2016**, *7*, 27067–27084.

M. Li, X. Jiang, G. Wang, C. Zhai, Y. Liu, H. Li, Y. Zhang, W. Yu, Z. Zhao, *J. Cancer* **2019**, *10*, 5223–5233.

M. L. S. Silva, *Cancer Lett.* **2018**, *436*, 63–74.

M. R. Carstens, R. C. Fisher, A. P. Acharya, E. A. Butterworth, E. Scott, E. H. Huang, B. G. Keselowsky, *Proc. Natl. Acad. Sci.* **2015**, *112*, 8732–8737.

M. Schirle, M. Bantscheff, B. Kuster, *Chem. Biol.* **2012**, *19*, 72–84.

M. Srinivasarao, P. S. Low, *Chem. Rev.* **2017**, *117*, 12133–12164.

M. T. Chiao, W. Y. Cheng, Y. C. Yang, C. C. Shen, J. L. Ko, *Autophagy* **2013**, *9*, 1509-1526.

M. V. Fournier, K. J. Martin, P. A. Kenny, K. Xhaja, I. Bosch, P. Yaswen, M. J. Bissell, *Cancer Res.* **2006**, *66*, 7095–7102.

M. Wenes, M. Shang, M. Di Matteo, J. Goveia, R. Martín-Pérez, J. Serneels, H. Prenen, B. Ghesquière, P. Carmeliet, M. Mazzone, *Cell Metab.* **2016**, *24*, 701–715.

M. Yu, A. Bardia, B. S. Wittner, S. L. Stott, M. E. Smas, D. T. Ting, S. J. Isakoff, J. C. Ciciliano, M. N. Wells, A. M. Shah, et al., *Science* **2013**, *339*, 580–584.

N. Barkalina, C. Charalambous, C. Jones, K. Coward, *Nanomedicine: N.B.M.* **2014**, *10*, e921–e938.

N. D. B. Le, G. Yesilbag Tonga, R. Mout, S. T. Kim, M. E. Wille, S. Rana, K. A. Dunphy, D. J. Jerry, M. Yazdani, R. Ramanathan, et al., *J. Am. Chem. Soc.* **2017**, *139*, 8008–8012.

N. D. B. Le, M. Yazdani, V. M. Rotello, *Nanomedicine* **2014**, *9*, 1487–1498.

N. Oishi, T. Yamashita, S. Kaneko, *Liver Cancer* **2014**, *3*, 71–84.

N. Parameswaran and S. Patial, *Crit. Rev. Eukaryot. Gene Expr.* **2010**, *20*, 87–103.

N. Takebe, P. J. Harris, R. Q. Warren, S. P. Ivy, *Nat. Rev. Clin. Oncol.* **2011**, *8*, 97–106.

O. Helm, J. Held-Feindt, E. Grage-Griebenow, N. Reiling, H. Ungefroren, I. Vogel, U. Krüger, T. Becker, M. Ebsen, C. Röcken, et al., *Int. J. Cancer* **2014**, *135*, 843–861.

O. R. Miranda, X. Li, L. Garcia-Gonzalez, Z. J. Zhu, B. Yan, U. H. F. Bunz, V. M. Rotello, *J. Am. Chem. Soc.* **2011**, *133*, 9650–9653.

P. B. Gupta, T. T. Onder, G. Jiang, K. Tao, C. Kuperwasser, R. A. Weinberg, E. S. Lander, *Cell* **2009**, *138*, 645–659.

P. Briand, O. W. Petersen, B. Van Deurs, *In Vitro Cell. Dev. Biol.* **1987**, *23*, 181–188.

P. C. Mahalanobis, *Proc. Natl. Inst. Sci. India.* **1936**, *2*, 49–55.

P. Ghosh, G. Han, M. De, C. K. Kim, V. M. Rotello, *Adv. Drug Deliv. Rev.* **2008**, *60*, 1307–1315.

P. J. Murray, J. E. Allen, S. K. Biswas, E. A. Fisher, D. W. Gilroy, S. Goerdt, S. Gordon, J. A. Hamilton, L. B. Ivashkiv, T. Lawrence, et al., *Immunity* **2014**, *41*, 14–20.

P. J. O'Brien, *Basic Clin. Pharmacol. Toxicol.* **2014**, *115*, 4–17

P. M. Lanctot, F. H. Gage, A. P. Varki, *Curr. Opin. Chem. Biol.* **2007**, *11*, 373–380.

P. Moreno-Layseca, C. H. Streuli, *Matrix Biol.* **2014**, *34*, 144–153.

P. R. Srinivas, B. S. Kramer, S. Srivastava, *Lancet Oncol.* **2001**, *2*, 698–704.

P. V Escribá, J. M. González-Ros, F. M. Goñi, P. K. J. Kinnunen, L. Vigh, L. Sánchez-Magraner, A. M. Fernández, X. Busquets, I. Horváth, G. Barceló-Coblijn, *J. Cell. Mol. Med.* **2008**, *12*, 829–875.

Q. Xu, J. T. Norman, S. Shrivastav, J. Lucio-Cazana, J. B. Kopp, *Am. J. Physiol. Physiol.* **2007**, *293*, F631–F640.

Q.-Y. Lei, H. Zhang, B. Zhao, Z.-Y. Zha, F. Bai, X.-H. Pei, S. Zhao, Y. Xiong, K.-L. Guan, *Mol. Cell. Biol.* **2008**, *28*, 2426–2436.

R. A. Butcher, S. L. Schreiber, *Curr. Opin. Chem. Biol.* **2005**, *9*, 25–30.

R. Ayala, C. Zhang, D. Yang, Y. Hwang, A. Aung, S. S. Shroff, F. T. Arce, R. Lal, G. Arya, S. Varghese, *Biomaterials* **2011**, *32*, 3700–3711.

R. Buttner, J. R. Gosney, B. G. Skov, J. Adam, N. Motoi, K. J. Bloom, M. Dietel, J. W. Longshore, F. Lopez-Ríos, F. Penault-Llorca, et al., *J. Clin. Oncol.* **2017**, *35*, 3867–3876.

R. Das, R. F. Landis, G. Y. Tonga, R. Cao-Milán, D. C. Luther, V. M. Rotello, *ACS Nano* **2019**, *13*, 229–235.

R. Derynck, R. A. Weinberg, *Dev. Cell* **2019**, *49*, 313–316.

R. F. Landis, A. Gupta, Y. W. Lee, L. S. Wang, B. Golba, B. Couillaud, R. Ridolfo, R. Das, V. M. Rotello, *ACS Nano* **2017**, *11*, 946–952.

R. Falcioni, A. Sacchi, J. Resau, S. J. Kennel, *Cancer Res.* **1988**, *48*, 816–821.

R. Gnanadesikan, J. R. Kettenring, *Biometrics* **2006**, *28*, 81.

R. M. Ransohoff, *Nat. Neurosci.* **2016**, *19*, 987–991.

12. R. Ostuni, F. Kratochvill, P. J. Murray, G. Natoli, *Trends Immunol.* **2015**, *36*, 229–239.

R. R. Arvizo, O. R. Miranda, D. F. Moyano, C. A. Walden, K. Giri, R. Bhattacharya, J. D. Robertson, V. M. Rotello, J. M. Reid, P. Mukherjee, *PLoS One* **2011**, *6*, e24374.

R. Scherz-Shouval, E. Shvets, E. Fass, H. Shorer, L. Gil, Z. Elazar, *EMBO J.* **2007**, *26*, 1749–1760.

R. Strauss, J. Bartek, A. Lieber, *Methods Mol. Biol.* **2013**, *1049*, 355–368.

R. Strauss, Z. Y. Li, Y. Liu, I. Beyer, J. Persson, P. Sova, T. Möller, S. Pesonen, A. Hemminki, P. Hamerlik, et al., *PLoS One* **2011**, *6*, e16186.

S. A. Mani, W. Guo, M.-J. Liao, E. N. Eaton, A. Ayyanan, A. Y. Zhou, M. Brooks, F. Reinhard, C. C. Zhang, M. Shipitsin, et al., *Cell* **2008**, *133*, 704–715.

S. Chung, H. Suzuki, T. Miyamoto, N. Takamatsu, A. Tatsuguchi, K. Ueda, K. Kijima, Y. Nakamura, Y. Matsuo, *Oncotarget* **2012**, *3*, 1629-1640.

S. Ding, C. Li, N. Cheng, X. Cui, X. Xu, G. Zhou, *Oxid. Med. Cell. Longev.* **2015**, *2015*, 1–11.

S. H. Lim, L. Feng, J. W. Kemling, C. J. Musto, K. S. Suslick, *Nat. Chem.* **2009**, *1*, 562–567.

S. J. Galli, N. Borregaard, T. A. Wynn, *Nat. Immunol.* **2011**, *12*, 1035–1044.

S. Katada, T. Hirokawa, Y. Oka, M. Suwa, K. Touhara, *J. Neurosci.* **2005**, *25*, 1806–1815.

S. Lin, K. Schorpp, I. Rothenaigner, K. Hadian, *Drug Discov. Today* **2020**, *25*, 1348–1361.

S. Liu, G. Dontu, I. D. Mantle, S. Patel, N. S. Ahn, K. W. Jackson, P. Suri, M. S. Wicha, *Cancer Res.* **2006**, *66*, 6063–6071.

S. Ngernpimai, Y. Geng, J. M. Makabenta, R. F. Landis, P. Keshri, A. Gupta, C. H. Li, A. Chompoosor, V. M. Rotello, *ACS Appl. Mater. Interfaces* **2019**, *11*, 11202–11208.

S. Ngernpimai, Y. Geng, J. M. Makabenta, R. F. Landis, P. Keshri, A. Gupta, C. H. Li, A. Chompoosor and V. M. Rotello, *ACS Appl. Mater. Interfaces*, **2019**, *11*, 11202–11208.

S. Rana, A. K. Singla, A. Bajaj, S. G. Elci, O. R. Miranda, R. Mout, B. Yan, F. R. Jirik, V. M. Rotello, *ACS Nano* **2012**, *6*, 8233–8240.

S. Rana, N. D. B. Le, R. Mout, B. Duncan, S. G. Elci, K. Saha and V. M. Rotello, *ACS Cent. Sci.* **2015**, *1*, 191–197.

S. Sharma, H. Byrne, R. J. O'Kennedy, *Essays Biochem.* **2016**, *60*, 9–18.

S. Vinogradov, X. Wei, *Nanomedicine* **2012**, *7*, 597–615.

T. A. Larson, P. P. Joshi, K. Sokolov, *ACS Nano* **2012**, *6*, 9182–9190.

T. Calinski, J. Harabasz, *Commun. Stat. Theory Methods* **1974**, *3*, 1–27.

T. D. Schmittgen, K. J. Livak, *Nat. Protoc.* **2008**, *3*, 1101–1108.

T. Ezashi, P. Das, R. M. Roberts, *Proc. Natl. Acad. Sci.* **2005**, *102*, 4783–4788.

T. Nunes, D. Hamdan, C. Leboeuf, M. El Bouchtaoui, G. Gapihan, T. Nguyen, S. Meles, E. Angeli, P. Ratajczak, H. Lu, et al., *Int. J. Mol. Sci.* **2018**, *19*, 4036.

T. R. Breitman, S. E. Selonick, S. J. Collins, *Proc. Natl. Acad. Sci. U. S. A.* **1980**, *77*, 2936–2940.

T. S. Gerashchenko, N. M. Novikov, N. V. Krakhmal, S. Y. Zolotaryova, M. V. Zavyalova,

N. V. Cherdyntseva, E. V. Denisov, V. M. Perelmuter, *J. Clin. Med.* **2019**, *8*, 1092.

T. Shibue, R. A. Weinberg, *Nat. Rev. Clin. Oncol.* **2017**, *14*, 611–629.

T. Vorup-Jensen, T. Boesen, *Adv. Drug Deliv. Rev.* **2011**, *63*, 1008–1019.

T.-C. Chou, *Cancer Res.* **2010**, *70*, 440–446.

U. Boehm, T. Klamp, M. Groot, J. C. Howard, *Annu. Rev. Immunol.* **1997**, *15*, 749–795.

U. Wellner, J. Schubert, U. C. Burk, O. Schmalhofer, F. Zhu, A. Sonntag, B. Waldvogel, C. Vannier, D. Darling, A. Zur Hausen, et al., *Nat. Cell Biol.* **2009**, *11*, 1487–1495.

W. J. Peveler, M. Yazdani, V. M. Rotello, *ACS Sensors* **2016**, *1*, 1282–1285.

W. J. Peveler, R. F. Landis, M. Yazdani, J. W. Day, R. Modi, C. J. Carmalt, W. M. Rosenberg, V. M. Rotello, *Adv. Mater.* **2018**, *30*, 1800634.

W. T. Kim, C. J. Ryu, *BMB Rep.* **2017**, *50*, 285–298.

12. W. Y. Cai, T. Z. Wei, Q. C. Luo, Q. W. Wu, Q. F. Liu, M. Yang, G. D. Ye, J. F. Wu, Y. Y. Chen, G. Bin Sun, et al., *J. Cell Sci.* **2013**, *126*, 2877–2889.

Wan, Y. Shan, Y. Fan, C. Fan, S. Chen, J. Sun, L. Zhu, L. Qin, M. Yu and Z. Lin, *Mol. Med. Rep.* **2016**, *14*, 4505–4510.

X. Li, H. Kong, R. Mout, K. Saha, D. F. Moyano, S. M. Robinson, S. Rana, X. Zhang, M. A. Riley, V. M. Rotello, *ACS Nano* **2014**, *8*, 12014–12019.

X. Yang, J. Li, H. Pei, Y. Zhao, X. Zuo, C. Fan, Q. Huang, *Anal. Chem.* **2014**, *86*, 3227–3231.

Y. C. Yeh, B. Creran, V. M. Rotello, *Nanoscale* **2012**, *4*, 1871–1880.

Y. Geng, H. L. Goel, N. B. Le, T. Yoshii, R. Mout, G. Y. Tonga, J. J. Amante, A. M. Mercurio, V. M. Rotello, *Nanomedicine N. B. M.* **2018**, *14*, 1931–1939.

Y. Geng, W. J. Peveler and V. M. Rotello*, Angew. Chemie Int. Ed.* **2019**, *58*, 5190–5200.

Y. Liu, C. Chen, P. Qian, X. Lu, B. Sun, X. Zhang, L. Wang, X. Gao, H. Li, Z. Chen, et al., *Nat. Commun.* **2015**, *6*, 5988.

Y. Tao, M. Li, D. T. Auguste, *Biomaterials* **2017**, *116*, 21–33.

Y. Y. Jang, S. J. Sharkis, *Blood* **2007**, *110*, 3056–3063.

Y.-C. Liu, X.-B. Zou, Y.-F. Chai, Y.-M. Yao, *Int. J. Biol. Sci.* **2014**, *10*, 520–529.

Z. Pode, R. Peri-Naor, J. M. Georgeson, T. Ilani, V. Kiss, T. Unger, B. Markus, H. M. Barr, L. Motiei, D. Margulies, *Nat. Nanotechnol.* **2017**, *12*, 1161–1168.

Z. Wang, C. Xu, Y. Lu, X. Chen, H. Yuan, G. Wei, G. Ye, J. Chen, *Sensors Actuators, B Chem.* **2017**, *241*, 1324–1330.

Z.-J. Zhu, P. S. Ghosh, O. R. Miranda, R. W. Vachet, V. M. Rotello, *J. Am. Chem. Soc.* **2008**, *130*, 14139–14143.